2016

DEVELOPMENT AND CHARACTERIZATION OF LUNG DERIVED EXTRACELLULAR MATRIX HYDROGELS

Robert A. Pouliot
Virginia Commonwealth University

DEVELOPMENT AND CHARACTERIZATION OF LUNG DERIVED EXTRACELLULAR MATRIX HYDROGELS

A Dissertation submitted in partial fulfillment of the requirements for the degree of Doctor of Philosophy in Biomedical Engineering at Virginia Commonwealth University.

by

ROBERT ADAM POULIOT
B.S. Clarkson University, 2011

Director: Rebecca L. Heise, Ph.D.
Assistant Professor, Department of Biomedical Engineering

Virginia Commonwealth University
Richmond, Virginia
August 2016

Table of Contents

Page

Table of Contents i

List of Tables iv

List of Figures v

List of Abbreviations vi

Abstract ix

Chapter

1 Chapter 1: Introduction 1

1.1 Chronic Inflammatory Lung Disease and Unmet Clinical Needs 2

1.4 Natural Barrier and Immune Systems in the lung 5

1.3 Mesenchymal Stem Cell Therapies for Chronic Inflammation 7

1.4 Naturally Derived Extracellular Matrix Biomaterials 11

2 Chapter 2: Research Design 16

Rationale and Major Hypotheses 16

Specific Aims 17

Overview 18

3 Chapter 3: Decellularization of Porcine Lung Tissue 19

3.1 Introduction 19

3.2 Materials and Methods 20

3.3 Results 23

3.4 Discussion 28

3.5 Conclusions 29

4 Chapter 4: Production and Characterization of Lung Derived Hydrogels.....30

4.1 Introduction 30

4.2 Materials and Methods 30

4.3 Results 34

4.4 Discussion 43

4.5 Conclusions 46

5 Chapter 5: Encapsulation of hMSCs and feasibility for Cell Delivery.....48

5.1 Introduction 48

5.2 Materials and Methods 49

5.3 Results 58

5.4 Discussion 70

5.5 Conclusions 74

6 Chapter 6: Tailoring ECM Hydrogels.....75

6.1 Introduction 75

6.2 Materials and Methods 75

6.3 Results 79

6.4 Discussion 86

6.5 Conclusions 87

7 Chapter 7: Conclusions and Future Research 88

References 93

Appendices 103

Appendix A: Detailed Decellularization Protocol 103

Appendix B: Scratch Assay Image Processing Methods 105

List of Tables

Table 4.1 Major Bands from Lung Derived ECM Powder

Table 4.2 Rheometrical Properties for Tissue Derived ECM Hydrogels in the Literature

Table 4.3. KGF Loading

List of Figures

Figure 1.1 COPD Pathology

Figure 1.2 TSG-6 Mechanism

Figure 2.1 Overview

Figure 3.1 Decellularization Scale-up

Figure 3.2 Porcine Lung Tissue Decellularization.

Figure 3.3. Intact vs. Decellularized Matrix Composition

Figure 3.4 Matrix Composition Between Intact and Decell

Figure 4.1. Intact Vs. Decell vs. Pregel SDS-PAGE

Figure 4.2 Fiber Size Comparison: Decellularized Lung Tissue vs. Lung ECM Hydrogel

Figure 4.3 Gelation Kinetics and Material Mechanics of ECM Hydrogels

Figure 4.4. Gelation Kinetics and Mechanics under 5% strain

Figure 4.5. Passive Release of protein from Hydrogels

Figure 4.6 Release of Loaded KGF from ECM Hydrogels

Figure 5.1 Cell Viability Within Hydrogels

Figure 5.2 Encapsulated hMSC Gene Expression

Figure 5.3. Scratch Assay using encapsulated hMSC conditioned media

Figure 5.4 LPS Activation of Encapsulated hMSCs

Figure 5.5 TNF-alpha Activation of Encapsulated hMSCs

Figure 5.6 Macrophage Activation on ECM Hydrogels

Figure 5.7 Cell Deposition in Elastase Treated Rat Lungs

Figure 6.1 SEM Comparison of Hydrogel Structure from timed digests

Figure 6.2 Hydrogel Interconnectivity

Figure 6.3. SDS- Page for Timed Digest Gels (Pre & Post Gelation).

Figure 6.4. SDS-Page Band Analysis for Pre & Post Gel Samples

Figure 6.5. Rheometry for Timed Digest hydrogels

Figure 6.6 KGF Release from Encapsulated hMSCs

Figure 6.7 SAEC Attachment and Proliferation

Figure 7.1 Generalized FDA Approval Process for Drugs and Biologics

List of Abbreviations

ECM	Extracellular Matrix
SEM	Scanning Electron Microscopy
MSCs	Mesenchymal Stem Cells
hMSCs	Human Mesenchymal Stem Cells
GAGs	Glycosaminoglycans
BCA	Bicinchoninic acid
MPO	Myeloperoxidase
PBS	Phosphate Buffered Saline
PPE	Porcine Pancreatic Elastase
H&E	Hematoxylin and eosin
COPD	Chronic obstructive pulmonary disorder
G*	Complex Modulus
G’	Storage modulus
G’	Loss Modulus
LVE	Linear Viscoelastic
TNF-alpha(α)	Tissue Necrosis Factor alpha
LPS	Lipopolysaccharide (also known as endotoxins)
KGF	Keratinocyte Growth Factor
FGF-7	Another name for KGF
HDAC2	histone deacetylase-2
M1	Pro-inflammatory Macrophage Phenotype
M2	Anti-inflammatory Macrophage Phenotype
VEGF	Vascular endothelial growth factor
TGF-β	Transforming growth factor beta
bFGF	Basic fibroblast growth factor
HGF	Hepatocyte Growth Factor

Alpha-gal	Galactose-alpha-1,3-galactose antigen
BEAS-2B	Bronchial Epithelial Cell (Lonza)
BEGM	Bronchial Epithelial Growth Medium
BEBM	Bronchial Epithelial Basal Medium
SAEC	Small Airway Epithelial Cell (Lonza)
CNS	Central Nervous System
SC	Spinal Cord
PGE_2	Prostaglandin E_2
IL-10	Interleukin-10
IL-6	Interleukin-6
IL-8	Interleukin-8
TSG-6	TNF-alpha Stimulated Gene 6
Fizz1	An M2 Macrophage marker in mice
MR	Manose Receptor
NOS2	Nitric Oxide Synthase 2
YM1	M2 Macrophage marker in mice
kDa	Kilodalton
CD	Cluster of Differentiation
CD44	Cell surface glycoprotein
SOX-2	Transcription factor essential for maintaining self-renewal
OCT-4	Gene associated with the ability to self-renew in embryonic stem cells
THY-1	Thymocyte antigen 1 (also known as CD90)
HA	Hyaluronic Acid
NF-κB	Nuclear factor kappa-light-chain-enhancer of activated B cells
C57BL/6	Specific Genetic Strain of Mice
DNA	Deoxyribonucleic Acid
dsDNA	Double Stranded Deoxyribonucleic Acid
cDNA	Double Stranded DNA synthesized from a single stranded RNA

RNA	Ribonucleic Acid
DAB	3,3'-Diaminobenzidine
1X TE	Tris – EDTA Buffer
DI	Deionized
STD	Standard
SDS-PAGE	(Sodium dodecyl sulfate) polyacrylamide gel electrophoresis
ELISA	Enzyme-linked immunosorbent assay
MTT	3-(4,5-dimethylthiazol-2-yl)-2,5-diphenyltetrazolium bromide
Decell	Decellularized
FITC	Fluorescein isothiocyanate
TRITC	Tetramethylrhodamine
NIH	National Institutes of Health
TC	Tissue Culture
PCR	Polymerase chain reaction
RT-QPCR	Real-time Quantitative PCR
MCSF	Macrophage Colony Stimulating Factor
GFP	Green Fluorescent Protein
EDTA	Ethylenediaminetetraacetic acid
HTAB	Hexadecyltrimethyl ammonium bromide
$\Delta ABS_{5\ min}$	Change in absorbance over 5 minutes
ANOVA	Analysis of variance
PPE	Porcine Pancreatic Elastase
TLR 4	Toll Like Receptor 4
MMPs	Matrix Metalloproteinases

Abstract

DEVELOPMENT AND CHARACTERIZATION OF LUNG DERIVED EXTRACELLULAR MATRIX HYDROGELS

By Robert A. Pouliot B.S.

A Dissertation submitted in partial fulfillment of the requirements for the degree of Doctor of Philosophy in Biomedical Engineering at Virginia Commonwealth University.

Virginia Commonwealth University, 2016

Director: Rebecca L. Heise, Ph.D.
Assistant Professor, Department of Biomedical Engineering

Chronic obstructive pulmonary disease (COPD) including emphysema is a devastating condition that is one of the only major diseases increasing in prevalence in the US and worldwide. Unfortunately, there remains no cure for COPD, rather only symptomatic treatment approaches. Lung architecture is highly complex and the tissue has several rapid clearance mechanisms that can quickly remove administered cell or drug therapies. For this reason, it has been difficult to translate therapies effective for acute lung damage to target chronic lung diseases like COPD. To address this, we have been investigating lung derived extracellular matrix (ECM) hydrogels as a novel approach for delivery of cellular therapies to the pulmonary system.

During this research we have validated out decellularization approach, confirming the removal of the immunogenic alpha-gal antigen as well as a ~95% reduction in dsDNA. We have

also characterized the disruption in ECM fiber organization and depletion of major ECM components between the native and decellularized tissues due to the harsh detergents. Further, we have processed these whole decellularized lung scaffolds into a dry ECM powder and solubilized the proteins to form a pregel solution using a pepsin digestion. The solubilized lung ECM pregel solution we have developed and characterized exhibits "injectability," a unique property where the pregel solution is liquid at room temperature, but undergoes rapid self-assembly as the temperature approaches the physiologically relevant 37°C. This property can be used to deliver a payload into the tissue, where it is encapsulated by self-assembly once it reaches body temperature. Physical properties of the hydrogel system were evaluated including: the average fiber size, gelation kinetics and mechanical properties of the formed gel, passive protein release, and ability to bind loaded growth factors.

To determine if this hydrogel is a feasible platform for cell delivery we have determined that the gel has the capacity to support 3D hMSC culture, encapsulated hMSC viability, and limited gene expression changes in hMSCs encapsulated over 7 days. The effect of encapsulation did not greatly reduce the capacity for hMSCs to respond to activating factors in the media. This was investigated by looking at inflammatory cytokine and growth factor gene expression resulting from exposure to LPS and TNF-alpha. We have characterized the response of naive (Mo) macrophages to culture on ECM hydrogels by looking at gene expression, finding that, while they do not express markers for classic M1 or M2 activation, they do have an upregulation of expression for secreted inflammatory mediators including IL-6, TNF-alpha, and IL-10. Finally, in an in vivo pilot study, we found that delivery of rMSCs in pregel increased cell retention over delivery in solution, 2 hours post-delivery, in a rat model of elastase induced emphysema.

As an extension of the previous work, we have started to investigate the effect of protein solubilization on the properties of the hydrogel. By varying pepsin digestion duration, we have been able to characterize significantly different, and controllable, properties of the hydrogel. These include: the branching and density of the hydrogel, the distribution of protein size, the gelation and mechanical properties, and the effect on cells cultured on or in the hydrogel. By lowering digestion times, the hydrogel architecture becomes denser and has significantly more interconnections. The resulting gel also has increased stiffness, and is better able to support epithelial cell growth. There are still some questions to investigate regarding this new approach, including the effect of digestion time on growth factor loading and release, the ability to encapsulate hMSCs, and the immunogenic response of macrophages to the materials.

The completed research has effectively demonstrated that the approaches taken to decellularize and produce an ECM hydrogel from porcine lung have resulted in a material that is feasible for cell and drug delivery. We have also demonstrated the ability to encapsulate and support hMSCs so that they are able to fill the proposed role for immunomodulation of an inflammatory environment. Continued research and development of this material and methods to expand its tailorability are novel to the field and can allow us to control material properties to address a wider range of applications. The work to develop and characterize the decellularization process is also the basis for two additional materials that include electrospun ECM polymer scaffolds and ECM nanoparticles.

Chapter 1: Introduction

* Sections taken from, Pouliot et. al., Development and Characterization of a Naturally Derived Lung Extracellular Matrix Hydrogel, JBMR, 2016 will be marked with [Pouliot et. al. 2016] *

Diseases categorized as chronic lower respiratory disease are the third leading cause of death in the US, resulting in almost 140,000 deaths in 2010. Included in this category are: asthma, chronic bronchitis, emphysema, and Chronic Obstructive Pulmonary Disease (COPD), which is solely responsible for killing over 120,000 Americans each year [1]. Unique challenges are encountered in developing treatment approaches for lung pathologies, including: (1) the complex architecture of interweaving airways, vasculature, and functional alveolar structures, (2) a volatile mechanical environment (respiration), and (3) multiple inherent mechanisms for removing administered agents from the lung tissue. The first and second challenges can be addressed using aerosol delivery for therapeutic drugs or molecular factors[2,3]. The shear forces generated in aerosolization limit cell delivery application, as a result, cell administration is done using an intra-tracheal injection of a cell suspension [4–6]. Current strategies do little to address the third challenge, there are several major mechanisms responsible for rapid removal of administered cells or drugs, including the physical action of the mucociliary escalator, coughing, uptake by alveolar macrophages, and absorption by the vasculature [7]. We have designed a lung derived extracellular matrix hydrogel approach, with the goal of address all three challenges.

1.1 Chronic Inflammatory Lung Disease and unmet Clinical Needs

COPD in large part is the result of an abnormal tissue response to inhaled toxic particles or gases. Most cases of COPD are directly related to long term cigarette/tobacco smoking; however, the rapid industrialization and increased pollution levels in developing countries is likely to be an increasing source of cases in the next decades. The majority of smokers without clinical symptoms of COPD are afflicted with low level infiltration of inflammatory cells into the large airways and peripheral lung parenchyma and have what is increasingly recognized as early disease. Further, in a significant proportion of smokers, the inflammatory process is amplified through as yet incompletely understood mechanisms and has long lasting effects. This amplified and prolonged inflammatory response is responsible for the tissue-remodeling events associated with chronic bronchitis and emphysema; hallmarks of COPD[8]. Figure 1.1 is a visual overview of the healthy vs COPD lungs, showing how chronic bronchitis and emphysema present in the tissue.

There is a clear association between atmospheric air pollution and the appearance of cytokines in the blood as well as an increase in the number of inflammatory cells, such as polymorphonuclear neutrophils (segmented and band) and monocytes. Increased levels of leukocytes in the blood is a predictor of decline in lung function, increased mortality, and potentially increases the likelihood of a smoker developing COPD. In COPD, the major source of increased ventilation resistance takes place in the peripheral airways. The increase in resistance is due to airway narrowing as the tissue thickens during inflammation, fibrosis, and mucous plugging, as well as increased airway closure resulting from reduced tissue elastic recoil [8].

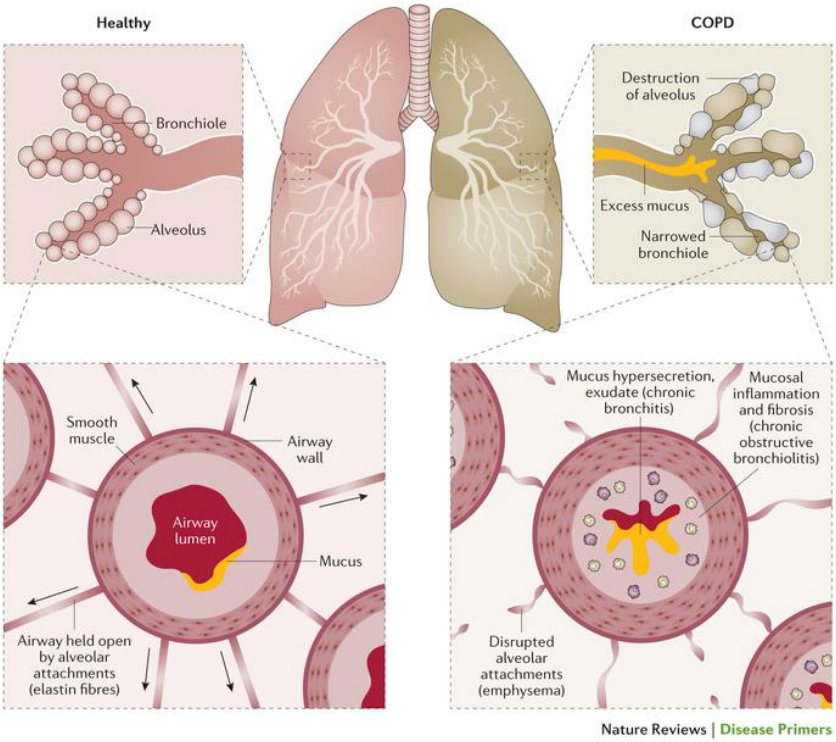

Figure 1.1 COPD Pathology This review figure shows all of the symptoms or damage that are commonly associated with the development of COPD. This includes chronic bronchitis with excess mucus production and inflamed airways, as well as damage to ECM damage and alveolar collapse[9].

In COPD, the recognition that cigarette smoke causes both alveolar emphysema and a fibrotic effect in small airways could be contradictive; however, this can be explained by a hypothesized imbalance between matrix component synthesis and degradation during the repair process [8]. The proteins most responsible for imparting healthy lung ECM mechanics are collagen, elastin, and glycosaminoglycans/proteoglycans. During the development of emphysema there is a loss of elastin and a weakening of ECM in the alveolar walls. This matrix weakening can result in a rupturing of the alveolar tissue leading to a large reduction in gas

exchange surface area. Chronic inflammation can further interfere with regular collagen cross linking, which further increases damage to both alveoli and to large and small airways[10]. The loss of functional tissue can dramatically change the distribution of mechanical forces on the remaining ECM during ventilation. As a result, the supportive collagen network, which is the underlying mechanical backbone for other matrix proteins (like fibronectin and laminin), is made to abnormally stretch and condense.

This disease is usually associated with long term smokers, and bronchodilator therapy only partially resolves lung hyperinflation in emphysema [11]. Corticosteroids are sometimes used to treat acute respiratory problems stemming from COPD, but long term treatments have shown little if any benefit. Corticosteroids work to reduce inflammation by suppressing several genes that are activated in chronic inflammatory diseases. They do this by reversing histone acetylation of inflammatory genes through a mechanism in which liganded glucocorticoid receptors are bound to coactivators, recruiting histone deacetylase-2 (HDAC2) to the transcription process [12]. However, in patients with COPD, oxidative /nitrative stress from smoking reduces expression of HDAC2 and become resistant to the anti-inflammatory action of corticosteroids [12].

Unfortunately, there remains no cure for COPD, rather only symptomatic treatment approaches. Lung volume reduction surgery decreases hyperinflation, but is associated with high morbidity and operative mortality[13]. For a relatively few patients, lung transplantation is utilized for end stage disease. However, the supply of donor lungs is limited and immune rejection[13] complicates transplantation such that 5 year survival of transplant recipients remains only

approximately 50%, making transplant an undesirable option. [14]. New approaches are desperately needed.

1.2 Natural Barrier and Immune Systems in the lung

Treatment of lung diseases is majorly complicated by several factors including the complexity of lung structures and architecture, the mucociliary escalator, and the cellular immune systems that protect the lung from inhaled vectors. The airway structure in the lung is a major limiting factor which controls the infiltration of any inhaled particulates depending on size, density, and shape[15]. Impaction of particles due to these lungs makes it much easier and speedier to remove these particulates with physical mechanisms including the action of the mucociliary escalator and coughing. The innate and adaptive immune systems control how the lung responds to foreign particulates, bacterial invasion, and inflammatory signaling. The component immune cells also play a major role in tissue hemostasis and controlling routine maintenance and remodeling.

The surface area of the endothelium of the lung is the largest in the human body and is constantly challenged with a large number of various microbes and particulate (toxic or not)[16]. Of the two, the innate immune system is much older in evolutionary timeline and is made up of soluble proteins and phagocytic migratory leukocytes traveling through the bloodstream or residing in the tissue[16]. The innate immune system is ready to quickly respond to stimuli, while the adaptive immune system is much slower and acts over a longer time scale. The cells on the front lines of the innate immune system include macrophages, neutrophils which respond to a

variety of inflammatory and stimulatory factors. They can be quickly and specifically activated through toll-like receptor (TRL) signaling which have evolved to bind antigens from an array of bacterial, fungal, and viral products without any help from the adaptive system[16].

The adaptive immune system is more advanced and has evolved to complement the innate system by responding to signals from the innate immune system. It does this by producing antibodies that are highly specific for antigens on invading viruses or bacterial membranes, making them much more susceptible to phagocytosis. One unique cell type, dendritic cells (DCs), are on the front line of innate immune response, however their complexity allows them to capture novel antigens from phagocytosed material, then migrate to and present the antigens on their surface for presentation to T and B cells[17,18]. This means that dendritic cells are the main points of interaction between he innate and adaptive immune systems that allow them to act together. The adaptive immune system also has a long term memory component, storing novel antigens in specialized T-cells for long term storage, this is the system that supports immunity to diseases due to past exposure, or vaccination.

Dendritic cells (DCs) and macrophages have a major role in response to inhaled virus or bacteria as part of the innate immune system. Normally there is a precarious balance in these situations between removing/dealing with the threat and limiting inflammatory responses that can cause acute lung failure[19] During the pathogenesis of COPD the ability of macrophages to clear pathogens and apoptotic cells is compromised, there is an increasing number of dendritic cells and the adaptive immune system is induced[22]. Neutrophils, a usually short lived cell type, are stimulated in increasing numbers to infiltrate the tissue, and they live for much longer[22].

Without targets to phagocytose, they mostly sit around and secrete an excess of matrix remodeling enzymes[22]. As the inflammatory chronic state continues, more and more specialized T-cells are called in which secrete a large amount of cytotoxic factors including perforins which add to the native cell death and apoptosis[22].

In smoking induced emphysema, chronically activated macrophages have actually been found to express upregulated levels of several proteinases and matrix metalloproteinases in both human smokers and some have been confirmed in mouse models[21]. Macrophages also play a crucial role in triggering the initial immune response in responding to smoking induced inflammation. Alveolar macrophages are usually kept in a quiescent state and actually work to suppress the adaptive immune system in the healthy lung, however in chronic inflammatory situation alveolar macrophages are the main source of pro-inflammatory amplification and play a significant role in causing an influx of other immune cells[20]. Macrophages contribute heavily to the pathogenesis and they play a key role in the inflammatory cascade that leads to pathogenic behavior of other immune cells; because of this, macrophage modulation is a compelling target for treating chronic inflammatory diseases like COPD.

1.3 Mesenchymal Stem Cell Therapies for Chronic Inflammation

Mesenchymal stem cells have been shown to be effective at sensing and responding to inflammatory environments through several pathways, making them a promising candidate for regenerative therapies. Mesenchymal stem cells are adult stem cells, and have been isolated from a growing number of sources including umbilical cord, endometrial polyps, blood from menstruation, bone marrow, and adipose tissues[23]. Mesenchymal stem cells have the ability to

differentiate into a several lineages of the mesoderm, ectoderm, and endoderm[23] into progenitor cell types for tissues including:: insulin-producing cells of the pancreas, neuron, muscle, chondrocytes, osteocytes, and adipocytes [24]. The ability to differentiate towards these targets may be limited by their isolation source, for example bone marrow derived mesenchymal stem cells may be limited to bone, cartilage, and adipose lineages. The differentiation of these cells has been shown to be controllable and directed by growth factors, substrate stiffness[25], and even geometric cues[26,27]. The question of whether stem or progenitor cells can engraft and acquire phenotype of structural lung cells following instillation remains controversial [28]. One recent study found that human bone marrow derived mesenchymal stem cells can be differentiated down a lung epithelial lineage when cultured on decellularized lung slices in small airway growth media [29]. However, MSCs infused into the lung directly to facilitate regeneration have not been found to engraft and participate in direct regeneration in significant number, instead they have been found to evert positive effects through anti-inflammatory activity[4].

Mesenchymal stem cells have demonstrated the ability to sense and respond to inflammatory factors in the environment. MSCs can target resident macrophages which are responsible for producing many of the pro-inflammatory factors and act on them in two ways. In one pathway, MSCs first sense tissue necrosis factor alpha (TNF-α) secreted by the macrophages, and respond by releasing tissue necrosis factor stimulated gene/protein 6. This released factor reduces nuclear factor-κB signaling in the macrophages and decreases pro-inflammatory cytokine release from the effected cells [30]. Another mechanism for MSC modulation begins when MSCs are activated to secrete prostaglandin E_2 by an extremely pro-

inflammatory environment. PGE_2 acts directly to convert macrophages from a pro-inflammatory phenotype, to a phenotype that produces pro-regenerative cytokine IL-10 [30].

TSG-6 modulation of inflammatory conditions has been described in several animal models including: rat cornea's (through both chemical and mechanical damage)[31], a mouse model for myocardial infarct [30],and a mouse model for peritonitis[32]. While there are several potential explanations for how TSG-6 could be operating in these systems, much of the data points toward a macrophage modulation mechanism. TSG-6 is a 35 kDa glycoprotein which can almost never be detected in tissue unless they are undergoing some form of inflammatory response such as ovulation, rheumatoid arthritis, or other general tissue inflammatory pathologies [33,34]. The TSG-6 protein specifically binds hyaluronic acid (HA) and increases or induces the binding of HA to CD44 (HA receptor). The underlying mechanism is thought to be caused by TSG-6 crosslinking of HA chains into an extended fiber. These cross –linked HA complexes have a greater affinity for the CD44 receptor causing increased substrate binding and CD44 receptor clustering on the cell surface [35]. This increase in CD44 activity is responsible for the inhibition of toll-like receptor signaling cascade and results in a down-regulation of NF-κB release and translocation to the nucleus. Endogenous macrophages release of TNF-α induces mesothelial cells to increase their production and release of additional inflammatory cytokines. This mechanism is exciting as modulation of the NF-κB signaling pathway can result in the down-regulation of the inflammatory cascade at the source of amplification [30]. Figure 1.2 depicts the pathway as described.

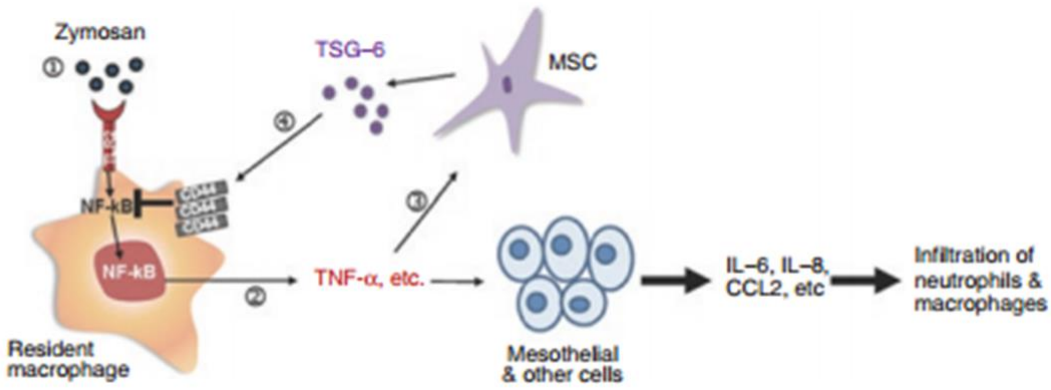

Figure 1.2 TSG-6 Mechanism This figure depicts the proposed method of action for TSG-6, which has been shown to play a major role in modulating inflammation[32].

Mesenchymal stem cells (MSCs) are currently being used therapeutically to promote regeneration of damaged lung epithelial tissue through immune-modulation of the pulmonary microenvironment [4,5]. MSC therapies are thought to act through their influence over pro-inflammatory resident macrophages[30–32]. MSCs have been successfully delivered in solution as a therapy for acute lung injury in several models[6,36–39]. Despite their success these therapies have failed to produce significant improvement when addressing chronic lung pathologies due to the low retention in the tissue over time [5,40]. Cell delivery strategies for encapsulating and maintaining the therapeutic efficacy of the dosed cells have been developed from both natural and synthetic materials[41–43]. Inclusion of extracellular matrix components in the cell delivery mechanism has been shown to help keep delivered cells in the tissue without negatively influencing the tissue environment. [Pouliot et. al. 2016]

Recently a synthetic poly-L-lysine/ECM (fibrin) hydrogel was used to deliver lung derived MSCs in a sheep emphysema model. These hydrogels increased cell retention and

resulted in better outcomes for the animals subjects.[44] In a similar strategy we have developed a tissue specific extracellular matrix (ECM) hydrogel derived from porcine lung tissue which could be used to deliver and shield inoculated cells from the clearance mechanisms of the lung. [Pouliot et. al. 2016]

1.4 Naturally Derived Extracellular Matrix Biomaterials

Tissue derived ECM is the next logical source to produce materials for organ transplant, tissue replacement, and novel tissue engineering approaches to cell and drug delivery [45–51]. Decellularized scaffolds are easily subjected to degradation and remodeling, and encourage macrophages to adopt the anti-inflammatory M2-like macrophage phenotype [52–54]. The organization, architecture, and composition of ECM components are tissue specific [55]. Lung derived ECM hydrogels retain native lung proteins, glycosaminoglycans, and glycoproteins that pulmonary cells can recognize and remodel. These material components can also sequester and present bioactive molecules and tissue specific growth factors important in guiding cell behavior including: migration, proliferation, differentiation, attachment, and signaling [56]. [Pouliot et. al. 2016]

Companies have been producing and selling decellularized ECM based products for at least 10 years now. Newer products are non-crosslinked to remove the potential for increased immune response. These products include a range of surgical and implantation materials including surgical meshes, wound dressing (Acell, Inc), vasculature replacement (Humacyte, Inc). Some companies have specialized in developing products from fetal tissues including wound healing matrix sheets derived from placenta tissue (MiMedx). Products derived from decellularized xenogenic sources have been developed and approved for human use as well. A

company called Miromatrix Medical Inc. just started selling a product called MIROMESH, a decellularized tissue mesh made from slices of highly vascular, decellularized porcine liver tissue. An ECM hydrogel product derived from decellularized human heart tissue called VentriGel (Ventrix, Inc) has been shown to successfully mitigate damage from a myocardial infarction and improve cardiac function in a porcine model[57], the treatment was approved for human clinical trials which started in 2015. As the science behind tissue decellularization and ECM processing progresses and acceptance of using these products in patients increases the demand and development of these products will scale up dramatically.

Scaffold behavior and cell interaction are paramount factors in determining their value. Decellularized scaffolds that are easily subjected to degradation and remodeling are more likely to influence macrophages into the anti-inflammatory M2 macrophage phenotype; likewise, scaffolds not easily modified or broken down prompt and M1 phenotypes [5]. Growth factors that might be sequestered in the matrix including vascular endothelial growth factor (VEGF), basic fibroblast growth factor (bFGF), and transforming growth factor beta (TGF-β) can be unleashed during degradation and remodeling. Scaffold degradation could also be used as a controlled release process for ECM subunits into the milieu, whose presence appears to mediate remodeling events through release of bioactive cryptic peptides [56,58]. Composition and structure of the ECM effect cellular activities and are subject to several factors. These include: current metabolic activity of resident cells, trends/changes in mechanical demands on the matrix, and age or disease states (such as fibrosis) [58].

Whole Organ Scaffolds

In the lung, a decellularized scaffold may provide a unique environment for the study of cell-ECM interactions in normal and diseased lung states and are increasingly used and as a scaffold for whole organ recellularization[46,55,59–61]. Whole organ extracellular matrix scaffolds retain tissue specific proteins, glycosaminoglycans, glycoproteins, bioactive molecules, and growth factors that are essential for cell-matrix recognition. The amino acid sequence and quaternary structure of matrix proteins in mammals are comparable across species; it is thought that ECM protein alone does not contribute much to scaffold immunogenicity in vivo [62]. They also maintain much of the organization, architecture, and mechanical composition of the native tissue [55,62]. For example, scaffolds derived from heart and lung tissue have higher levels of elastin because the source tissue needed facilitate dynamic mechanical systems while minimizing energy loss (and damage). ECM components are important in cell matrix interactions through membrane bound integrin proteins which function in attachment and pass information about another cell or the composition of the matrix.

Direct organ transplantation and development of biomaterials from xenogenic sources is complicated by the presence of the alpha gal epitope, especially in cases in which intact or fixed tissue is used without prior depletion of the antigen[63,64]. In humans a significant 1% of all circulating immunoglobulins are specific for the alpha-gal epitope which is responsible for the catastrophic failure of such implants [65]. The immune response to alpha-gal recognition should be limited following effective removal of cellular material through decellularization. However, incomplete decellularization or re-sequestration of cellular factors, including alpha-gal, in the extracellular matrix could activate both innate and acquired immune response. The quantification

of the alpha –gal epitope in decellularized tissues or scaffolds should be an effective indicator of the removal of cellular debris because it is present on all porcine cell membranes.

Fundamental differences in normal vs diseased scaffolds have been discovered. For examples, scaffolds produced from lungs of patients with idiopathic pulmonary fibrosis induce pathogenic myofibroblast differentiation of fibroblasts [66]. Notably, emphysematous scaffolds are structurally different from normal scaffolds and importantly don't support growth of normal lung epithelial, vascular endothelial, or stromal cells nearly as well as scaffold derived from healthy lungs[67]. Decellularized lung tissue is already being explored as a scaffold for whole organ recellularization[46,55,59–61] as well as a platform for investigation of cell differentiation, and the effects of age, injury, and disease states on the matrix[29,66–68]. Recellularization of acellular lung scaffolds has been successful and co-cultures of alveolar epithelial cells and vascular endothelial cells have displayed migration and hierarchical organization in the scaffold [53,60].Recellularization approaches are also progressing significantly and co-cultures of alveolar epithelial cells, vascular endothelial cells, and lung stromal cells such as fibroblasts or mesenchymal stromal cells (MSCs) have displayed hierarchical organization on acellular scaffolds [53,60].

Decellularized Matrix based Biomaterials

ECM hydrogels have been developed from an increasing number of tissues, including: cardiac, epidermal, bladder, articular cartilage, nerve, and adipose sources [69–74]. These materials exhibit "injectability", a unique property based on their gelation behavior. The ECM pre-gel solution is liquid at room temperature, but undergoes rapid self-assembly as the temperature approaches 37°C. This property allows the material to fill an area or settle into a defect just prior

to gelation, encapsulating any cells or drugs delivered in the solution. Like other biomaterials, ECM hydrogels benefit from a high surface area to volume ratio which provides ample area for integrin binding [56]. *In vitro* studies have determined that several cell types exhibit a positive response to hydrogels derived from tissue specific sources including CNS [74] derived ECM and cardiac ventricular [47] derived ECM hydrogels. Recently, cardiac tissue derived ECM hydrogels have been shown to increase migration of endogenous cells into the damaged tissue when delivered in an infarct model[69]. Naturally derived gels, which retain a significant portion of sulfated glycosaminoglycans, can effectively bind and deliver heparin binding growth factors *in vivo* [75]. A lung derived ECM hydrogel could be an effective material for delivery and encapsulation of cells, drugs, or molecular factors at difficult to reach sites in lung disease models where epithelial cell and ECM defects at injury sites are observed. [Pouliot et. al. 2016]

Tissue specific differentiation has also been shown in hydrogels derived from native tissue using progenitor cells. Cardiac progenitors grown in cECM were shown to increase expression of early cardiac markers while a culture of these cells on adipose derived ECM gels did not produce the same differentiation towards a mature cardiomyoctye cell type, suggesting that the ECM hydrogels maintain important tissue specific biochemical cues [47]. In another example, a hydrogel derived from brain ECM promoted increased neuron length in 3D culture over non-tissue specific derived materials such as spinal cord and urinary bladder derived hydrogels[74]. The ability ECM hydrogels to influence progenitor differentiation as well as promote specific cell morphology without the same guiding tissue matching mechanical properties or structures of whole tissue scaffolds suggests that biochemical cues are intact and active in these derivative materials.

Chapter 2: Research Design

2.1 Rationale and Major Hypotheses

This research was initiated with the goal to design and develop an ECM hydrogel from decellularized lung tissue in order to increase MSC engraftment into the lung tissue for direct regeneration. Over the past four years the goal has shifted towards developing an ECM hydrogel for the purpose of cell or drug delivery, to encapsulate and maintain delivered factors in the tissue for an extended period of time. This shift in direction was directed by findings and opinions in the field that MSCs delivered into the lung fail to engraft[4] and are unlikely to differentiate. The purpose of using hydrogels to deliver hMSCs into the diseased lung evolved with the field to embrace MSCs for their immunomodulatory functions. The **main hypothesis** for this research is that a lung derived ECM hydrogel can be developed and validated as a feasible platform for delivering and maintaining therapeutic cells or drugs in the tissue. As an extension of this work we have also **hypothesized** that novel changes in the ECM solubilization protocol can be used to produce hydrogels with controlled properties. In order to test these hypotheses, we developed four specific aims.

2.2 Specific Aims

Aim 1 Evaluate the proposed lung decellularization approach with regards to removal of immunogenic material, disruption of the extracellular matrix organization, and depletion of key ECM components including elastin, collagen, and glycosaminoglycans.

Aim 2 Characterize the resulting hydrogel biomaterial including fiber size, gelation kinetics, mechanical properties, and passive protein release. Determine the capacity of the hydrogel to bind and sequester growth factors as an additional functionality, using KGF as a representative group.

Aim 3 Investigate the ECM hydrogel as a feasible platform for cell and drug delivery by investigating the viability of encapsulated cells and if they maintain their mesenchymal phenotype. Confirm that encapsulated cells maintain their ability to secrete immunomodulatory factors and respond to strong activating factors in the environment, while encapsulated. Determine if naïve macrophages are significantly polarized by growth on ECM hydrogels.

Aim 4 Determine if ECM hydrogel physical and mechanical properties can be significantly changed and controlled using modifications to the ECM solubilization protocol. Conduct some pilot studies using several cell lines to determine how changes in digestion time can effect cell growth, signaling, and behavior.

2.3 Overview

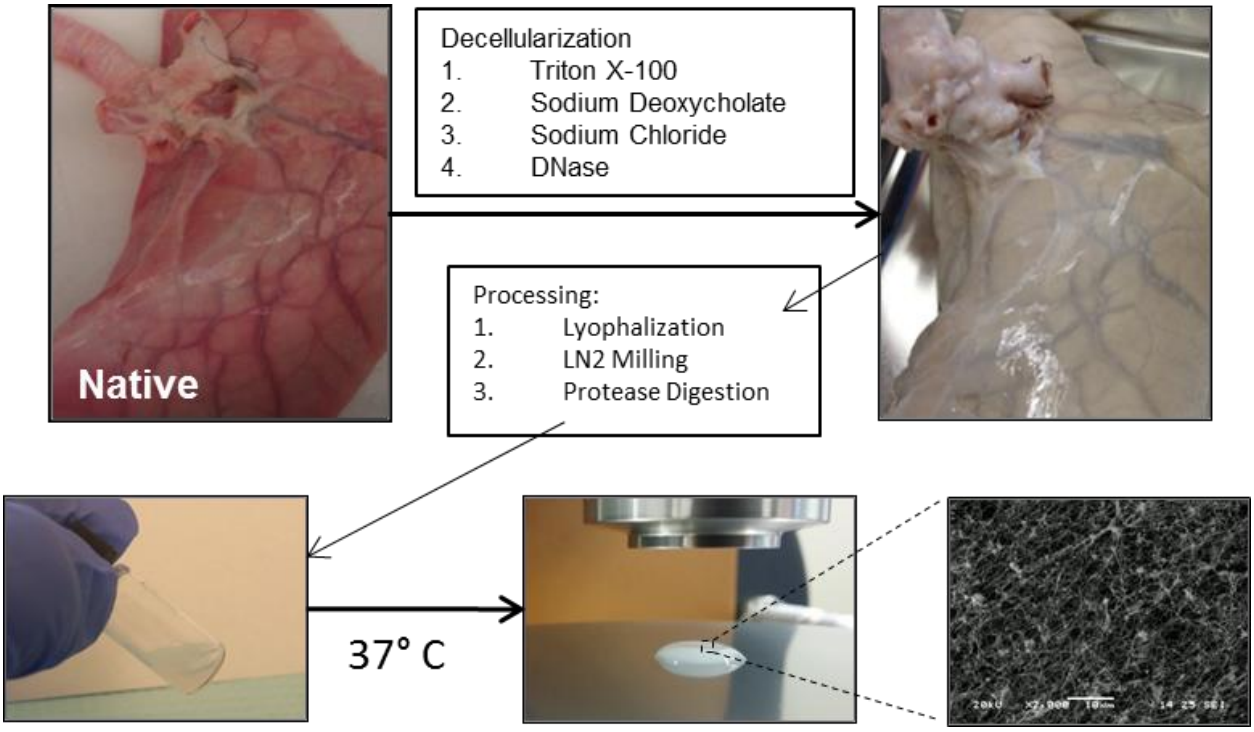

Figure 2.1 Overview Figure showing the major steps in creating porcine derived ECM hydrogels with some of the characterization techniques used including gel rheometry and SEM.

Chapter 3: Decellularization of Porcine Lung Tissue

3.1 Introduction

Decllularization of porcine lung tissue was adapted from a protocol for C57BL/6 mice [60]. Over the course of this research we have scaled up from mice, to rats, to pigs in order to greatly increase the amount of material we have for characterization and feasibility experiments (Figure 3.1). Processed lungs provide about 5 mg, 40 mg, and 10 g of ECM powder respectively (estimated). This chapter describes the methods for decellularization of porcine lung tissue and the evaluation of the extent of decellularization including the removal of double stranded DNA (dsDNA), and the immunogenic antigen alpha-gal. We also investigated the disruption of major elastic components and the physical morphometry of essential lung structures including: alveoli, airways, and vasculature, using SEM imaging and histological staining.

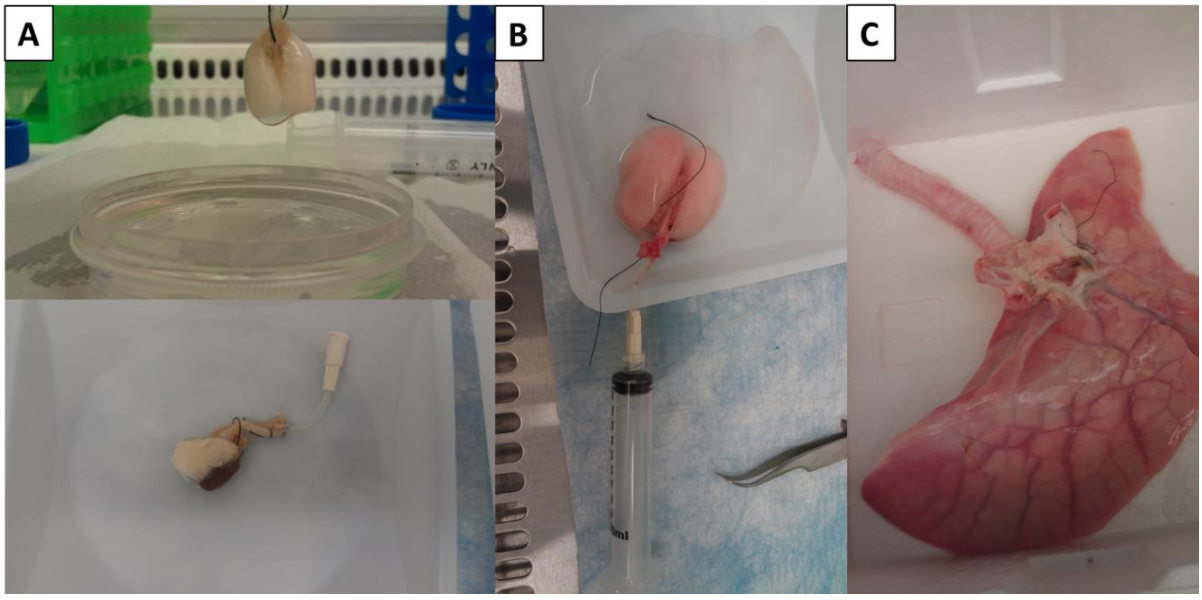

Figure 3.1 Decellularization Scale-up Images of lung tissue for decellularization, isolated from (A) C57BL/6 mice, (B) Sprague-Dawley Rats, and (C) Slaughterhouse Pigs.

3.2 Materials and Methods

Porcine Lung Tissue

Lung tissue was donated from slaughterhouse animals by Smithfield-Farmland Inc. The lungs, heart and trachea were isolated *en bloc* from a 6 month old pig at the facility, packed in ice, and delivered overnight in a sealed insulated container. Upon arrival, the heart was carefully removed to preserve the pulmonary artery for cannulation. Connective tissues surrounding the trachea, bronchi, and pulmonary artery were carefully excised to expose the vascular and airway structures necessary for perfusion. The right lung was removed at the main bronchus and the vasculature was dissected. The vasculature and airways previously connected to the right lung were then clamped or sutured shut to create a closed system for perfusion decellularization of the left lung. Both the trachea and pulmonary artery were sutured with tubing to streamline tissue perfusion. [Pouliot et. al. 2016]

Decellularization

Tissue decellularization was adapted from a protocol for C57BL/6 mice [60] and scaled to fit to work for porcine lung tissue. Briefly, the lung was perfused three times with sterile filtered water with 1X penicillin/streptomycin (Life Technologies) though the trachea and vasculature. Between every rinse the solution was removed passively, driven by the elasticity of the tissue. After rinsing the tissue, 1L 0.1% Triton X-100 (Fisher Sci) was injected through the pulmonary vasculature and 1.5L was injected into the airways through the trachea. Treated tissue was submerged in the same solution and incubated for 24 hours at 4°C. Following incubation, the tissue was again rinsed three times with sterile filtered water to remove the chemical solution and all cellular debris. Tissue was then perfused again using a 2% sodium deoxycholate (Sigma) and

incubated for an additional 24 hours. On day three, tissue was rinsed and a DNase solution was pumped into the tissue, incubated for 60 minutes and rinsed. A sodium chloride (Fisher Sci) solution was administered for an additional 60 minutes. Following the decellularization the tissue was rinsed with water three more times before being rinsed with sterile 1X PBS five times to remove as much decellularization agents and loose debris as possible. Decellularized tissue was sectioned and all discernable cartilaginous airways were removed before storage at -80°C. [Pouliot et. al. 2016] A more thorough decellularization protocol has been added in Appendix A.

Tissue Histology

A minimum of 3 representative samples were taken from distal areas of both intact and decellularized lung, paraffin embedded, sectioned, and mounted. The slides were subsequently deparaffinized in xylenes and hydrated from 100% ethanol using stepwise rinses with increasing water to ethanol ratio. One set of lung sections were stained with hematoxylin and eosin (H&E) to confirm decellularization and additional slides were stained using the ACCUSTAIN elastic stain kit (Sigma) to compare elastin and collagen organization before and after decellularization. A final set of slides was exposed overnight to 1 to 5 dilution of mouse α-Galactosidase primary antibody (Enzo), then washed and incubated with mouse SignalStain Boost Detection Reagent and stained with DAB chromogen solution (Cell Signaling) for 5 minutes. Stained slides were rinsed, dehydrated with xylenes, and mounted using Permount mounting medium (Fisher) prior to imaging using an Olympus IX71 Microscope (Olympus). [Pouliot et. al. 2016]

Picogreen Double Stranded DNA Quantification

The DNA content of native and decellularized tissues was completed using the Quant-iT PicoGreen dsDNA assay kit. Briefly, intact and decellularized porcine lung tissues were sectioned into 100 mg samples and then diced using a razor blade. Each sample (n=3 per tissue) was digested in 1mL of papain digestion solution at 60 °C overnight. The next day the samples were lightly centrifuged and diluted in 1X TE buffer for the following dilutions: 1:1, 1:4, 1:9, 1:19, 1:29, 1:49, 1:79, 1:99 and added to a solid black 96 well plate in 100ul volumes in triplicate. A dsDNA standard was also prepared in the following [ug/mL] concentrations: 2, 1, 0.5, 0.25, 0.125, 0.0625, 0.03125, and 0. Picogreen reagent was then added to samples and standards and incubated in the dark at room temperature for 3 minutes. The samples were quantified in using a fluorescent plate reader with an excitation wavelength of 480 nm and emission wavelength of 520 nm. [Pouliot et. al. 2016]

Quantification of Matrix Components

Elastin/ Collagen Quantification

Both elastin and collagen quantification were completed using a protocol from Tranquillo et al[76]. Collagen quantification was performed using a hydroxyproline assay. Elastin quantification was performed using the ninhydrin assay. Briefly, 50 mg samples were taken from both intact and decellularized porcine lung tissue and solubilized in 0.1M NaOH at 98 °C for 45 minutes. Samples were then centrifuged (3000g, 10 minutes), and the soluble proteins in the supernatant were removed, frozen, and lyophilized. Both the remaining insoluble elastin pellet and the lyophilized soluble proteins from the supernatant were hydrolyzed for 24 hours in 6M HCl at

110°C. These hydrolyzed solutions were lyophilized and then diluted in 2mL of DI water. The insoluble elastin samples were quantified using a ninhydrin assay and the collagen from the soluble protein samples was quantified using a hydroxyproline assay (Sigma). [Pouliot et. al. 2016]

Glycaosamnioglycan (GAG) Quantification

Sulfated GAGs were quantified using an Alcian Blue colorimetric assay described in Frazier et al[77]. Initially 100 mg sections of both intact and decellularized tissue was diced and incubated at 4°C in a 4M guanidine HCL solubilization buffer (with 0.05M NA-Acetate and 2% w/v Triton x-100) for 12 hours. An initial dilution of dye test reagent was made with 100mg of 8Gs Alcian blue powder (Sigma) in 10mL of 0.018 M H_2SO_4. This initial solution was diluted to a working solution 1/100 in 0.018 M H_2SO_4 and Triton X-100 was added so that the final solution had 0.25%. The final solution was centrifuged at 10,000g to remove any insoluble dye particles. 200 uL of the solubilized tissue samples was added to 300 uL of the final dye solution and rigorously vortexed. These tubes were centrifuged (16,000g, 10 mins) at 4°C and then the resulting stained GAG pellet was isolated and dissolved in 500uL of 8M guanidine HCL solution. 300uL of each sample was transferred to a 96 well plate and absorbance was measured at 600 nm using a Biotek plate reader. [Pouliot et. al. 2016]

3.3 Results

Intact vs. Decellularized Lung Tissue

An investigation of the porcine lung tissue before and after decellularization was completed using histology, immunohistochemistry, scanning electron microscopy, dsDNA

quantification, and evaluation of key matrix components to determine the extent of decellularization and to describe the disruptive effects of detergents on the organization of matrix proteins. Slides from intact and decellularized tissue were stained using hemotoxylin and eosin to illustrate the removal of nuclei and most nuclear remnants from the remaining matrix (Fig. 3.2, A). Staining showed a depletion of the immunogenic membrane epitope, α-galactosidase, and is an indicator for the removal of cellular remnants from the matrix (Fig. 3.2, B). Picogreen quantification shows that dsDNA was reduced from 1,239.4 (+/- 62.7) [ng dsDNA/mg Tissue] to 57.4 (+/- 3.52) [ng dsDNA/mg Tissue] as a result of decellularization (Fig. 3.2, C).

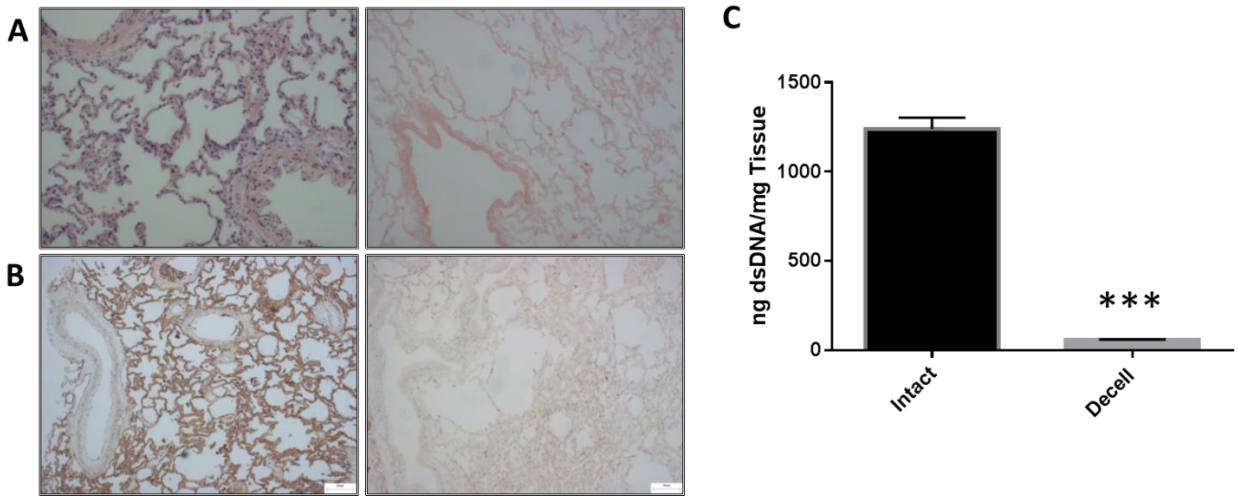

Figure 3.2 Porcine Lung Tissue Decellularization. (A) H&E staining of porcine lung tissue fixed before and after decellularization indicating the removal of most nuclei, (B) α-galactosidase staining shows a reduction of the immunogenic alpha-gal membrane epitope, (C) dsDNA picogreen assay confirmed a 95.3% reduction in double stranded DNA. Data are mean +/- st.dev. n=3 per group. *** $p<0.001$ compared to the intact. Scale bars are 100μm.

A qualitative study comparing intact porcine lung tissue slices to decellularized lung tissue slices shows that the decellularization process preserves many of the structures of the lung. Conserved feature structures include airways, alveolar spaces, and vasculature (Fig. 3.3). Histologic sections stained with Accustain Elastic stain show that elastic fibers are present in the tissue following decellularization but are depleted and much less organized (Fig 3.3 A-C, J-L). [Pouliot et. al. 2016]

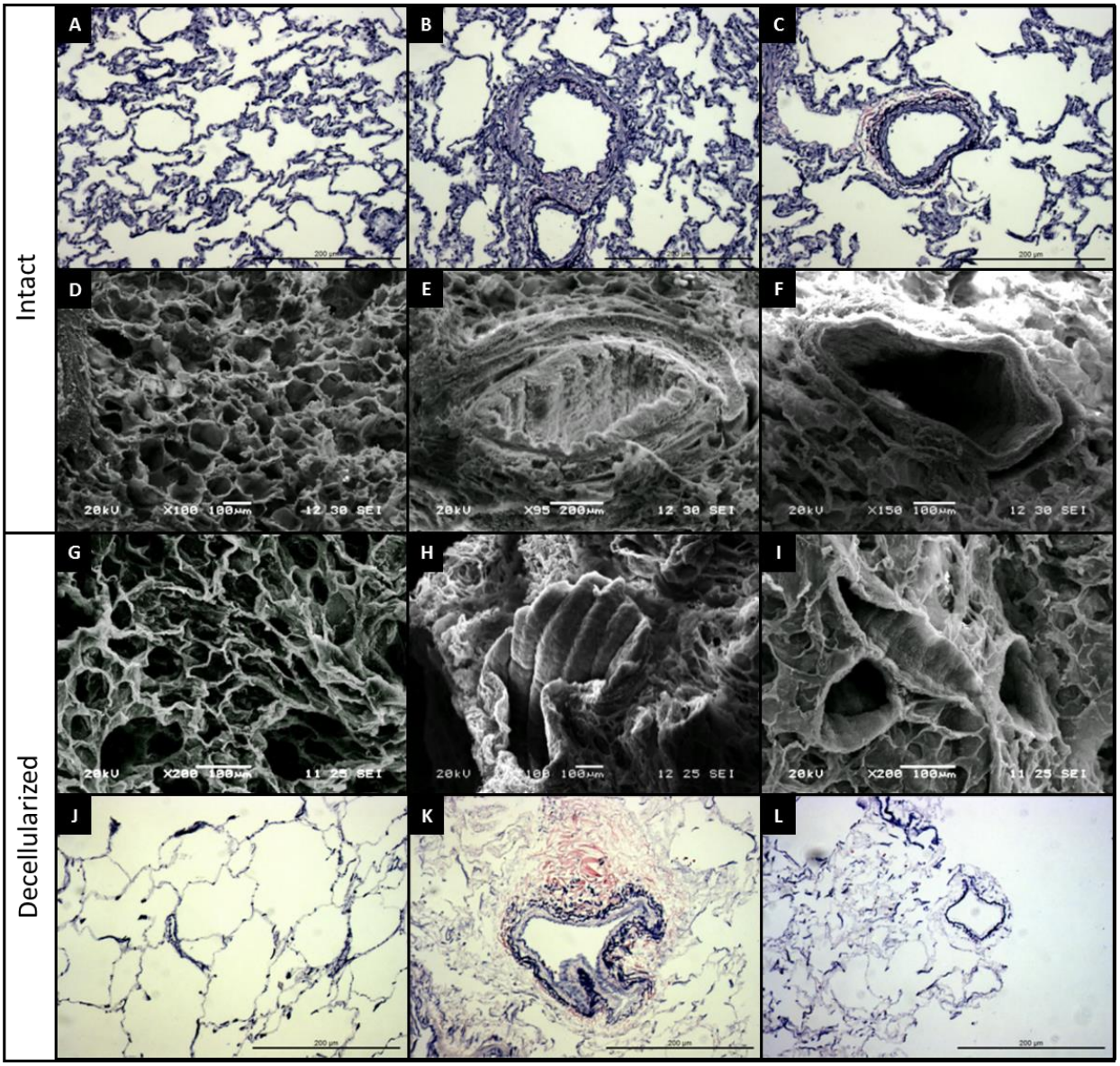

Figure 3.3. Intact vs. Decellularized Lung Tissue Comparison. SEM & Histology images from both intact (A-F) and a decellularized (G-L) lung slices comparing similar structures: first column (A,D,G,J) Alveolar Tissue; second column (B,E,H,K) airway structures; third Column (C,F,I,L) vasculature Structures. Histology samples stained using Accustain Elastic Stain: Black/Dark Purple: Elastic Fibers; Red/Pink: Collagen. Scale bars are 100μm for SEM and 200μm for light images.

Quantification of Matrix Components

Decellularization using detergents is known to reduce the amounts of matrix proteins in the remaining scaffold. We quantified the changes in elastin, collagen, and sulfated glycosaminoglycans (GAGs) and found that there was a significant decrease in all three. Absorbance data was collected for each colorimetric assay and normalized by the intact sample values to show the relative amount that each component is depleted during the decellularization process (Fig. 3.4). [Pouliot et. al. 2016]

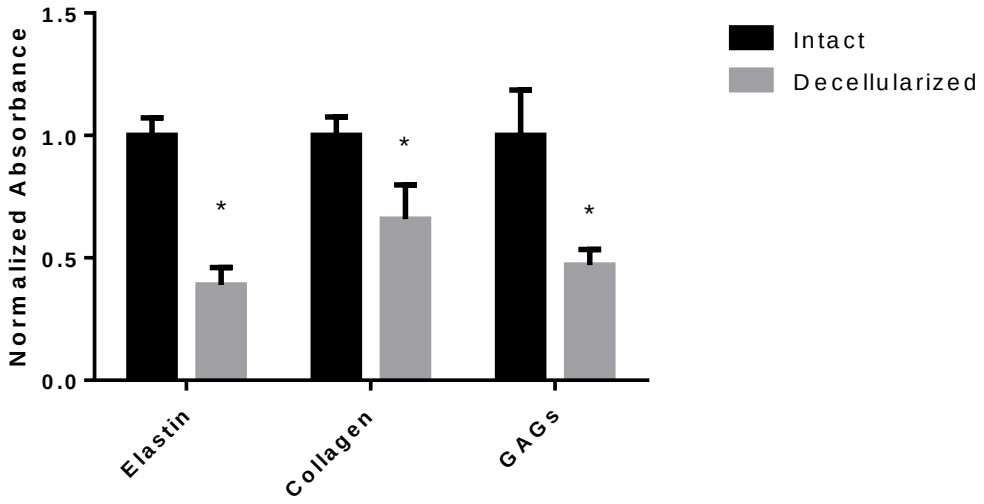

Figure 3.4. Intact vs. Decellularized Matrix Composition. Quantification of major ECM components: elastin, collagen, and GAGs, showing the relative reduction caused by the decellularization process. Data are presented as mean +/- st.dev, n=3-4 per group *$p<0.05$ as measured by t-test.

3.4 Discussion

The sodium deoxycholate/triton approach effectively decellularized porcine lung tissue and conserved many of the important structural components from the native ECM. Staining with hematoxylin and eosin confirmed that a large majority of the nuclear structures were removed and further quantification of total double stranded DNA indicates a 95.7% reduction after decellularization (Fig. 3.2 A, C). Evaluation of remnant nuclear structures or DNA in the scaffold is often used as a primary method for gauging effectiveness of the decellularization regimen used. Development of biomaterials from xenogenic sources is complicated by the presence of immunogenic antigens. One major consideration is the alpha gal epitope, which can result in an acute rejection response without prior depletion of the antigen[63,64]. The alpha gal antibody specifically recognizes the alpha-gal epitope found on the cell surface in the majority of mammals with the exception of Old World monkeys, apes, and humans. In humans a significant 1% of all circulating immunoglobulins are specific for the alpha-gal epitope which can lead to catastrophic failure of xenogenic materials without depletion of the antigen[65]. Comparative DAB staining using a primary antibody for alpha galactosidase before and after decellularization suggests that cell remnants including matrix bound membrane sections, debris, and intracellular proteins were mostly removed and prevented from sequestration in the matrix (Fig. 3.2, B). [Pouliot et. al. 2016]

Every approach for tissue decellularization influences the quantity and quality of extracellular matrix components retained in the acellular framework[48,50,78]. The resulting profile of depleted or damaged matrix proteins plays a major role in determining the ultimate physical properties of the hydrogel and its capacity for supporting cell-matrix interactions [78–80].

Comparison of the elastin and collagen organization in major lung structures pre and post decellularization (Fig. 3.3) hints at the disruptive nature of the deoxycholate/triton approach used. Colorimetric assays confirmed a reduction of key matrix components during the decellularization process including elastin, collagen, and sulfated GAGs (Fig. 3.4 A). The assay also indicates that there are still robust amounts of these matrix components present in the decellularized matrix prior to pepsin digestion. [Pouliot et. al. 2016]

3.5 Conclusions

During this investigation we have validated our decellularization approach in its ability to remove potentially immunogenic components from the matrix including a 95% reduction double stranded dsDNA and as well as removal of the alpha gal epitope from the matrix. We have also characterized the disruption to essential lung structures including their elastic fiber organization and reduction of essential matrix components including elastin, collagen, and glycosaminoglycans. This work represents a firm foundation for further investigations using decellularized porcine lung tissue.

Chapter 4: Production and Characterization of Porcine Lung Derived Extracellular Matrix Hydrogels

4.1 Introduction

The approach used to prepare and solubilize ECM powder derived from decellularized porcine lung matrix was adapted from Freytes et. al. In fact, the overwhelming majority of the ECM hydrogels prepared from decellularized tissue have been prepared using this approach, with only a few investigating changes to the overall protocol. This chapter describes our investigation to thoroughly characterize the resulting pregel solution, including SDS-PAGE analysis of the solubilized protein profile, rheometrical measurements to describe the gelation mechanics and mechanical properties. This also includes SEM image analysis of fiber sizes present in the native and decellularized tissue, compared to the fiber sizes found in the hydrogel. Fiber size and mechanical properties of the gel are important factors which will influence how cells will respond to the hydrogel. Finally, we investigated the ability of the platform to sequester growth factors and other charged therapeutics, using human KGF as a representative target. KGF, also known as FGF-7, is a critical regulator of epithelial cell proliferation in the lung and plays an important role in repair following acute injury[81] which makes it a prime candidate for delivery studies.

4.2 Materials and Methods

Preparation of Porcine Lung Derived ECM Hydrogels

Processing and digestion of the decellularized scaffold into a pre-gel solution were adapted from a protocol for urinary bladder matrix[73]. Frozen tissue sections were lyophilized

using a Flexi-Dry Lyophilizer (FTS Systems) and then milled using a SPEX model 6700 freezer mill. ECM powder was digested in a 0.01M HCl solution with pepsin from porcine gastric mucosa (Sigma-Aldrich) in order to solubilize the ECM components. ECM digestions were run for 48 hours under constant agitation and ended using a 0.1M NaOH and a 10X PBS solutions bringing the pre-gel solution pH to 7.4 (+/- 0.2) and PBS concentration to 1X. The pre-gel solution will self-assemble into a hydrogel at these conditions when incubated at 37 °C. [Pouliot et. al. 2016]

SDS-PAGE Protein Size

Protein lysates were prepared for SDS page from intact porcine lung tissue, decellularized ECM powder, and ECM pre-gel solution (pepsin digested powder) using a 25mM/1%SDS/4.5M Urea solubilization buffer and heating at 60 ° for 1 hour. Lysates were centrifuged (12,000g, 10 minutes) at 4°C and supernatants were sampled for soluble protein levels using a Bicinchoninic Acid (BCA) protein assay (Pierce). BCA values were used to balance protein levels by dilution. 25 uL of each balanced sample was added to 2x Laemmli buffer (Biorad) with 5% 2-mercaptoethanol (Fisher) and heated to 100°C for 5 minutes. Samples were cooled on an ice block before being loaded into an Any-kd Mini-Protean TGX Stain-Free Gel (Biorad) and run. Stain free gels were activated for 45s and imaged using a ChemiDoc Touch imaging system (Biorad). [Pouliot et. al. 2016]

Additional analysis of the protein profile found in the decellularized ECM powder was completed using Image Lab Software (BIORAD, Inc). The standard used for SDS-PAGE, the BIORAD Precision Plus Stain Free STD, was identified by the software in 2 separate lanes. This calibration allows us to identify the molecular weights of the unidentified bands. By isolating the

individual bands in the software we were also able to quantify the relative volume of the protein in each band. This Data will be used to compare identified bands to the predicted molecular weights of major lung matrix components to determine potential proteins that each band might represent. It also allows us to quantify a percentage of the total protein that each band represents.

Scanning Electron Microcopy (SEM) Imaging and Histology

ECM hydrogels were formed from pre-gel solution incubated for 30 minutes before being fixed in glutaraldehyde. After fixation the gels were sectioned and removed from the well using a biopsy punch. Lung tissue slices for imaging were isolated from both intact and decellularized porcine lung tissue and fixed in 4% paraformaldehyde for 48 hours. Samples fixed for SEM imaging were rinsed in PBS and then incubated in 4% osmium tetroxide for an additional hour. After several washes tissue and gel samples were transferred from PBS to an ethanol solution using serial dilutions of ethanol from 25% to 100% incubating for up to 10 minutes between steps. Samples were then critical point dried using an autosamdri-814 critical point dryer (Tousimis) and mounted using conductive adhesive tabs (TED PELLA, inc) for imaging. Samples were plasma sputter coated before imaging with a scanning electron microscope (JEOL 6330F). [Pouliot et. al. 2016]

SEM images of decellularized tissue and ECM hydrogels were captured to characterize average fiber diameter and organizational patterns. The average diameter was determined by measuring the width of the fiber in three locations with approximately equal distribution along the fiber or fiber bundle using Matlab. For the tissue samples, a threshold of 300nm was used to separate fibrils from more organized fiber bundles. [Pouliot et. al. 2016]

Rheometry

Rheometery was used to assess the mechanical properties of the hydrogels. Gel rheometry was completed using an ARG2 rheometer (TA Instruments) with a 20mm parallel plate geometry. ECM digests were completed less than 1 day prior to mechanical testing. An amplitude sweep was conducted for both 8 and 4 [mg/mL] ECM hydrogels to find an acceptable strain range for the experiment. To test the hydrogels 100 [ul] of the pre-gel solution was loaded onto the Peltier plate set at 4°C. The gap distance was then truncated to 300 to enclose the solution between the plate and the geometry. The temperature of the plate was increased from 4 to 37 C° at 5 [°C/min] and then held constant for 15 minutes. The oscillatory modulus of the sample was monitored continuously at a constant 0.1Hz with a strain of 0.5% during the experiment. Samples were subjected to an oscillatory strain, developing a sinusoidal stress, G*, which represents the frequency dependent complex modulus. From G*, G' and G" were determined; where G' is the real part of the complex modulus, the storage modulus, and G" is the imaginary portion of the complex modulus, the loss modulus. [Pouliot et. al. 2016]

Passive Protein Release

An in vitro assay was performed to determine the amount of protein that is passively released from the gel following complete gelation. In a 96-well TC plate 100µL of ECM pre-gel solution was incubated at 37ºC for one hour then gently washed with 200µl 1X PBS which was collected and replaced. PBS was collected from replicate wells at predetermined time points and stored for a Bicinchoninic Acid (BCA) protein assay (Pierce) to determine the amount of protein released from the gel over time. Absorbance values were measured at 562 nm and converted to

protein concentration [μg/mL] using values from the protein standard. Data is presented as total protein [μg] in each sample volume. [Pouliot et. al. 2016]

Loading of Growth Factors – KGF

KGF was loaded into 300 uL ECM pregel samples and incubated to form hydrogels. 200 uL of 1X PBS was added to the formed hydrogels as a simulated environment to facilitate KGF release. The KGF concentrations loaded were 312.5, 625, 1250, 2500, 5000, 10,000, and 20,000 [ng/mL]. The PBS was collected for analysis and replaced at 5 minutes (initial release), and 1, 2, and 5 Days and the samples were analyzed using a KGF DuoSet ELISA kit (RnD Systems, Inc.), the ELISA had 3 plate replicates for each sample. The mass of KGF released from each gel was calculated by multiplying the concentration released by the PBS collected, 200 uL, and summed to get total KGF release over time.

4.3 Results

SDS-PAGE

Protein lysates from intact tissue, decellularized tissue powder, and pepsin digested ECM pre-gel solution were run on a wide band SDS-PAGE gel to separate proteins by size (Fig. 4.1). Intact tissue has the most bands as it includes both extracellular and intracellular matrix proteins. Decellularized matrix powder also has a significant number of distinct bands representing the spectrum of remaining extracellular matrix proteins following decellularization and processing. Pepsin is a fairly non-specific protein enzyme and will act between any two unshielded amino acids responsible for the SDS-PAGE size distribution. Most of the largest proteins have been segmented and represented in the smaller bands. The non-specific nature of pepsin also leads to a "smear" of protein sizes outside of the clear banding. [Pouliot et. al. 2016]

A table describing the predicted bands for several essential proteins that should be present in the lung matrix has been added to Figure 4.1. Additionally, the BIORAD, image lab software has allowed for the determination of relative molecular weight and volume of each of the bands. With this information we were able to identify some of the potential proteins present in the bands as well as their quantity relative to the other measured bands. This information has been tabulated in table 4.1.

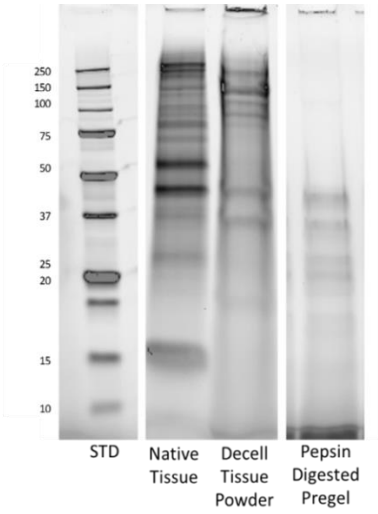

Potential Lung Matrix Proteins		
Protein	**Size**	**Source**
Collagen 1	250; 125-135	human kidney tissue
Collagen 3	140-150	mouse pancreas
Collagen 4	50	mouse heart
Fibroectin	250; 100; 70	NIH T3T Cells
Laminin	70; 35 - 32	Human Heart Tissue
Vitronectin	87-72	human serum
Tenacin-C	250-260	abcam (predicted)
Versican	70	human aorta
Decorin	46-48	BxPC-3 Cells
Nidogen-1	136	human placenta
Perlecan	350;240;105	COLO 320 Cells

Figure 4.1. **Intact Vs. Decell vs. Pregel SDS-PAGE.** This gel shows how protein size and distribution change as tissue is processed to a powder and further digested into a pre-gel solution. The table attached lists the predicted size of some of the essential matrix components found in Lung Tissue.

Band	Description	Mol. Wt. (KDa)	Volume (Int)	Percent of Measured	Potential Proteins
1	Several Bands	250.0	1.27E+07	5.9	Collagen 1, Fibronectin, Tanscin-C
2	Several Bands	192.1	3.04E+07	14.1	
3		137.5	1.70E+07	7.9	Collagen 3
4	Think Band	118.8	7.87E+07	36.6	Collagen 1
5		101.8	1.99E+07	9.3	Fibronectin
6		83.9	8.55E+06	4.0	Vitronectin, Versican
7	faint	61.0	7.32E+05	0.3	Collagen 4, Decorin
8	faint	46.7	1.97E+06	0.9	
9	faint	40.6	2.33E+06	1.1	
10		32.7	1.11E+07	5.2	laminin
11		18.4	7.04E+06	3.3	
12		13.9	2.46E+07	11.5	

Table 4.1 Major Bands from Lung Derived ECM Powder. This table lists the major bands identified from the solubilized lung derived ECM powder. The molecular weight and intensity volume of each band have been calculated using the BIORAD Image Lab software. Potential proteins present in each band have been identified using the table in Figure 4.1

Fiber Size and Organization

While the ECM hydrogel lacks the highly organized matrix formations of collagen bundles seen in the decellularized tissue, it does have comparable fiber size to those found in the tissue. SEM imaging was used to evaluate ECM fibrils and fiber bundles in the hydrogel and in the tissue (Fig. 4.2, A-C). Measurement of fibrils found in the decellularized tissue and in the fixed hydrogels (<300 nm) found no significant difference between the groups, 138.03 ± 25.96 nm (tissue) and 87.104 ± 13.77 nm (hydrogels). The more organized fiber bundles (>300 nm), found only in the decellularized tissue sections, were determined to have an average thickness of 974.97 ± 81.33 nm, and were significantly different from both of the fibril groups. [Pouliot et. al. 2016]

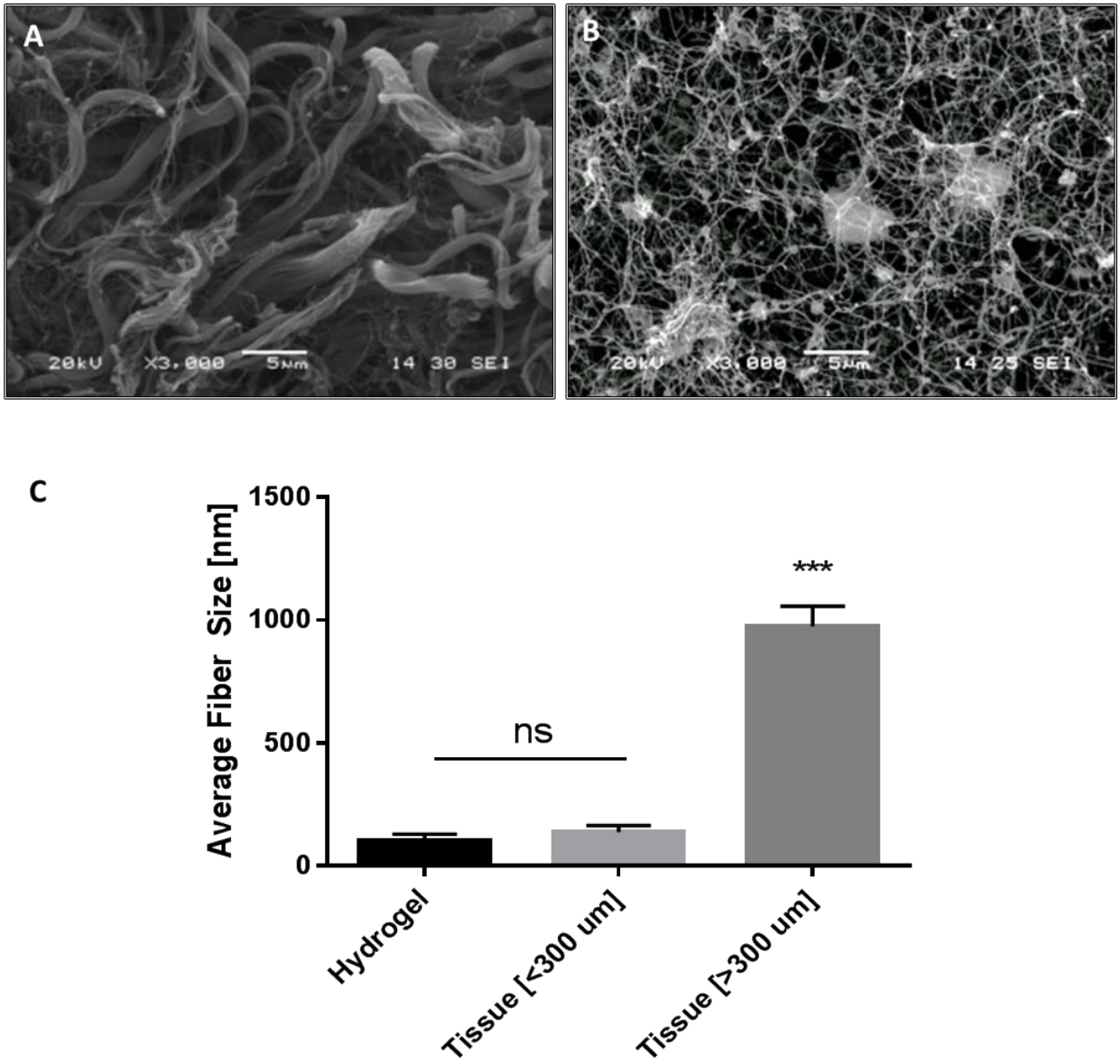

Figure 4.2 Fiber Size Comparison: Decellularized Lung Tissue vs. Lung ECM Hydrogel. SEM of (A) pig lung tissue after decellularization and (B) a pig lung derived ECM hydrogel. (C) Quantification of average fiber size found in each set of samples, measured using Matlab image processing. While fiber bundles in the tissue samples are much larger, the small fibers (<300 nm) are more similar to those found in the hydrogel. *** $P<0.0001$ for comparison to both the hydrogel and tissue small fiber size groups. n = 3-5 for all groups. SEM scale bars are 5µm.

Rheometry

A preliminary amplitude sweep was conducted to determine the acceptable strain range to test our material within the linear viscoelastic region (Fig. 4.3, A). This range was found to be between 0.1 and 1% strain for our samples; 0.5% was used for the experiments. The rheological properties of pig lung ECM hydrogels at 8 & 4 [mg/ml] were examined during a temperature ramp and both the storage modulus (G') and loss modulus (G") were found to increase as the pre-gel liquid solution self-assembled into a gel (Fig. 4.3, B, C). Results were compared to ECM hydrogels derived from other tissues (Table 4.2). The measurements taken during a temperature ramp 4°C to 37°C at 3°C increments show that the self-assembly mechanism of the pre-gel solution start around 35°C and that the majority of the mechanical change related to the gelation occur shortly after the gel reaches physiologic body temperature of 37°C. The strain used to test the hydrogels was found to have a significant impact on the results.

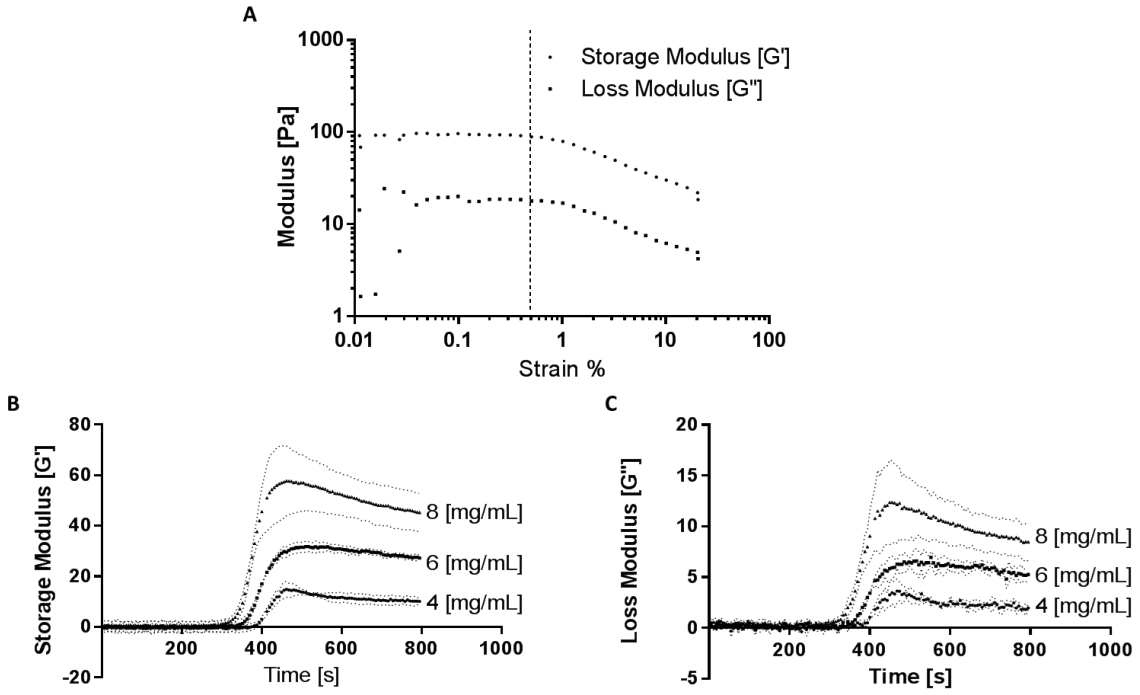

Figure 4.3 Gelation Kinetics and Material Mechanics of ECM Hydrogels. (A) Representative amplitude sweep for an 8 [mg/mL] ECM hydrogel from 0.01% to 20% strain (B) Storage modulus and (C) Loss modulus at the temperature is ramped from 4 to 37°C and then held constant. Rapid self-assembly takes place as the material approaches 37°C with the majority of gelation occurring within 3 minutes. Data are mean +/- st.dev. n=3 per group.

Rheometry experiments conducted using 5% strain resulted in irreversible deformation of the ECM hydrogels at 8 and 4 [mg/mL] and significantly lower modulus values as the temperature was ramped to induce gelation (Fig. 4.4 A, B). Testing on similar materials derived from other sources used a range of testing conditions, including different strains, which could be partially responsible for the large spectrum of mechanical properties amongst published results (Table 4.2). [Pouliot et. al. 2016]

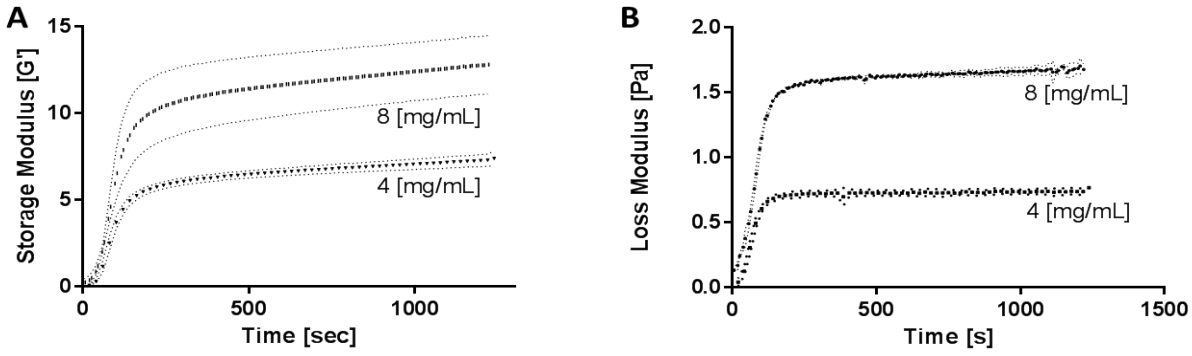

Figure 4.4. Gelation Kinetics and Mechanics under 5% strain (A) Storage modulus and (B) Loss modulus at the temperature is ramped from 4 to 37°C and then held constant using a strain of 5%. Samples at this strain are irreversibly damaged, they still exhibit self-assembly behavior,

but measurements are not representative of the hydrogels mechanical properties. Data are mean +/- st.dev. n=3 per group.

Material	Concentration	Storage Modulus [Pa]	SD	Reference
Lung	8 [mg/ml]	59.02	± 13.53	
	6 [mg/ml]	32.02	± 1.87	
	4 [mg/ml]	15.27	± 2.87	
Adipose	4 to 12 [mg/ml]	10 to 15		*Young et al. Acta Biomat. 2011*
Cardiac	8 [mg/ml]	9.52	± 3.77	*Johnson et al. Nanotech. 2011*
	6 [mg/ml]	5.28	± 0.41	
Dermis	8 [mg/ml]	466.5	± 64.3	
UBM	8 [mg/ml]	143.8, 182.2	± 84.1, ± 36.5	*Medberry et al. Biomat. 2013/ Wolf et al. Biomat. 2012*
	4 [mg/ml]	11.43	± 4.9	
Brain	8 [mg/ml]	61.8	± 11	*Medberry et al. Biomat. 2013*
	4 [mg/ml]	20.3	± 16.0	
SC-ECM	8 [mg/ml]	757	± 74.9	*Medberry et al. Biomat. 2013*
	4 [mg/ml]	138.5	± 33.8	

Table 4.2 Rheometrical Properties for Tissue Derived ECM Hydrogels in the Literature

Passive Protein Release

Proteins passively released from the material could have a significant effect in addition to the actual degradation products of the hydrogel *in vivo*. During our investigation we found that there is a significant amount of non-soluble or non-assembled protein that is initially trapped during gelation but quickly released into the milieu. Using 1X PBS to collect these proteins over time we determined that measurable passive protein loss occurs over 14 days, with the maximum protein release occurring within the first 48 hours after gelation (Fig. 4.5, A). Comparison of hydrogels directly following gelation and after 14 days of protein release using SEM yields an observable difference in the quantity and organization of proteins in the hydrogel network (Fig. 4.5, B) There was also a visual difference in the density of non-integrated proteins from day 1 to day 14 which suggests that much of the measured protein release could have been diffusion from the hydrogel. [Pouliot et. al. 2016]

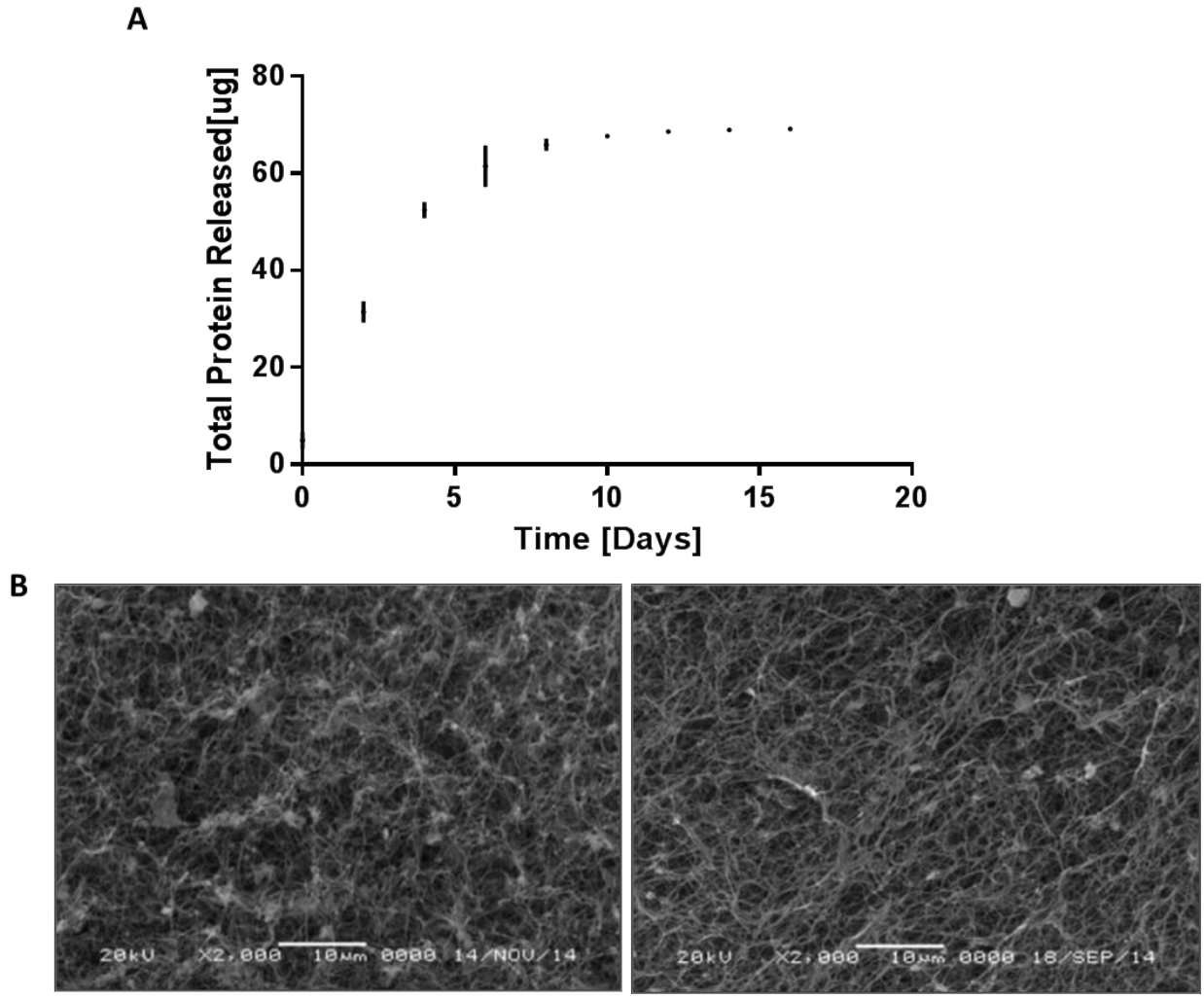

Figure 4.5. Passive Release of protein from Hydrogels. (A) Protein release from hydrogels based on BCA Analysis of PBS supernatant, most protein loss occurs before day 8, data are mean +/- st.dev. n=3 per group; (B) SEM comparison images from hydrogels fixed at Day 1 compared to those fixed at day 14. Scale bars are 10 μm.

Loading of Growth Factors – KGF

The ability to sequester growth factors could become an impactful functionality of the ECM hydrogel platform. During our investigation we loaded ECM pregel samples with several

concentrations of KGF before incubation. PBS was used as a medium to simulate the environment and a KGF ELISA kit was used to measure KGF release form each of the samples, which was converted to grams and presented as total release over time as shown in figure 4.6, A. The data shows that there is a similar proportionality in the higher loaded concentrations (5k +) that is not seen as much in the lower samples. The percentage of protein that was released from each gel is available in table 4.3. The trend is that more KGF can be released, as a percentage of the loaded amount, at those higher concentrations.

KGF Conc. [ng/mL]	Total KGF Loaded [ng] in each 300 uL gel	Summed Protein Release [ng]	Percent KGF Released
20000	6000	332.2	5.54
10000	3000	185.2	6.17
5000	1500	77.7	5.18
2500	750	17.0	2.27
1250	375	5.9	1.58
625	187.5	4.9	2.61
312.5	93.75	0.7	0.73

Table 4.3. KGF Loading. This table tabulates the starting concentration, total KGF loaded per gel, the total amount [ug] of protein released over 5 days, and the percentage of the total protein released. At higher concentrations the percentage of KGF released from each gel is relatively consistent, which is not the case for the lower values released from the bottom 4 samples.

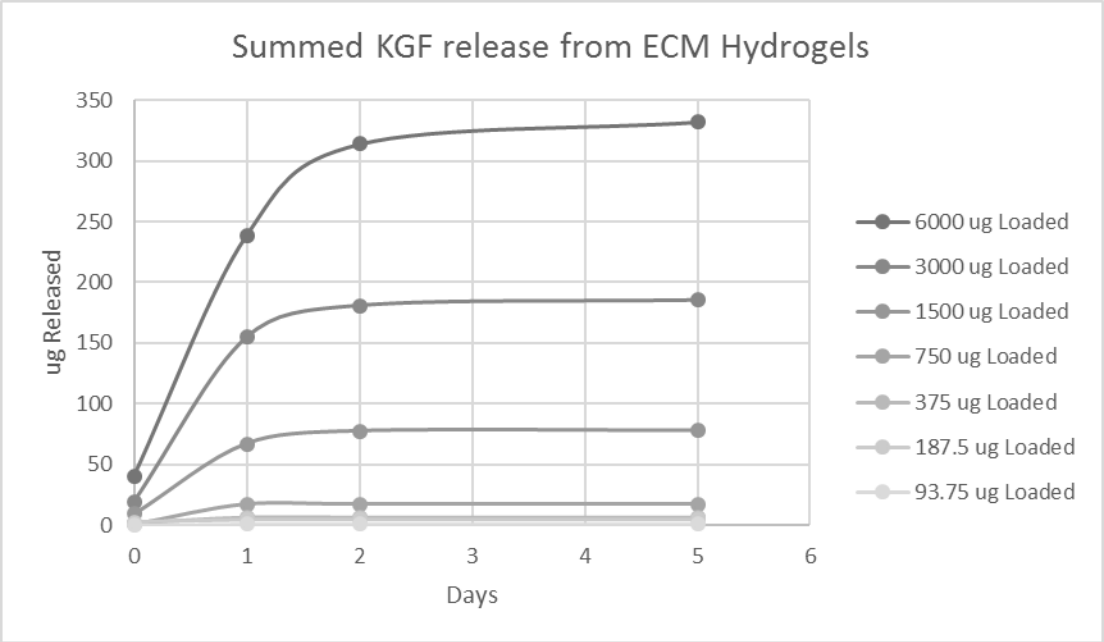

Figure 4.6 Release of Loaded KGF from ECM Hydrogels. KGF released from loaded hydrogels was quantified using ELISA, (A) shows the release from 7 individual gels loaded with concentrations of KGF from 312.5 to 20,000 ng/mL. Concentration measured in the release samples was converted to mass release and presented as total release over time (n=3, plate replicates).

4.4 Discussion

The changes in the profile and size distribution of proteins resulting from decellularization, processing, and digestion are evident in the SDS-PAGE data presented in Figure 4.1. There are distinct matrix components input into the pepsin digestion. However, due to the unspecific cleavage it is difficult to determine the state of each of these components following digestion in the pre-gel. This unspecific cleavage of the pepsin digestion makes it difficult to apply traditional matrix quantification and mass spec approaches to the pre-gel solution. The lyophilization, milling, and digestion to transform the acellular matrix into a hydrogel results in the reduction of highly organized extracellular matrix structures, bundles, and

fibers into a less dense and more randomly organized material (Fig. 4.2). A quantification of fiber sizes revealed that the organized fiber bundles were much more prevalent in the decellularized tissue. The fibers measured in the hydrogel sample were much thinner with less variance suggesting that proteins from the tissue had been reduced to subunits during the digestion and then reassembled during gelation. [Pouliot et. al. 2016]

Solid tissue engineering scaffolds are appropriate for addressing tissue engineering needs in tissues with a static mechanical environment. They are, however, much less applicable in tissues that undergo complex deformation such as the heart or lungs. The deformability of hydrogels can prevent damage to the native tissue under strain while protecting encapsulated cells or drugs. The novel lung ECM hydrogels we have developed have mechanical properties comparable to similar scaffolds (Table 4.2). In general the shear modulus of soft tissues are significantly higher than what we have determined for lung derived hydrogels [82]. However, for a therapeutic delivery vehicle, the ability to maintain cells or drugs at target locations in the tissue is more important than a perfect match with native the tissue mechanics. [Pouliot et. al. 2016]

The gelation behavior of the hydrogel contributes to the practicality of the hydrogel system, especially for use in injectable delivery. We determined that our lung derived hydrogel shows little to no gelation activity until the temperature of the material exceeds 32 °C, the pre-gel solution then completely self assembles in 3 minutes once the material reaches 37 °C (Fig. 4.3). This can potentially allow drugs or cells to be delivered in an injectable liquid solution, encapsulating the payload once the solution reaches the target tissue. For an intratracheal delivery, the goal would be to deliver the pre-gel solution to the alveolar spaces before gelation

to reduce the chances that airways are obstructed. Studies using ECM gels derived from other tissues suggest that the mechanical properties and gelation time can be directed by modifying the starting temperature, protein concentration, pH, or ion concentration[56,83] which could be tailored using our model to ensure that the majority of the solution reaches the alveolar spaces before gelation. [Pouliot et. al. 2016]

A comparison of the published rheometry data for other tissue derived ECM hydrogels revealed a large variation in the experimental methods and conditions used. We have demonstrated that there is a significant difference in the modulus found using strains of 0.5 and 5%. We attribute this difference to the larger strain being outside of the linear viscoelastic (LVE) region as determined by an amplitude sweep. While 5% strain could be in the LVE region for some of the more robust materials derived from highly collagenous tissues such as bladder, dermis, and spinal cord, it is possible that such a large strain irreversibly damages hydrogel samples during the first rheometric measurements. [Pouliot et. al. 2016]

Degradation products of previously described ECM biomaterials have been found to have additional beneficial functions including antibacterial properties [84] and chemo attractant promoting cell taxis [85]. In this study, our analysis of the passive release profile of the hydrogel revealed that a large amount of protein can be collected in the wash immediately after complete gelation, and that the majority of protein release happens within the first 48 hours (Fig. 4.5, A). This suggests that not all constituents of the pre-gel solution are involved in self-assembly of the hydrogel and that possibly not all of the isolated protein been solubilized with our current digestion protocol. While it is not clear that proteins passively released from a lung derived

hydrogel are beneficial they have not been found to be cytotoxic in preliminary in vitro experiments or in the acute in vivo model. [Pouliot et. al. 2016]

The functionality of being able to sequester and delivery growth factors as a therapeutic or as a guide for progenitor differentiation is a major augmentation to the hydrogel platform we have developed. The KGF loading results shows that lung derived ECM hydrogels sequester KGF in a concentration dependent manner as shown in Figure 4.6, A. The higher concentrations (5k, 10k, 20k [ng/mL]) release a similar percentage, between 25 and 30% of the KGF that was loaded, while the lower concentrations release less overall as shown in table 4.3. The difference between the highest three concentrations and the lower four are either because the loaded KGF in these samples has a higher affinity to the matrix, which would make sense if there were more binding sites available in these gels, the other explanation is that the ELISA could not accurately measure KGF at these levels. I suggest that both of these could play a role in the results. It is likely that remodeling and degradation of the ECM hydrogel by immune cells would lead to an increase in the KGF released in vivo. KGF has previously been sequestered in fibrin gels by attaching a matrix binding peptide to the growth factor[86]. This augmentation was able to increase KGF loading in the gel to control release of the growth factor from 90% in 24 hours, to 15%. Controlled release is beneficial for KGF because it has a short unbound half-life[86].

4.5 Conclusions

We have successfully demonstrated that decellularized lung tissue can be processed and digested to create a smart material which is liquid at room temperature, but undergoes self-assembly into a hydrogel as the environment approaches 37 °C. During this study we have

thoroughly characterized the composition, structure, gelation kinetics, mechanical properties, and protein release behavior of the material. Additionally, we have confirmed an additional functionality of the hydrogel platform, finding that growth factors can be sequestered in the pregel solution. We have characterized the concentration dependent release of KGF from the hydrogel and found that the protein can retain at least 70% of the loaded KGF over 5 days. These findings support the use of this material for a feasibility investigation for cell and drug delivery.

Chapter 5: Encapsulation of hMSCs and demonstration of ECM hydrogel feasibility for Cell and Drug Delivery

5.1 Introduction

One of the major goals of this research has been to demonstrate that ECM hydrogels are a feasible platform as a delivery vehicle for cell and drug delivery. This chapter describes our investigation into this subject. The essential starting point was determining if hMSCs can be successfully encapsulated inside of ECM hydrogel, and remain viable; while maintaining their phenotype. This is important because we want encapsulated hMSCs to continue to be able to sense and respond to the inflammatory environment when delivered in the hydrogels. From there we investigated both sides of the activation/secretion question, looking into if cells can be activated by factors outside of the hydrogel, and also if secreted factors could escape from the hydrogel. This capability is essential in order for delivered cells to be able to respond to and modulate a chronic inflammatory environment. Specifically, we wanted to see how these encapsulated cells would respond to a simulated environment in which TNF-alpha is abundant, like in COPD (REF). Another feasibility question that we addressed is whether or not injected hydrogels would cause significant immune response and polarization of immune cells. Finally, an in vivo dosing trial was completed to see if ECM hydrogels did in fact increase retention of delivered cells in the tissue.

5.2 Materials and Methods

In vitro Cell Culture

All *in vitro* cell studies were completed using human bone marrow derived mesenchymal stem cells (hMSCs) obtained from Rooster Bio, Inc. Cells were defrosted and expanded in culture in enriched basal medium (RoosterBio) which was changed every 2-3 days. When cells were 80 – 90% confluent they were trypsinized, counted, and plated for attachment and encapsulation experiments. Cells used for these experiments were from the first three passages and quantification experiments were performed using a Quant-iT™ PicoGreen® dsDNA Assay Kit (Life Technologies). Background levels of dsDNA sequestered in the ECM material were normalized for using non-cell controls for protein coatings and gel encapsulation. These background values were subtracted so that only dsDNA from cultured cells is represented in the data. [Pouliot et. al. 2016]

Encapsulated Cell Viability

Viability of hMSCs encapsulated in formed ECM hydrogels was evaluated over 48 hours. hMSCs were suspended at $3*10^4$ [cells/gel] at four concentrations: 2, 4, 6, and 8 [mg/mL]. The solutions were plated into 96 well plates in triplicate and incubated for 30 minutes to form 500 [μm] thick hydrogels. Following gelation, 100μL of media was carefully added to each well. After 2 days the media was aspirated and samples were digested in papain digestion solution overnight at 65 °C. Double stranded DNA was quantified using a picogreen assay as previously described. [Pouliot et. al. 2016]

Encapsulated hMSC Live/Dead Staining

A Live/Dead viability kit (Invitrogen) was used to visualize the performance of encapsulated hMSCs over time. In a 96 well clear TC plate hMSCs were encapsulated in pre-gel solution at a density of 10,000 cells/well. The plate was incubated for 30 minutes to form 500µm thick hydrogels and 100µL of hMSC media was added to each well. The Live/Dead staining components were defrosted and added to 1X PBS to make a solution with 2µM calcien AM (green, Live) and 4µM EthD-1 (red, Dead). The media was first aspirated and 100µL of Live/Dead staining solution was added to each well and incubated at room temperature for 30 minutes. The plate was then imaged using an Olympus IX71 Microscope using fluorescent light source and FITC (~490 nm, Live) and TRITC (~530 nm, Dead) filters. Images taken using each filter were colored and merged using FIJI to create Live/Dead composite images. Image quantification and cell counting was performed with NIH Image J on a minimum of 3 fields per sample. [Pouliot et. al. 2016]

QPCR Gene expression Analysis

The gene expression values obtained from all of the QPCR experiments performed was determined using the delta delta Cq (sometimes called Ct) approach commonly used in the literature. Briefly, the average of the Cq values was taken for the housekeeping gene and the gene of interest, for both the control group (plate control, or non-activated control depending on experiment) and the experimental group(s). The housekeeping gene average Cq value is subtracted from the experimental gene Cq for the control and each experimental group. The purpose of this first calculation, ΔCq, is as another control for the amount of cDNA loaded. The housekeeping gene is supposed to be a gene that has little change in expression no matter what,

the outcome of this operation is an additional control for loading errors, normalizing Cq values so that they represent the same relative number of cells. The second operation, ΔΔCq, is to take the ΔCg for the control group, and subtract it from the ΔCq from the experimental groups. The fold change can be calculated from these ΔΔCq values for each group using $2^{\wedge-}$ΔΔCt. Using the experimental replicates, you can determine average fold change for determining statistically significant differences between the control group and the experimental groups. There is some controversy over the presentation of standard deviation with this data due to manipulation of the data leading to these values, it has been argued that these calculations are not representative of the source signals due to the data manipulation. We have presented the standard deviation here because it still depicts useful information on the variance of fold change within each group.

Gene Expression of Encapsulated hMSCs

Gene Expression was performed using a CFX Connect real-time PCR machine (Biorad) to determine gene expression changes in MSCs when encapsulated in ECM hydrogels. hMSCs (~100k cells/well) were either encapsulated in 300uL ECM hydrogels or seeded onto TC plastic in 6 well plates. At 3 and 7-day time points RNA was collected and purified using a Qiagen RNeasy kit. RNA concentrations were balanced using nuclease free water and converted to cDNA using a high capacity cDNA reverse transcription kit (Applied Biosystems). Following conversion, the cDNA was probed using primers for Thy1, Sox2, and Oct4, with 18s as a housekeeping gene using SybrGreen (Applied Biosystems). Fold change for each experimental group is reported in reference to the 3-day plate control. [Pouliot et. al. 2016]

Scratch Assay

A scratch assay was performed to investigate the ability of hMSCs to modulate a simulated wound environment while encapsulated inside ECM hydrogels. For this experiment we used BEAS-2B cells for our confluent epithelial layer. BEAS-2B cells are a commercially available cell line (Lonza) that was derived from normal human bronchial epithelium. BEAS-2B cells were plated in 200 uL of BEGM (Lonza) media, at 50,000 cell/well, in a 48 well TC plate. Plates at this density these cells take 2 days to reach confluency appropriate for a scratch assay, media was changed 1 day after initial plating to remove unattached cells. At the same time the experimental and control conditioning wells were plated, these groups included an unconditioned media control, hMSCs plated at 50,000 cells/well in 48 well plates, and hMSCs encapsulated in 50 uL of pregel solution at 50,000 cells/well. After 24 hours the hMSC media plated on the experimental hMSC groups was replaced with conditioning media which includes both BEBM and BEGM conditioning groups (n=3 for each conditioning group). This media was conditioned by the plate control and encapsulated hMSCs for 24 additional hours.

At 2 days the media has been conditioned and the epithelial BEAS-2B cell layer should be confluent. A black permanent lab marker is used to draw a reference line horizontally across the middle of each row in the scratch plate. Each well of the BEAS-2B plate was scratched using a sterile 200 uL pipette tip, lining the plate cover up down the middle of each lane to use as a physical guide to keep the tip straight. The goal of the scratch procedure is to maintain a steady pressure along the whole length, without pushing into the well, just enough to remove the cell layer. After all of the wells have been scratched the existing BEGM media is used to rinse the plates to remove unattached cells and then aspirated. The conditioning media groups are then added to the scratch wells to start the scratch assay; this is time 0. The assay is imaged using a

black and white camera attached to an Olympus IX71 Microscope, at 4x magnification, each well is imaged at each time point. For continuity, the frame is oriented so that the black reference line is at the very bottom, and so the scratch in the well is in the middle of the image. The assay was imaged at 0, 12, 24, 36, 48, and 60 hr time points.

Images from this assay were stacked using image J, creating one image file for each well encompassing all six of the time points. The scale was set in the software using the scale bars that were burned into each image (200 um = 124 pixels). Each image stack was analyzed using the MRI wound healing tool plugin. This tool uses variance in image pixels to find the edges of the scratch and draw a mostly accurate border on each image, this border can be measured for all of the time points on each well to get a scratch area for each time point. Occasionally the MRI tool was not able to accurately draw parts of the scratch due to shadows or other obscuring irregularities on the raw images. These borders were manually corrected using the selection tool in Image J. Data from each well was averaged for each group and presented as percentage of scratch closed, using:

$$Closure = (Scratch_i - Scratch_x)/Scratch_i$$

Where "i" is the initial area, and "x" is the time point of interest

A more thorough description of how to manipulate and analyze scratch assay images using Image J and additional plugins has been added in Appendix B.

Activation of Encapsulated hMSCs with LPS and TNF-alpha

In order to investigate whether hMSCs encapsulated within ECM hydrogels can sense and respond to stimulating factors in the milieu an activation experiment was conducted. Cells were activated by incubation with normal hMSC growth media (Rooster Bio) that included either

200 ng/mL Lipopolysaccharide (LPS) or 50 ng/mL TNF-alpha. hMSCs were plated at 100,000 cells/well in 6 well TC plates, in four groups: (1) plate control, (2) plate activation, (3) gel control, and (4) gel activation. The gel groups used previously described methods to suspend the cell pellets in 300 uL of pregel/well; which were allowed to incubate for 30 minutes before growth media was added. After 24 hours of incubation the normal growth media was aspirated and replaced with serum free hMSC media which included the activating LPS or TNF-alpha. After 24 hours of activation the media was aspirated and RNA was collected as previously described. RNA form the samples was balanced to ~21.6 ng RNA/uL and converted to cDNA as previously described. The LPS and TNF-alpha cDNA were run in separate QPCR plates. The primers used for the LPS assay included the primers for inflammatory mediators IL-6 and IL-8 as well as primers for growth factors including keratinocyte growth factor KGF (FGF-7), hepatocyte growth factor (HGF), and vascular endothelial growth factor (VEGF). The same primers were used for the TNF-alpha activation, with the addition of tissue necrosis factor stimulated gene 6 (TSG-6) to the inflammatory mediator group. Plates were run using a CFX-Connect RT-QPCR (BIORAD) as previously described and gene expression data was processed using the non-activated gel control as the reference.

Comparing M0 macrophage activation on ECM hydrogels to M0, M1 and M2 Macrophages

Gene expression was also used for the approach to determining naïve macrophage activation on ECM hydrogels. Naïve bone marrow macrophages were isolated from C57BL/6 mice. The cell suspension isolated from the bone marrow was plated and macrophage colony stimulating factor (MSCF) was used to isolate naïve macrophages. This method was previously validated using flow cytometry in our laboratory. Established methods were used to get control

data for phenotypic gene expression, using LPS doped media for M1 macrophages and TNF-alpha for M2 macrophages. For the experimental group, 300 uL/well ECM hydrogels were plated in a 6 well plate and allowed to gel as previously described. Following gelation naïve macrophages were plated onto the gels at a concentration of 1 x 10^6 cells/well. After 24 hours incubation the RNA was collected, balanced to the M0, M1, and M2 RNA at 30 ng/uL and converted to cDNA. Gene expression was determined using QPCR as previously described with primers for both phenotypic markers: NOS2 (M1), Fizz1 (M2), Manose Receptor (M2), and YM1 (M2); and inflammatory mediators: IL-6, TNF-alpha, and IL-10. Fold change was calculated using naïve macrophage (M0) gene expression as the reference.

In vivo studies

To examine whether the lung ECM hydrogels enable initial lung delivery and retention of MSCs following administration intracheally, a feasibility study was performed in a rat model of emphysema. Emphysema was induced in male Sprague-Dawley rats weighing 250-300g with an orotracheal solution spray instillation (0.2 ml) of porcine pancreatic elastase (PPE, Elastin Products) at 240U/kg. On day 21, an impaired cardiopulmonary functionality was confirmed with a reduced exercise endurance on the treadmill according to the training and testing protocol established previously in-house [87]. Like our previous study[46], emphysematous rats ran for only 9.85 ± 5.04 min in average, compared to 47.6 ± 3.8 min in healthy animals. On day 22, rats received an orotracheal solution instillation (0.1 ml) of 1 x 10^6 rat GFP-labeled bone-marrow derived MSCs (passage 3-5; Cyagen) with or without 4 mg/mL pre-gel porcine lung ECM hydrogel solution. At 24h, rats were euthanized by exsanguination under sodium pentobarbital (i.p.;. 50 mg/kg), and lungs were inflated with 4 % low-melting point agarose solution introduced

at 20 cmH_2O hydrostatic pressure. After placing in ice for 5 min, the lungs were fixed with 10% formalin, paraffin embedded, sectioned to 5 micron thick slices, and mounted on slides. For visualization of the rat GFP positive MSCs, rat lung sections were deparaffinized in xylenes and rehydrated in a series of graded ethanol. Following blocking with 5% goat serum (Cell signaling), the slides were incubated for overnight at 4°C with a rabbit antibody to GFP (1:100; SC-8334 Santa Cruz;), followed by another 1h incubation with Alexa Fluor 594-conjugated anti-rabbit antibody (1:1000; FisherSci) at room temperature. The slides were mounted in a Prolong Gold Antifade reagent with DAPI (ThemoFisher) and imaged on Olympus fluorescent microscope. Counts of GFP positive cells were performed using NIH Image J. Ten field images were taken per rat and three rats were used per treatment group. [Pouliot et. al. 2016]

The elastase treatment was an effective approach for modeling the matrix depletion and inflammatory environment of clinical emphysema. Using this approach allowed us to avoid the much more time consuming and expensive methods used to induce emphysema through cigarette smoke inhalation. Cell retention was compared at 24 hours post inoculation to allow us to determine the significant difference in cell retention related to our approach.

The green fluorescent protein has an excitation range between 350 – 450 nm and has a fluorescent emission between 500 – 550 nm. Lung tissue autoflourescence occurs in this same excitation and emission range so it obscures the signal from the protein. To get around this, the GFP positive cells had to be visualized using a GFP-primary antibody and a secondary antibody, Alexaflour 594. This allowed us to visualize the protein in the cells without the interference from the tissue autoflourescence, which was very important in identifying positively stained cells. This works because the secondary antibody is excited at ~590 nm so it can be visualized with the TRITC channel, which has an excitation range between ~500 - 600 nm.

Myloperoxidase Assay

Myeloperoxidase (MPO) activity in each group of animals was quantified as a measure of lung tissue neutrophil accumulation using an approach developed by Goldblum et al.[88] and modified by Sakagami et al[87]. The groups included healthy animals, positive elastase control, elastase treated animals dosed with rMSCs only, and elastase animals dosed with rMSCs in ECM pre-gel solution. Briefly, 100mg of rat lung tissue was homogenized in 0.5mL 0.02M EDTA (pH4.7) and brought to 0.75mL with additional EDTA. After centrifugation (12,000g, 15 min) at 4°C the supernatant was discarded and the tissue was re-homogenized in 0.5mL in 0.5% hexadecyltrimethyl ammonium bromide (HTAB). After another centrifugation (12,000g, 15 min) at 4°C, the supernatant was collected and saved. 10uL of each supernatant was added to a 96 well plate in triplicate and 190uL of test solution (0.17mg/mL O-dianisidine dihydrochloride and 0.0005% H_2O_2) was added to the wells. Immediately after adding the test buffer the plate was read using a Biotek Synergy 2 plate reader at an absorbance of 405 nm every minute for 5 minutes. The change in absorbance was normalized with the BCA protein levels found in each supernatant, data is reported as $\Delta ABS_{5\ min}$ / μg protein. [Pouliot et. al. 2016]

Statistical Analysis

All quantitative hydrogel characterization and in vitro experimental studies were performed with a minimum of n=3 in triplicate. In vivo treatment studies were performed with n=3 rats per treatment group. Statistics were performed on each experimental measure with multiple groups with one-way ANOVA with Tukey tests for pair wise comparisons. When only comparing 2 groups, 2-tailed student's t-tests were performed. P values of <0.05 were

considered significant, *p<0.05, **p<0.01, ***p<0.001 as indicated in the figure legends. We used GraphPad Prism 5 statistical analysis software. [Pouliot et. al. 2016]

5.3 Results

Encapsulation of hMSCs

hMSCs encapsulated in lung derived ECM hydrogels were found to maintain viability at higher levels than encapsulation in a commercially available collagen hydrogel (Fig. 5.1, A). In addition to hMSC experiments using dsDNA quantification, cell viability was confirmed by staining encapsulated hMSCs grown in hydrogels using a Live/Dead staining kit. Quantification of these images showed that there are a significantly greater number of cells alive at the 5 days indicating active proliferation in the gel (Fig 5.1, B). This is clearly demonstrated visually in representative images taken from day 2 and day 5 (Fig. 5.1 C, D), minimal dead cells were observed at either time point. In addition, cell attachment to and contraction of the hydrogels demonstrates their ability to recognize and use binding sites inherent in the matrix derived material. [Pouliot et. al. 2016]

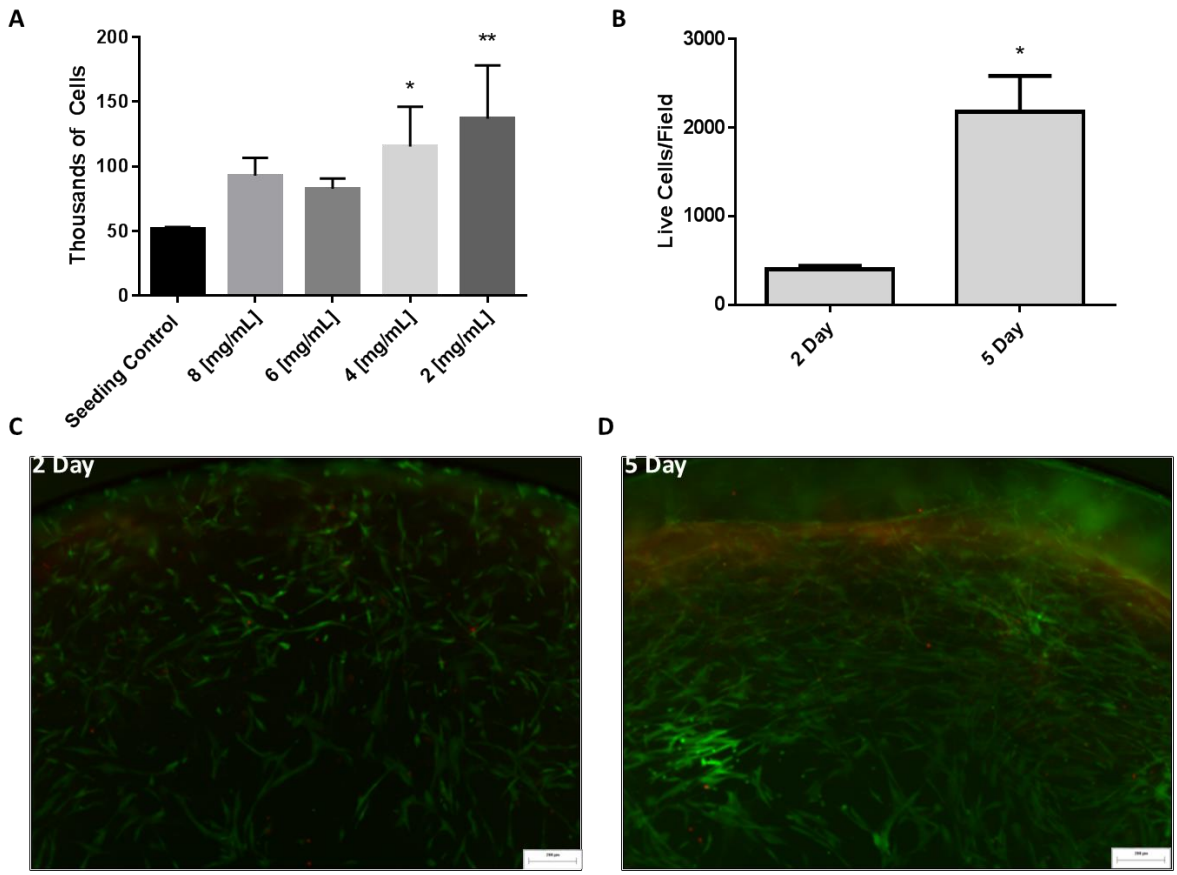

Figure 5.1 Cell Viability Within Hydrogels. (A) 2 day encapsulated hMSC viability assay shows that cells remain viable following encapsulation. Data are mean +/- st.dev. n=3 per group * $p < 0.05$, ** $p < 0.01$ compared to the seeding control; (B) Image analysis quantification of live/dead assay. Live cells are reported as dead cells were negligible. Data are presented as mean +/- st.dev. n=3 per group. *$p<0.05$ comparing 2 and 5 days, indicating cell proliferation (C, D) Representative images from hMSCs encapsulated in lung ECM hydrogels and stained using a Live/Dead kit at 2 and 5 days of culture.

Encapsulated MSC Gene Expression

In vitro gene expression analysis of MSCs grown within lung ECM hydrogels indicates that several markers maintain their expression during encapsulation (Fig. 5.2). Thy1 showed no significant change compared with cells grown on a tissue culture plate control. Sox2 and Oct4 expression were significantly increased compared to plate control on Day 3, and the expression returned to plate control levels at Day 7. [Pouliot et. al. 2016]

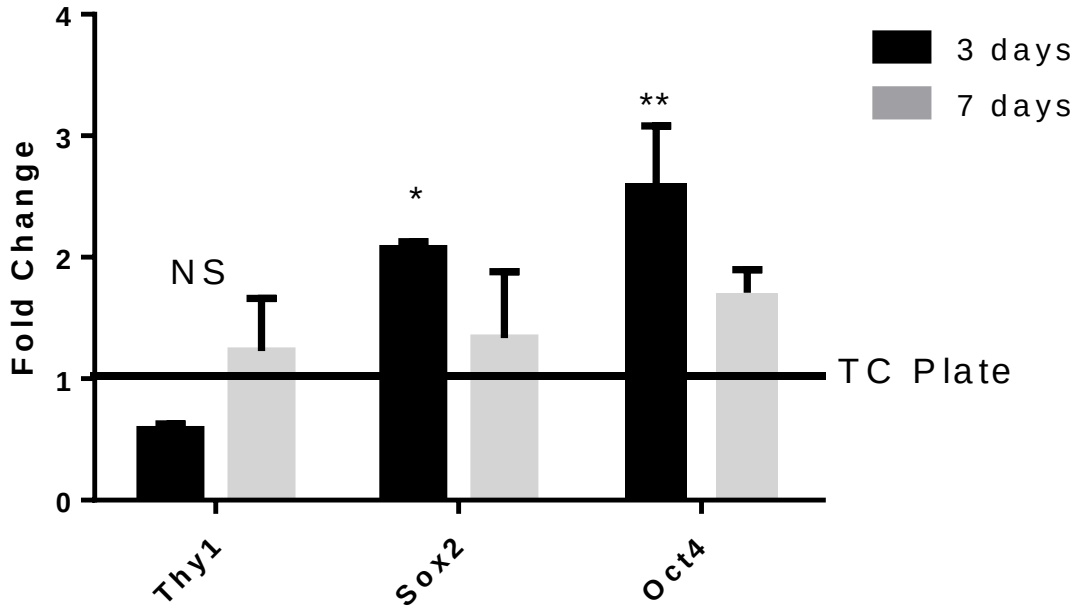

Figure 5.2 Encapsulated hMSC Gene Expression. QPCR data from cells encapsulated in ECM hydrogels for 3 and 7 days and compared to a 3 day plate control. Gene expression indicates that both Sox2 and Oct4 are upregulated at 3 days of encapsulation but all three genes return close to their control levels by 7 days of encapsulation. Data are presented as mean +/- std. dev. n=3 per group. *$p<0.05$ compared with plate control.

Scratch Assay

The results of the scratch assay suggest that hMSCs encapsulated inside of ECM hydrogels maintain their ability to positively influence simulated wound closure in vitro, results shown in figure 5.3. Groups exposed to both basal and growth media conditioned by hMSCs encapsulated in ECM hydrogels significantly increased wound closure compared to the non-conditioned basal and growth media controls. MSC controls were found to significantly increase wound closure in the conditioned growth media group over the non-conditioned control. No significance was found between the hMSC control and the encapsulated hMSC controls in either basal or growth conditioning groups; however, there is a visual trend of higher wound closure in the encapsulated hMSCs in both conditioning groups.

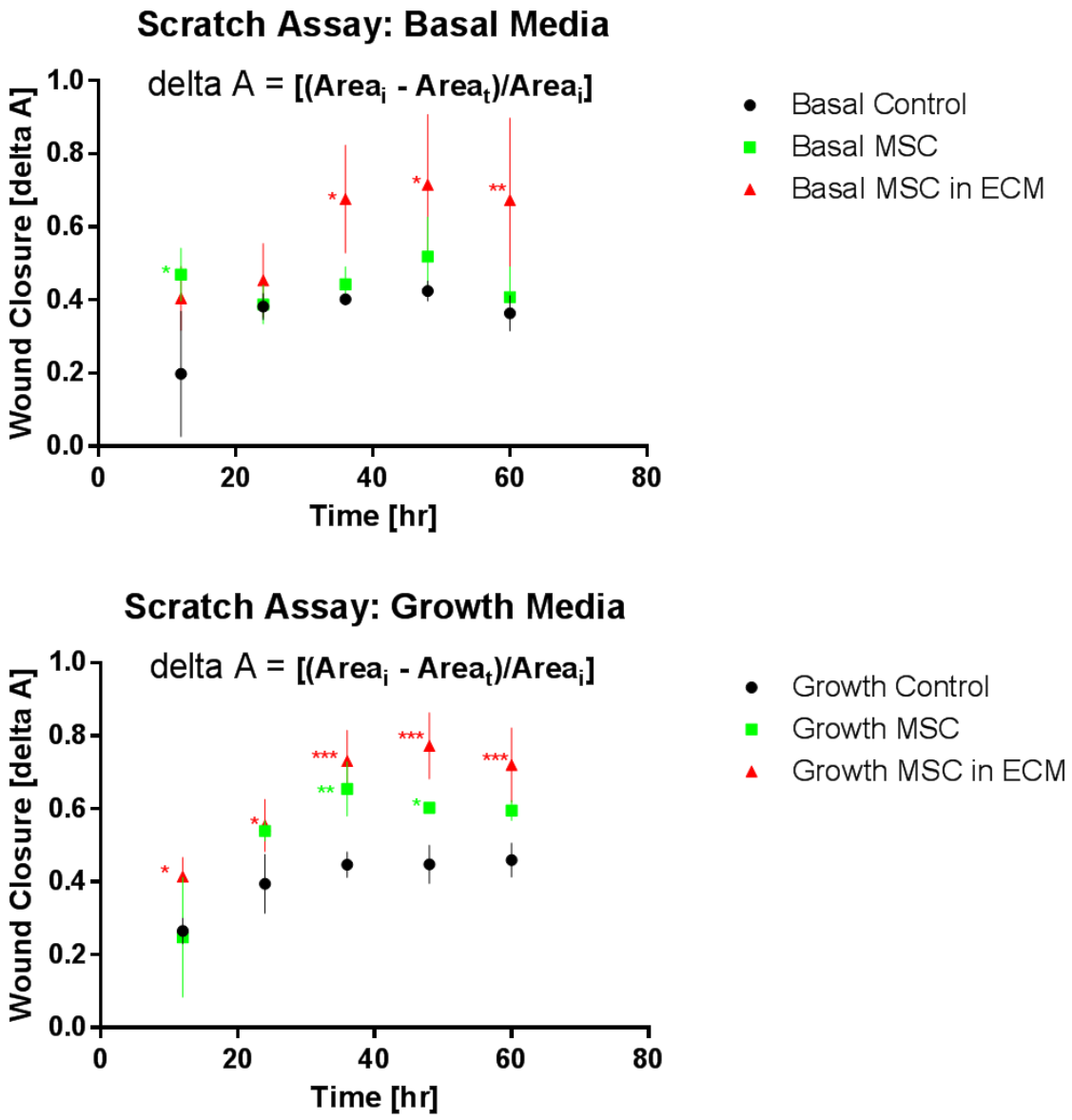

Figure 5.3. Scratch Assay using encapsulated hMSC conditioned media. A scratch assay performed using conditioned media from both plated and encapsulated hMSCs demonstrates that conditioned media from encapsulated hMSCs can significantly increase the closure of an epithelial scratch in vitro. n=3 at each time point. *p<0.05 **p<0.01 *** p<0.001.

Activation of Encapsulated hMSCs with LPS and TNF-alpha

LPS activation had a significant impact on the gene expression of several groups, as shown in figure 5.4. Relationships between the inflammatory mediators IL-6 and IL-8 showed similar trends when comparing the control to their activated counterpart (gel control compared to gel activation and plate control compared to plate activation). IL-6 is significantly lower in the plated groups than in the gel groups, IL-8 is significantly higher in both the activated gel and plate groups. For growth factor expression, the same trends within each group (gel/gel, plate/plate) are also present. The plate control for KGF is significantly higher than all of the other groups, HGF is downregulated in both of the plate groups, and VEGF is significantly lower in the LPS activated plate groups.

TNF-alpha activation also had some very significant effects on gene expression in all of the groups as seen in figure 5.5. Activation significantly increased the expression of inflammatory mediators IL-6, IL-8, and TSG-6 and both the gel and plate activated groups. Growth factor expression for these groups were different, with the TNF-alpha activation increasing KGF expression in gel group, but decreasing it in the plate activation group. HGF was significantly decreased for both of the plate groups. VEGF returned to the trends seen for other genes with the gel and plate activated groups being significantly lower than the gel control.

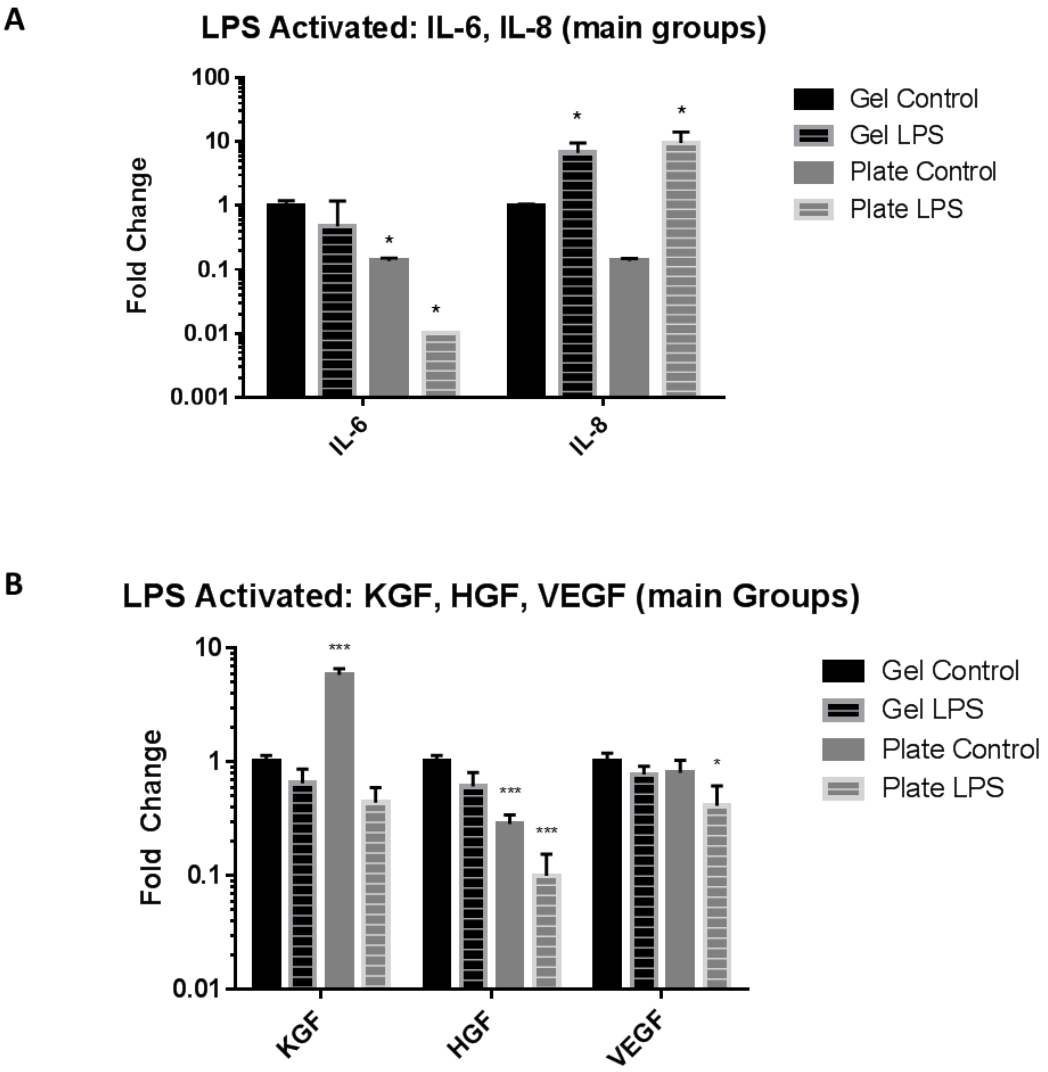

Figure 5.4 LPS Activation of Encapsulated hMSCs. Gene expression for plated and encapsulated hMSCs activated with 200 [ng/mL] LPS, the gene expression data is organized into (A) inflammatory mediators, and (B) growth factors, all gene expression data is referential to the gel control group (n=3). The results indicate that encapsulated hMSCs are similarly activated to the plate activated cells, especially with respect to the inflammatory mediator IL-8. There are some differences in the expression of IL-6, KGF and HGF; although the trends within groups remain very similar. *$p<0.05$ **$p<0.01$ *** $p<0.001$ (n=3, each gene analyzed separately with 1 way anova, and combined on the graph).

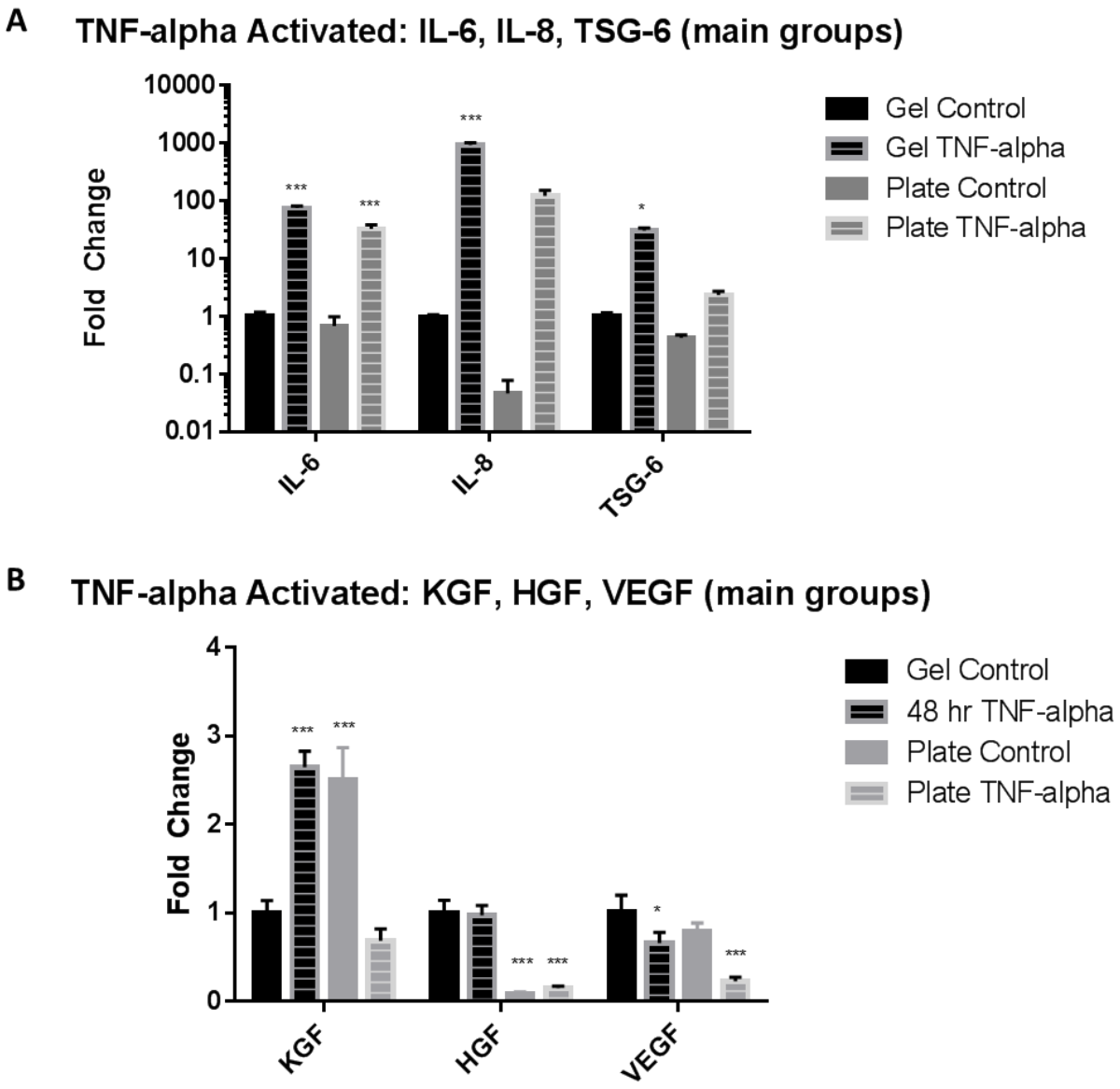

Figure 5.5 TNF-alpha Activation of Encapsulated hMSCs Gene expression for plated and encapsulated hMSCs activated with 50 [ng/mL] hrTNF-alpha, the gene expression data is organized into (A) inflammatory mediators, and (B) growth factors, all gene expression data is referential to the gel control group. The results indicate that encapsulated hMSCs are similarly activated to the plate activated cells, especially with respect to the inflammatory mediators IL-6, IL-8, and TSG-6. There are some differences in the expression of KGF and HGF. *$p<0.05$ **$p<0.01$ *** $p<0.001$ (n=3, each gene analyzed separately with 1 way anova)

Comparing M0 macrophage activation on ECM hydrogels to M0, M1 and M2 Macrophages

Gene expression for M1 and M2 phenotypic markers and several inflammatory mediators resulted in several significant findings, shown in figure 5.6. The M2 activated naive macrophages expressed high levels of Fizz1, Manose Receptor, and YM1; all M2 phenotypic markers. They also had a significant downregulation of IL-6. The M1 activated naive macrophages had an upregulation of the M1 phenotypic marker NOS2, as well as IL-10. The experimental group of naïve macrophages grown on ECM hydrogels dig not have any significant expression of and of the M1 or M2 phenotypic markers. They did have significant upregulation of all of the inflammatory mediators including IL-6, TNF-alpha, and IL-10.

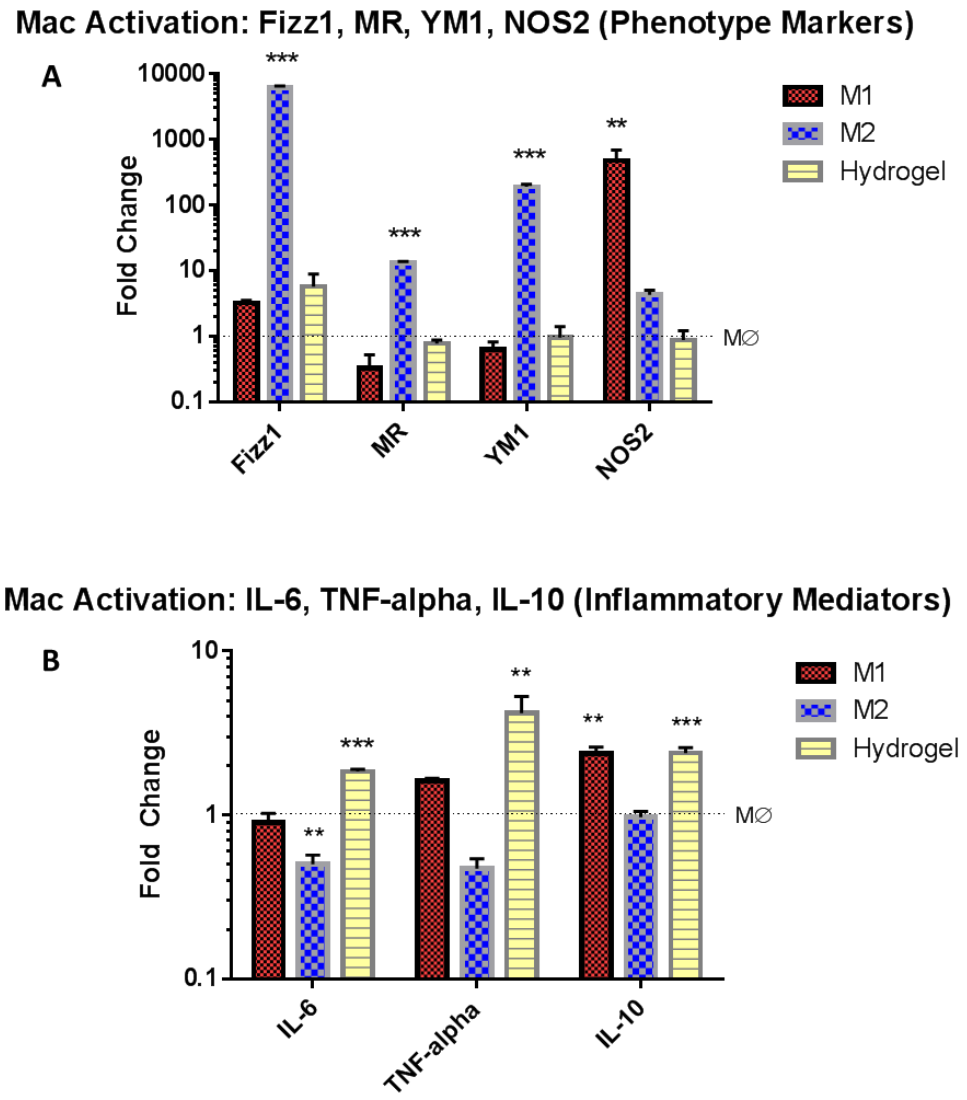

Figure 5.6 Macrophage Activation on ECM Hydrogels. Gene expression from Naïve, M1, and M2 C57BL/6 bone marrow isolated primary macrophages grown on ECM hydrogels for 24 hours showing the expression of (A) phenotypic markers indicative of M1 and M2 macrophages, and (B) the expression of some common macrophage secreted cytokines. Naïve macs on the gels are clearly not activated to become M1 (NOS2) or M2 (Fizz1, MR, YM1), they do however have a dynamic cytokine response to being grown on gels which includes increase in expression for both pro and anti-inflammatory mediators. *p<0.05 **p<0.01 *** p<0.001 (n=3, each gene analyzed separately with 1 way ANOVA, and then added to the graph together)

In Vivo Delivery and Inflammatory Indicator

Delivery of rat MSCs intratracheally using the lung ECM hydrogel was determined to significantly increase the number of GFP positive cells in the tissue by nearly 2.5 times the amount after 24 hours when compared to rat MSCs delivered in saline (5.7, A). Representative images from each group are shown in Figure 5.7A and 5.7B showing GFP tagged MSCs in the alveolar regions in the elastase treated rat lungs. MPO is a granular enzyme expressed by polymorphonuclear neutrophils and alveolar macrophages, catalyzing the synthesis of hypoclorous acid, a by-product of hydrogen peroxide and is indicative of inflammatory response. PPE induced emphysema is not expected to cause large amounts of MPO. Treatments of MSC and MSC+ ECM in the PPE treated rats did not significantly increase MPO activity compared with Saline in the PPE rats, indicating that the treatment at did not cause increased inflammation (Fig 5.7D). [Pouliot et. al. 2016]

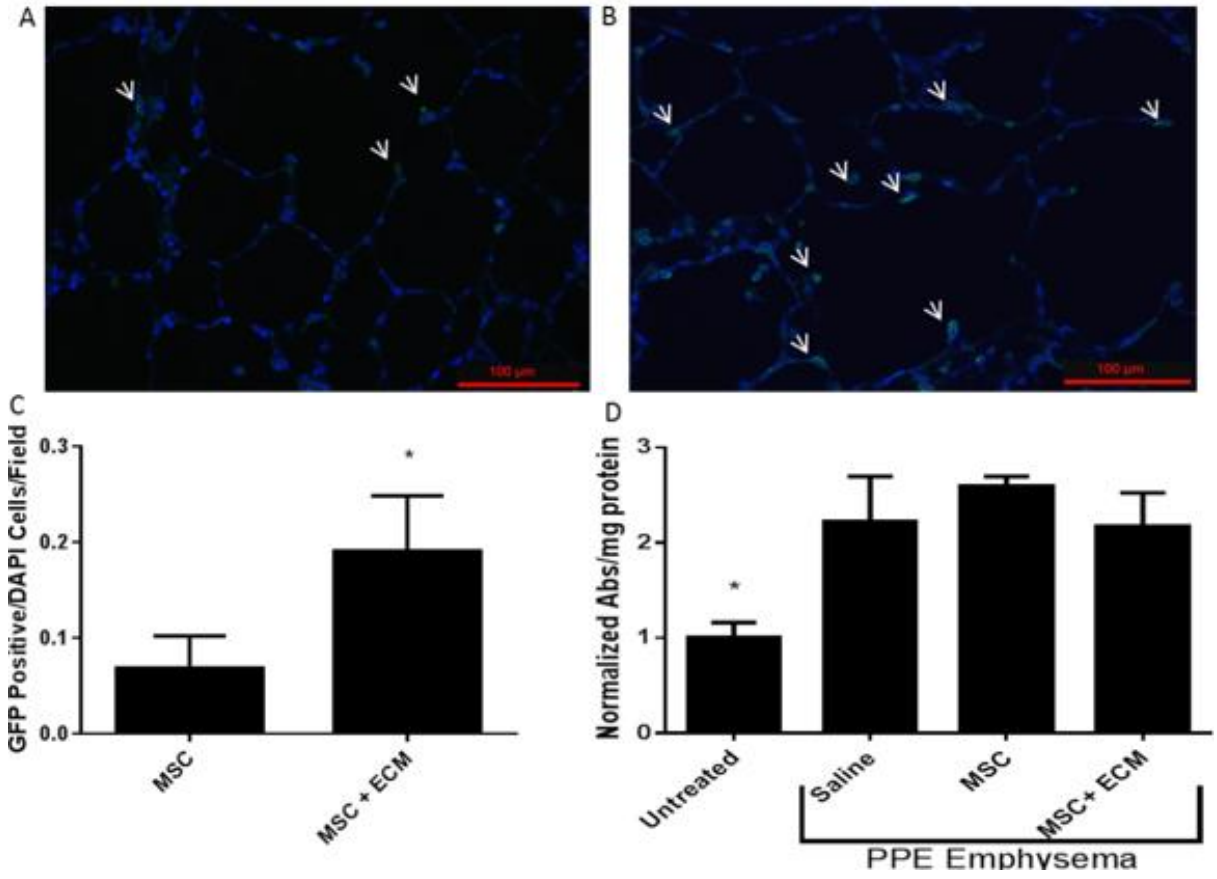

Figure 5.7 Cell Deposition in Elastase Treated Rat Lungs. Cell deposition in elastase treated rat lungs. (A) Representative image from MSCs delivered in saline stained with anti-GFP to track the MSCs. (B) Representative image from MSCs delivered in ECM pre-gel solution stained with anti-GFP to track the MSCs. Arrows point to GFP+ cells. Scale bars are 100 μm. (B) Quantification of GFP positive rat MSCs per field in elastase treated rat lungs. Significantly greater numbers of GFP positive rat MSCs were present in the damaged lungs in the MSCs delivered in the ECM pre-gel solution compared with MSCs delivered in saline. Data are presented as mean +/- St. dev. n=3 rats per group. Counts were from 10 fields/rat. *$p<0.05$. (D) MPO assay of treated rat lungs. All elastase treated animals had significantly greater MPO activity compared with healthy animals. No statistical differences were observed between treated

groups, indicating that MSC and MSC+ECM do not cause any additional inflammatory response at 24 hours. Data are presented as mean +/- St. dev. *$p<0.05$. Scale bars are 100 μm.

5.4 Discussion

The behavior of cell types grown on tissue specific ECM is a driving force behind proponents of tissue specific ECM for tissue engineering scaffold materials. Many whole organ decellularization studies have investigated the differentiation and organization of tissue progenitor cells in culture on whole organ scaffolds[46,61,78,89]. Decellularized whole organ materials have the advantage of mechanical properties closer to those of the native tissue, physical cues from intact tissue structures, as well as the biochemical cues of the ECM. All of these help guide seeded cells find their functional identity. [Pouliot et. al. 2016]

In vitro investigations with ECM derived materials have found that the materials are non-cytotoxic [71,74], promote migration of relevant cell types [90], and are equal or better at maintaining cell viability when compared to control collagen hydrogels [47,72]. During our investigation we found that hMSCs encapsulated in lung ECM hydrogels remain viable at higher or comparable levels to those encapsulated in a commercially available collagen type I hydrogel. We also observed that cells proliferate more in lower concentration ECM hydrogels, we believe that this difference is due to there being less support and encapsulation in the 4 [mg/mL] and 2 [mg/mL], and which may allow the cells to sink to the bottom of the gels to sense the stiffness of the tissue culture plastic. [Pouliot et. al. 2016]

In addition to the activity and viability of cells encapsulated in ECM hydrogels we were interested in determining the effect of encapsulation on the genetic expression of hMSCs. We looked at Thy1 (CD90) which is a common MSC marker, and Sox2 and Oct4 which are prominent actors in the signaling pathways responsible for mesenchymal stem cells retaining their pluripotency. Many of the therapeutic functions of MSCs come from their immunomodulatory functions which would be minimized if encapsulation caused differentiation. Significant increases in Sox2 and Oct4 suggest that the cells are responding as they attach and migrate through the hydrogel, but their return to plate control levels by day seven suggests that encapsulated MSCs maintain their original phenotype. [Pouliot et. al. 2016]

One of our major goals was to determine if encapsulated hMSCs maintained their ability to secrete factors that could positively modulate an inflammatory environment. One of the concerns that we have had is that the ability of the hydrogel to sequester proteins could inhibit either the influx of pro-inflammatory cytokines for the hMSCs to respond to, or the efflux of secreted factors from the encapsulated hMSCs, or both. The scratch assay was completed using non-activated cells so the results are only based on the baseline secretion from encapsulated hMSCs which only addresses the second part of our concerns. The results of the scratch assay, shown in figure 5.3 suggest that they do in fact maintain this ability. It is possible that the large number of cytokines was able to overwhelm the protein sequestering reservoir allowing the majority of secreted factors to reach the conditioning media.

In order to address the first concern, that the encapsulation would inhibit inflammatory factors from the milieu from reaching the hMSCs we investigated gene expression of

encapsulated hMSCs activated with either LPS or TNF-alpha. LPS, which is present on the membrane of infiltrating bacteria, was used to simulate an immune response to bacterial infection, by activating the TLR 4 receptor[91,92]. TNF-alpha is a pro-inflammatory mediator that is present in many chronic inflammatory pathologies and is known to be a strong activator of MSCs[93] and has been shown to promote secretion of angiogenic factors[94]. The results from both of these assays, shown in figures 5.4 and 5.5 thoroughly demonstrate that encapsulated hMSCs can be activated through these mechanisms. Another finding from these assays is that encapsulated hMSCs have a higher baseline expression of all of the genes analyzed except for KGF. It is possible that encapsulation of the hMSCs has some inherent activation on its own. The activation of hMSCs with TNF-alpha lead to much more dramatic change in gene expression. Fold change values for all of the inflammatory mediators were significantly increased from baseline. KGF was upregulated in activated encapsulated hMSCs, but downregulated in the plate activated groups, while HGF expression was not effected by activation, but baseline levels in gel groups were higher than plate groups. This suggests that the gene expression for these growth factors may in some part be subject to the mechanical stiffness of the gel, or the due to the 3D culture conditions.

An additional feasibility topic we were interested in looking at in vitro is the potential immunogenic response to the ECM hydrogel. To look at this we took naïve macrophages plated them on ECM hydrogels, then compared their gene expression of M1 and M2 markers and additional inflammatory mediators to classically activated M1 and M2 expression. From the results presented in figure 5.6 it is clear that the 24-hour exposure to ECM hydrogels significantly change the expression of the phenotypic markers towards M1 or M2, in fact the

expression did not change much from baseline M0 expression. However, the significant increase in expression of all three of the inflammatory mediators we tested indicated that the macrophages are responding to the hydrogel different than they do to tissue culture plastic.

The expression of genes for pro-inflammatory mediators IL-6 and TNF-alpha is not significantly increased from naive macrophage expression levels, while the macrophages grown on ECM hydrogels have upregulation of these and the anti-inflammatory cytokine IL-10. Normally there would be an upregulation of TNF-alpha and IL-6 in M1 cells compared to naïve cell expression[95], the lack of this paradigm may suggest that the primers used for these genes are not suitable for PCR at the temperature we used or have products with other sequences that we did not account for. It is also possible that our control M1 group was not adequately polarized by our experimental setup. To address this, we can add some more M1 markers to analyze, and also try some other primer pairs for these genes.

We were not able isolate macrophages grown on these same conditions for flow cytometry because they had remodeled and infiltrated the hydrogel so much that we could not separate them. I would suggest that paired with the gene expression data, these macrophages are infiltrating and working to break down the hydrogel, in this scenario the increase in inflammatory mediator would be to direct other cells to secrete MMPs and other enzymes. This is a research question that could be investigated much more thoroughly in the future.

Finally, the in vivo feasibility study for intratracheal cell delivery in Figure 5.7 confirmed that the ECM hydrogel vehicle increased cell retention when compared to a non-vehicle control. In both groups there are examples of the GFP antibody localizing to immune cells suggesting that some cells are phagocytosed regardless of delivery method. However, it is clear that there

are more intact GFP-tagged cells when delivered in a pre-gel solution when compared to the non-vehicle control. Additionally, the absence of apoptotic cells as indicated by an apoptotic staining assay on serial sections used for quantification of dosed cells in the tissue suggests that the GFP tagged cells found in the tissue remain viable. Further investigation of the treated animal groups revealed that additional inflammation was not caused in the short term as evidenced by the MPO data; however, longer term studies will need to be perform to more extensively assess the pro- or anti-inflammatory effects of the hydrogel as a treatment. The successful encapsulation and maintenance of viable MSCs in a lung derived ECM hydrogel both in vitro and in vivo supports further investigation of this material for cell delivery purposes. [Pouliot et. al. 2016]

5.5 Conclusions

We have conducted initial in vitro experiments which suggest mesenchymal stem cells remain viable and maintain their expression of genes associated with pluripotency during encapsulation in hydrogels for up to a week. We have also determined that encapsulated hMSCs maintain their ability to secrete factors into the environment as well as their ability to be activated by several mechanisms. Macrophage experiments with ECM hydrogels determined that while macrophages are not activated to an M1 or M2 phenotype they do respond to the gel differently than TC plastic, a topic which should be investigated further. Delivery of MSCs intratracheally in a rat model demonstrated that encapsulation of the cells in the hydrogel resulted in increased retention of the cells after 24 hours. The results of this study support continued investigation of lung derived ECM hydrogels as a cell or drug delivery vehicle.

Chapter 6: Tailoring ECM Hydrogels for Specific Applications

6.1 Introduction

Tissue derived extracellular matrix based materials are increasingly being investigated for applications including: cell and drug delivery, in vitro modelling, and biomaterial coatings. The effect of matrix preparation variables could play a large role in determining the final material properties and, as previously mentioned in chapter 4, have yet to be investigated. We looked at varying digestion times in the ECM powder digestion protocol and the resulting changes in the size of the solubilized proteins and gelation behavior. These investigations include SEM characterization, a quantitative method for determining network density, and additional SDS-PAGE analysis on both pre and post gelled samples, and rheometric characterization of the gelation properties for each digestion time variant. Additionally, we started to investigate an area that we haven't looked at before, using the KGF ELISA to characterize KGF release from encapsulated hMSCs in normal conditions, and when activated with LPS. Finally, we looked at the attachment and proliferation of SAECs to coated plates and on ECM hydrogels respectively. This research represents a first step towards a novel area that has not been investigated by previous groups working with ECM hydrogels.

6.2 Materials and Methods

Hydrogel Preparation

ECM hydrogels were prepared as previously described in chapter 4, briefly, 100 mg of ECM powder and 10 mg of pepsin was weighed and added to 10 mL of 0.01 M HCl. The

digestion solution was agitated in a 50 mL conical tube using a stir bar which was rotated at speeds fast enough to mix all levels of the digestion. 2.5 mL of the digestion solution was taken out of the reaction tube and chilled on ice for 2 minutes at time points of 4 hr, 16 hr, 36 hr, and 72 hours (4, 12, 24, and 48 for some experiments). The extracted digests were neutralized with 250 uL of 0.1 M NaOH and with 278 uL of 10X PBS. The digests were stored at 4 degrees Celsius and used within 7 days.

SEM Imaging

Pregel from 4, 16, 36, and 64 hour digests was plated in a 48 well plate and allowed to gel for 30 minutes before being fixed in 5% glutaraldehyde. These 200 uL gels were then transferred to a 24 well plate for further fixation in a 4% osmium tetroxide solution. In preparation for SEM imaging the samples were dehydrated to 100% ethanol, critical point dried, and plasma sputter coating in preparation for imaging as previously described. Qualitative images for visual comparison were taken at 2000x magnification using the Jeol SEM at the NCC, and images for further quantitative processing were taken at 5,000x magnification.

Hydrogel Interconnectivity

The 5000x magnification images taken previously were used in an image processing protocol to determine the physical interconnectivity of the resulting gels at the different digestion time points. Three representative images were taken for this analysis. The images were uploaded into Image J and overlaid with a 12 section grid, the number of branches in each section of the grid were counted and recorded. The total number of interconnections for each image were

averaged and divided by the total image area to present the data as network density using interconnections per um^2.

SDS-Page on Pre and Post gelled ECM Hydrogels

Samples were prepared for SDS-PAGE as previously described except they were run on a 15 lane gel. Each sample was prepared as both a pregel and post-gel to determine if the self-assembly leads isolated proteins with a different molecular weight profile. The experiment included the intact native tissue and ECM powder groups for comparison. Gels were imaged and processed using the BIORAD software to sync with the standards on the gels and determine the approximate molecular weight and density of the bands in the samples. The protein measured for each the bands of each sample was summed in order to visualize the difference in identifiable protein as a function of digestion time.

Rheometry

Pregel solutions from the timed digests were also characterized using rheometry as previously described. Each sample was run at least three times at 0.5% strain using a temperature ramp from 4 degrees C to 37 C and the results were averaged. Data was averaged to quantify the relative gelation behavior of the hydrogels at each digestion time point.

KGF Release from LPS activated hMSCs in Gels

hMSCs were encapsulated in 4, 12, and 48 hour timed digest pregel solutions and plated in a 48 well plate. 50,000 cells were plated in each well in 50 uL of pregel solution, along with a non-gel TC plate control. The solutions were incubated to induce gelation and then normal

hMSC media was added. After 24 hours the media was aspirated and replaces with basal hMSC media loaded with LPS at 200 ng/mL to activate the hMSCs. 24 hours later the media was aspirated and collected for a KGF release ELISA. The wells were refilled with basal media and 20 uL of MTT labeling reagent (Roche) was added to each well; four hour later the MTT solubilization buffer was added to the wells and incubated overnight. The KGF ELISA was completed and read using a Biotek plate reader. The MTT data was used to normalize the KGF release data to the relative number of cells that were in each group.

Small Airway Epithelial Cells on ECM Coated Plates and ECM Hydrogels

SAEC attachment to ECM coated plates was determined for 30 and 60 minute time points. ECM pregel solution from timed digests neutralized at 4, 12, 24, 48, and 72 hours were used to coat TC plates for an attachment assay. 50 uL of each pregel solution was added to each well in a 96 well plate and then incubated at 4 degrees Celcius for 4 hours, before being aspirated and rinsed with 1X PBS. SAECs were plated at 10,000 cells/well in SAGM media (Lonza). Media was aspirated and wells rinsed at 30 and 60 minutes respectively, following removal of non-adherent cells basal SABM was added to each well and cell number was determined using MTT as previously described.

SAEC proliferation when plated on formed ECM hydrogels was determined over a two-day period. 50 uL of each ECM pregel solution from timed digests neutralized at 4, 12, 24, 48, and 72 hours were added to wells and allow to gel in the incubator. Following this SAECs were plated at 10,000 cells/well in growth media and cultured for 2 days. Following this the relative number of cells in each well was determined using MTT as previously described.

6.3 Results

SEM Imaging

The hydrogel structure resulting from each digest were investigated using SEM imaging. Images taken from 2, 4, 20, 36, and 64 hour digests show a clear progression of protein organization, as shown in figure 6.1. Shorter digests have much more highly branched and networked appearance, where longer digests have a much more porous and less diverse fiber organization.

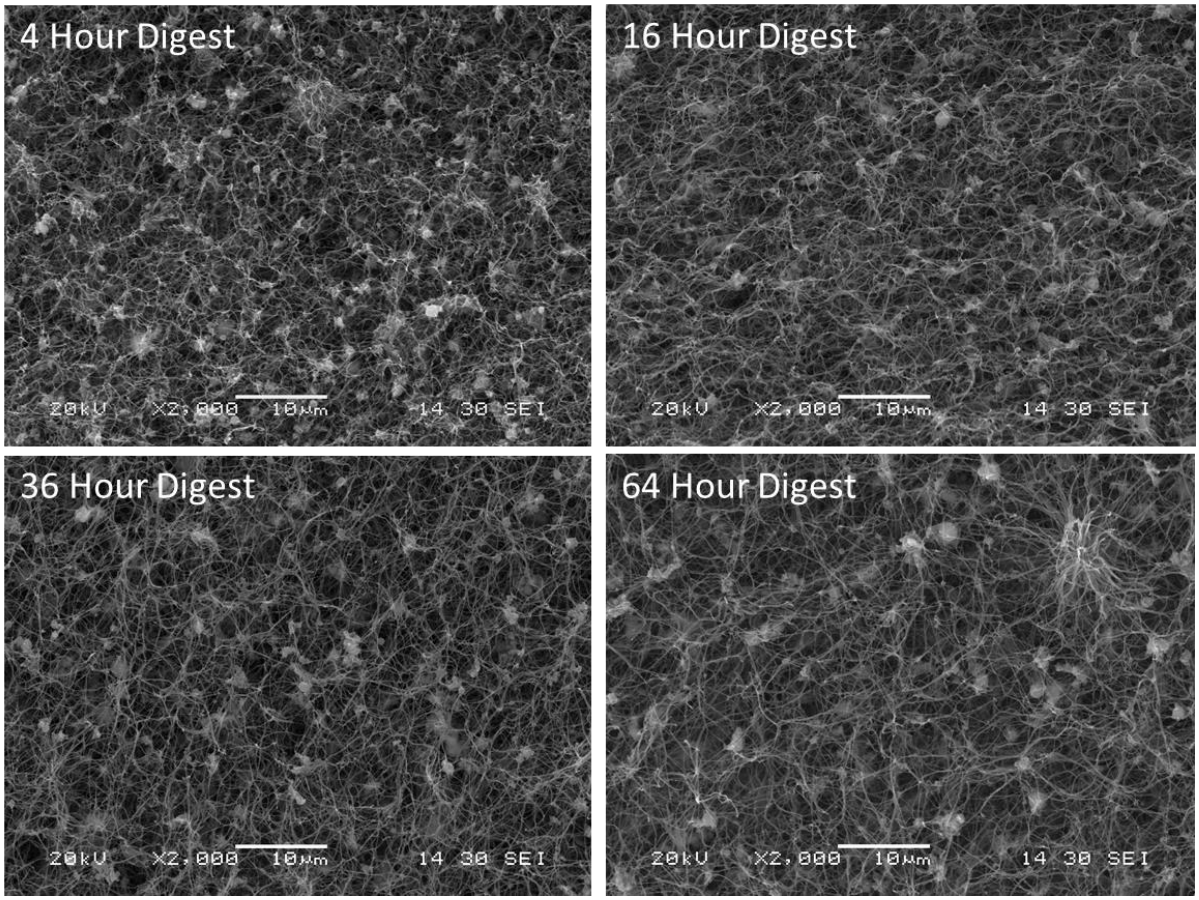

Figure 6.1 SEM Comparison of Hydrogel Structure from timed digests. Hydrogels prepared from pregel solutions neutralized at 4, 16, 36, and 64 hour into the digest were SEM imaged to investigate changes resulting from the digest time. Visual observation shows that the proteins in shorter digests have a much higher degree of branching and there is a progression to less branched and less dense over time.

Hydrogel Interconnectivity

Using the SEM images taken for each of the timed digest samples we were able to use Image J to determine the network density as defined by protein [interconnections/area]. The results of this approach are shown in figure 6.2. From this analysis we were able to determine that the quantitative data matches the qualitative observations made from the corresponding images. That is, that the density of the hydrogel architecture decreases as digestion time increases.

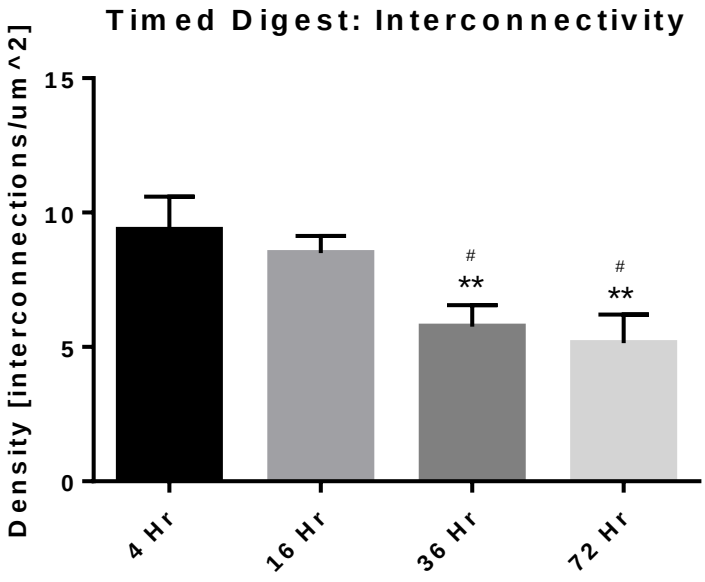

Figure 6.2 Hydrogel Interconnectivity. SEM images were analyzed using Image J to determine the change in interconnectivity of the protein structures each digestion time. There is a clear trend, as digestion time increases the hydrogel network has a lower density of interconnected proteins. The 36 and 64 hour samples are significantly different from both the 4 and 16 hour samples. *$p<0.05$ in comparison to 4 hour group, #$p<0.05$ in comparison to 16 hour group (n=3 images per gel, only one gel was imaged for each time point).

SDS-Page on Pre and Post gelled ECM Hydrogels

SDS-PAGE results in 6.3 show how bands for larger proteins lose volume as digestion time is increased and become even fainter as digestion time increases. The quantitative confirmation of this observation is available in figure 6.4, which includes measurements of band volume by intensity as well as total relative protein in all the bands measured for each sample. Additionally, this SDS-PAGE experiment allowed us to investigate the difference in protein molecular weight profile between pre and post gelled samples for each digestion time point.

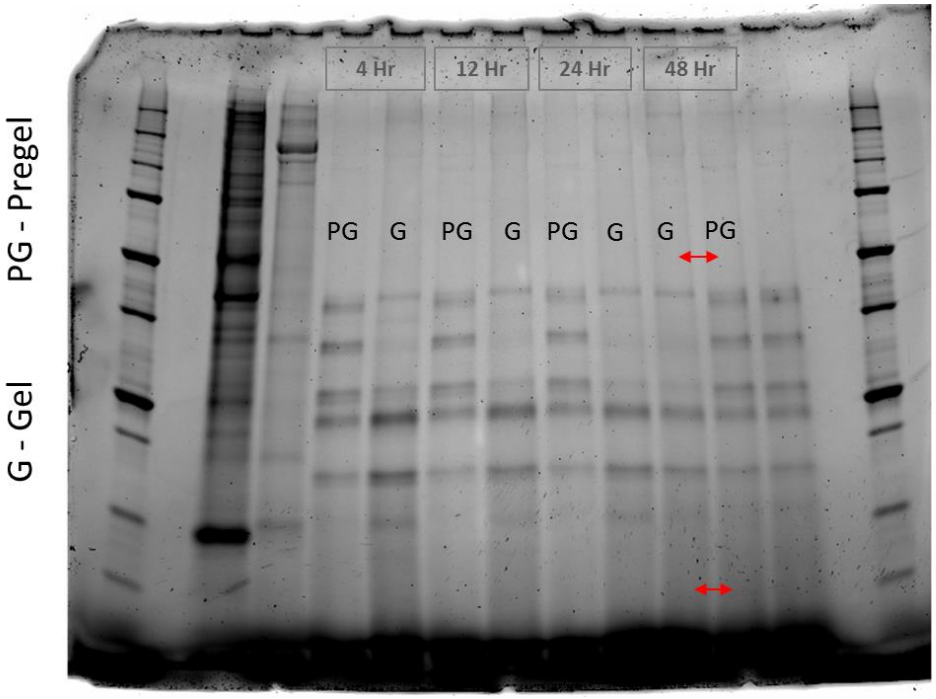

Figure 6.3. SDS- Page for Timed Digest Gels (Pre & Post Gelation). This SDS-PAGE gel shows the progression and change in protein profile, for both pre and post gelled samples, as digestion time increases. The first two lanes after the standard are intact and decellularized lung tissue for reference.

A

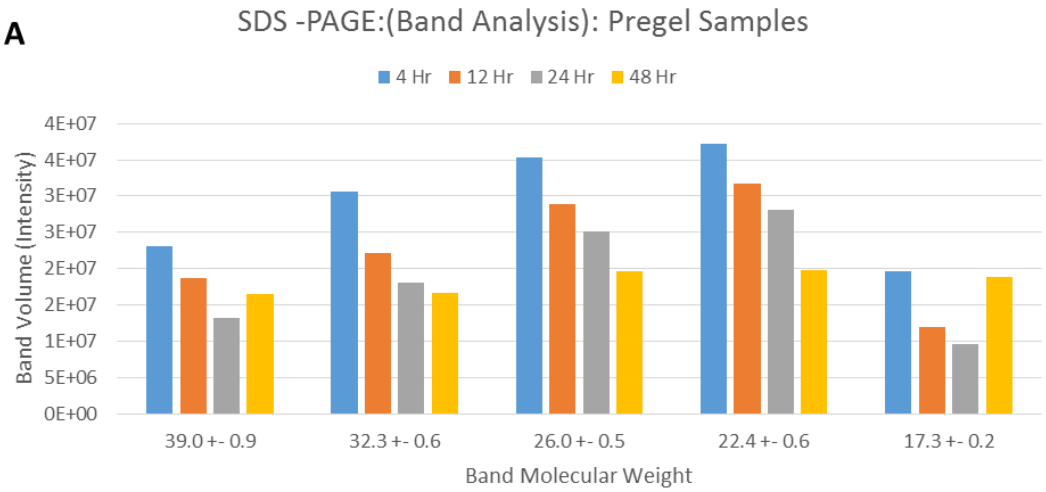
SDS -PAGE:(Band Analysis): Pregel Samples
4 Hr
12 Hr
24 Hr
48 Hr
Band Volume (Intensity)
4E+07
4E+07
3E+07
3E+07
2E+07
2E+07
1E+07
5E+06
0E+00
39.0 +- 0.9
32.3 +- 0.6
26.0 +- 0.5
22.4 +- 0.6
17.3 +- 0.2
Band Molecular Weight

B

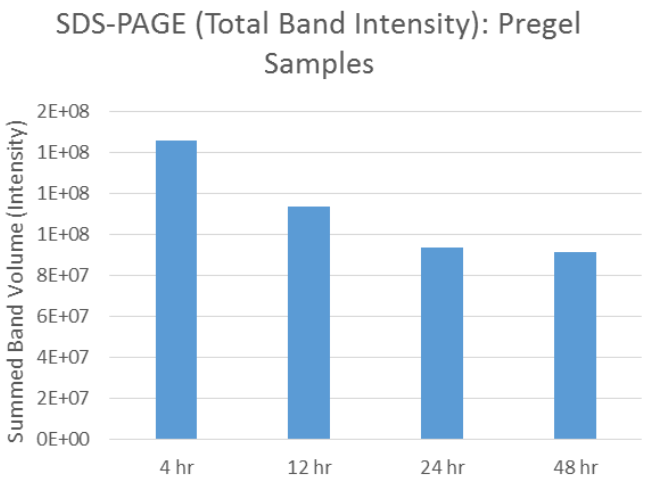
SDS-PAGE (Total Band Intensity): Pregel Samples
Summed Band Volume (Intensity)
2E+08
1E+08
1E+08
1E+08
1E+08
8E+07
6E+07
4E+07
2E+07
0E+00
4 hr
12 hr
24 hr
48 hr

C

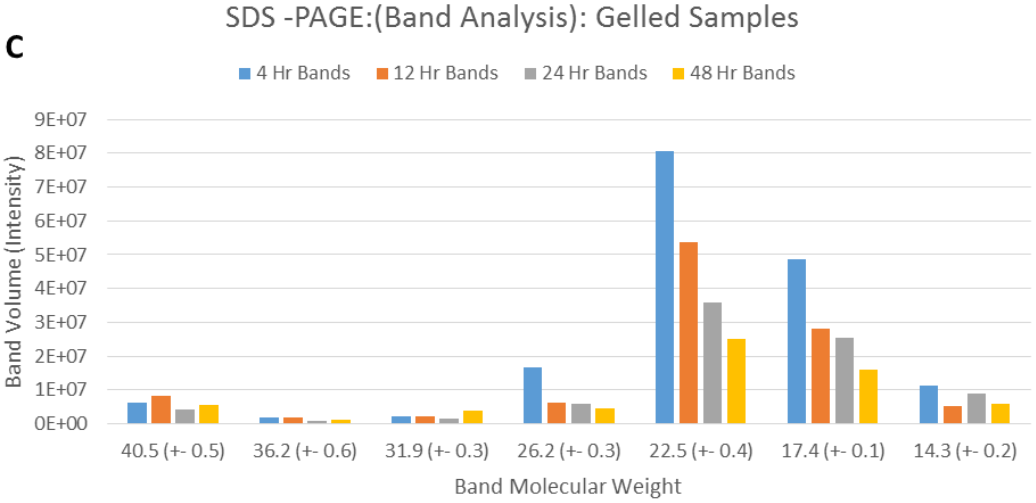
SDS -PAGE:(Band Analysis): Gelled Samples
4 Hr Bands
12 Hr Bands
24 Hr Bands
48 Hr Bands
Band Volume (Intensity)
9E+07
8E+07
7E+07
6E+07
5E+07
4E+07
3E+07
2E+07
1E+07
0E+00
40.5 (+- 0.5)
36.2 (+- 0.6)
31.9 (+- 0.3)
26.2 (+- 0.3)
22.5 (+- 0.4)
17.4 (+- 0.1)
14.3 (+- 0.2)
Band Molecular Weight

D

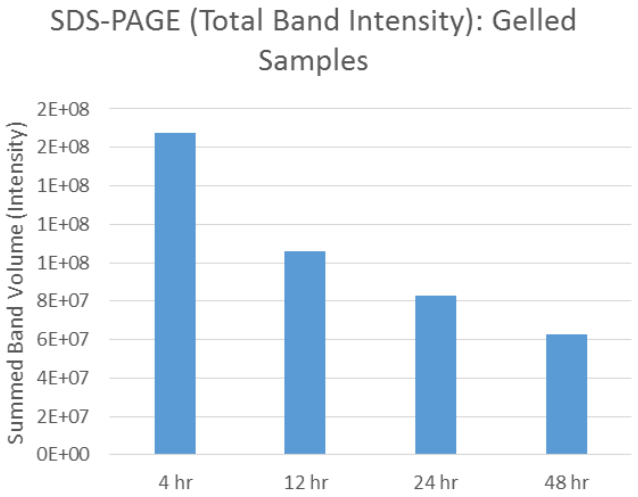
SDS-PAGE (Total Band Intensity): Gelled Samples
Summed Band Volume (Intensity)
2E+08
2E+08
1E+08
1E+08
1E+08
1E+08
8E+07
6E+07
4E+07
2E+07
0E+00
4 hr
12 hr
24 hr
48 hr

Figure 6.4. SDS-Page Band Analysis for Pre & Post Gel Samples. SDS-PAGE quantification of identified bands using the BIORAD Image Lab software. (A, C) show the relative protein volume determined for each molecular weight band, across the timed digest samples; (B, D) are a summation of the total protein volume(intensity) measured from bands in each timed digestion sample. There is only n=1 per group.

Rheometry

Rheometrical characterization of the gelation behavior and mechanical propertied of the timed digest samples was determined for samples from 4, 12, 24, 48, and 96 hour digests, as shown in figure 6.5. The results indicate that all digests start to self-assemble into a hydrogel as the plate approaches 37°C. There is a clear difference in gel stiffness as the lower time digests (4 and 12 hour) have a higher storage modulus, and the other digestion times all have similar, lower, properties.

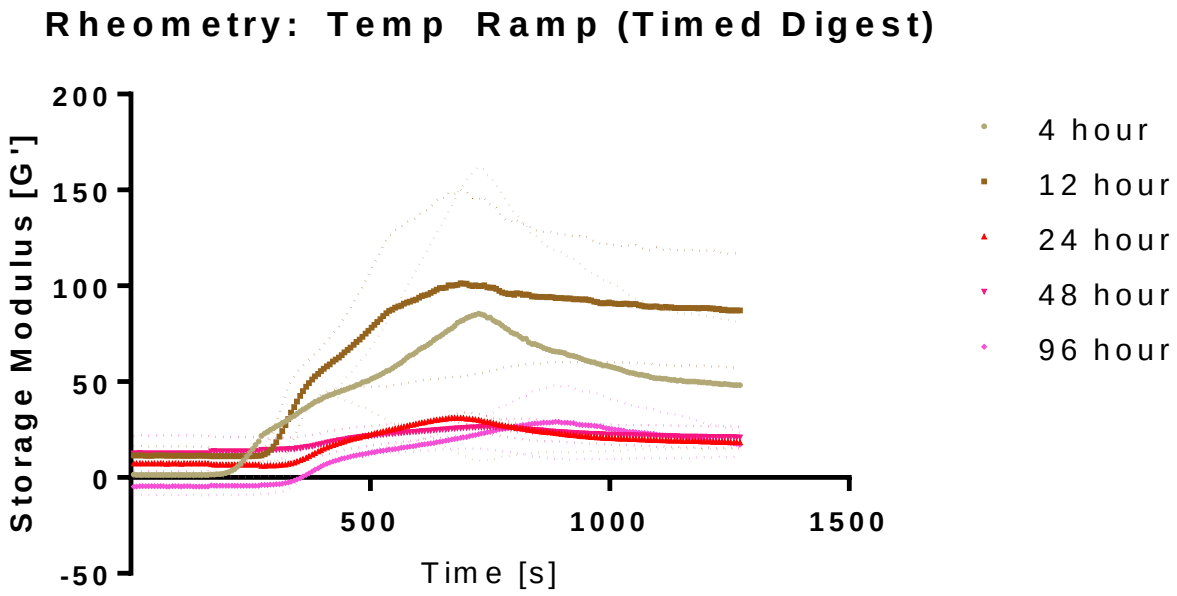

Figure 6.5. Rheometry for Timed Digest hydrogels. Rheometry data for ECM pregel solutions neutralized at 4, 12, 24, 48, and 96 hours.

KGF Release from LPS Activated hMSCs encapsulated in Timed Digest Gels

A conditioning media experiment was plated to determine if hMSCs could be activated to produce different amounts of KGF when encapsulated by several timed digest groups. The MTT data revealed that there were more cells in the plate control than in any of the encapsulated wells, so the KGF release data was normalized to the MTT. Based on this combined data it seems the only conclusion that can be drawn is that longer digestion time results in more KGF released per cell under both control and activated conditions.

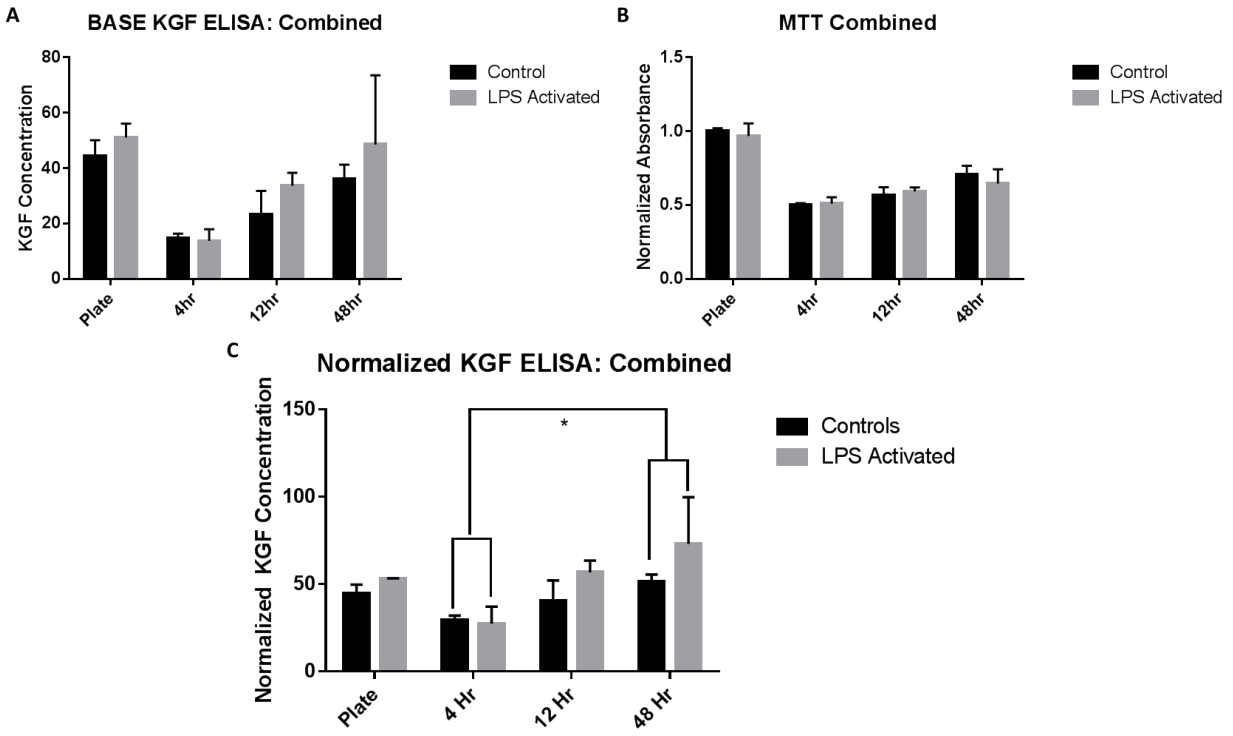

Figure 6.6 KGF Release from Encapsulated hMSCs (A) KGF ELISA results from media samples collected from encapsulated hMSCs activated with LPS or controls, (B) MTT data for the encapsulated hMSCs, (C) ELISA data normalized to the MTT data. *$p<0.05$ for the indicated groups (n=3 per group, data was analyzed using 2 way ANOVA)

Small Airway Epithelial Cells on ECM Coated Plates and ECM Hydrogels

SAECs attachment, shown in figure 6.7 A and B, was significantly increased on plates coated with 4 and 12 hour digest samples at 30 minutes, and to 12 hour alone by 1 hour of attachment. Significance is relative to the 48 hour digest group, which is the main digest time used for the majority of the research completed. SAEC proliferation on timed digest samples, shown in figure 6.7 C, was significantly increased for the 2 and 4 hour groups, and significantly decreased in the 72 hour group. There also seems to be a consistent trend were increasing digestion time corresponds to decreased SAEC proliferation over 2 days.

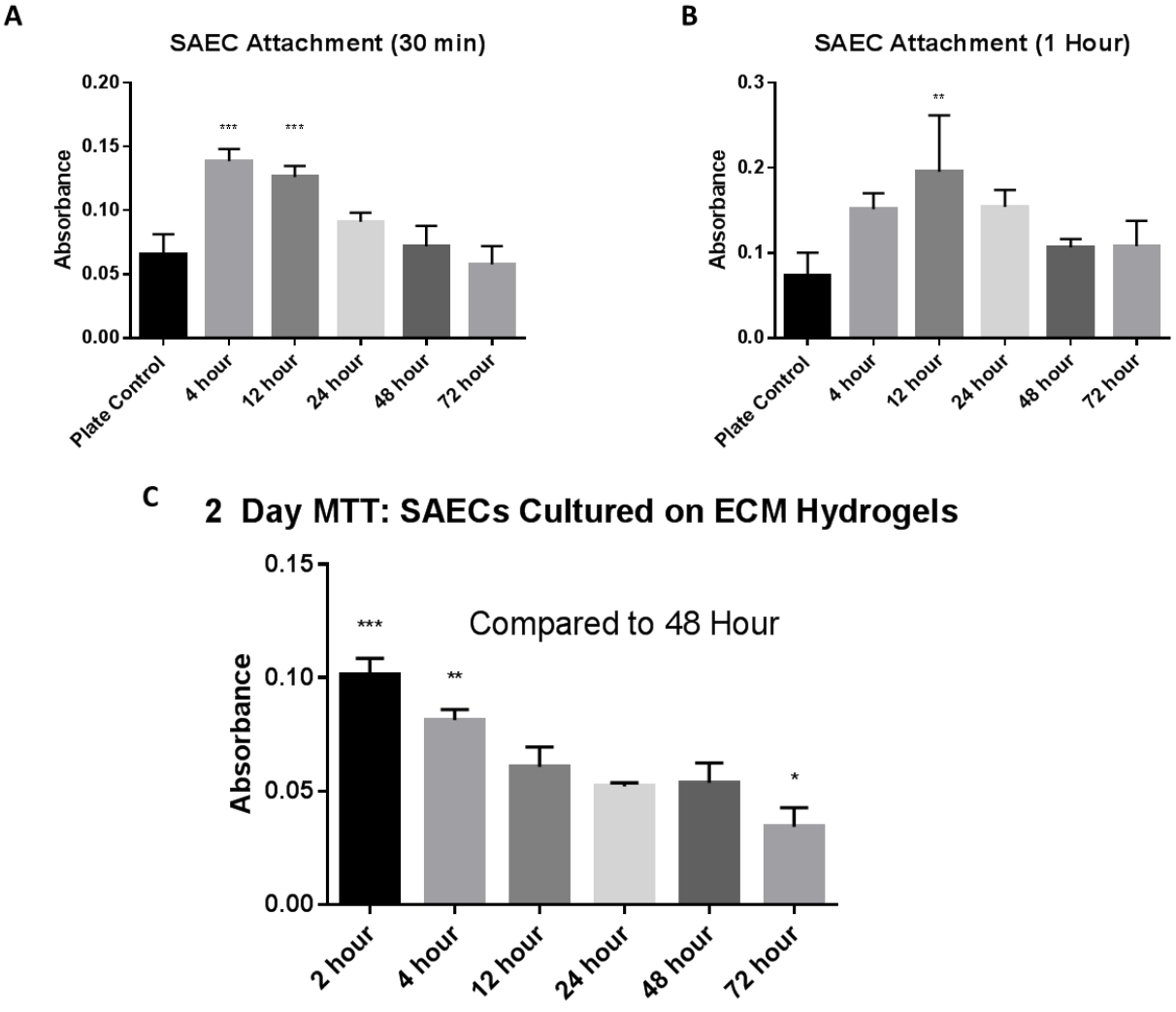

Figure 6.7 SAEC Attachment and Proliferation SAEC attachment to cold coated plates that were rinsed to dislodge unattached cells at (A) 30 minutes and (B) 1 hour; (C) Proliferation data for SAECs plated onto formed ECM hydrogels and cultured for 2 days in growth medium. *$p<0.05$, **$p<0.01$, *** $p<0.001$ for comparison to the 48 hour group.

6.4 Discussion

By varying digestion time, we have been able to control several key properties of ECM hydrogels including: protein architecture, network branching/density, relative protein size, and hydrogel mechanics and gelation behavior. Based on this data it is clear that lower digestion times result in higher branching, with more large protein retained. Increase hydrogel branching and density is likely responsible for the increase in mechanical properties at shorter digestion times. By modifying the solubilization approach we might be able to produce materials suited for specific applications. For example, stiffer more branched materials might be better suited for supporting in vitro cell culture and are more likely to support cell spreading and migration. It is also likely that pregel samples from different digestion times will have varying ability to sequester growth factors and drugs. This property could potentially be used to tailor controlled release in the future.

One major question that was answered by the SDS-PAGE analysis is whether increased digestion time was resulting in more protein being broken down into an unidentifiable smear. This has been confirmed as shown in figure 6.4, B and D, where the summed total volume of all the proteins measure in each lane, decreases as the digestion time increases. Another question that is at least addressed by this data is how the protein profiles change between pregel and

hydrogel samples. Pregel samples only have 5 identifiable bands while the post gelled samples have 7. We expected the self-assembled gel to have higher relative amounts of large ECM proteins when compared to the pregel samples; however, they actually have less of the first band.

The KGF release experiment demonstrated that digestion time may play a role in regulating cytokine release from encapsulated cells. This was either because of the mechanical properties of the gel effected the MSC signaling pathways responsible for this gene, or because the lower digestion time gels have a higher capacity for sequestering released factors. If the second one is the case, it would likely be because the larger and more branched protein structures in the gels are better at binding cytokines. I also believe that the increased branching and mechanical properties were responsible for the increased proliferation values for groups grown on shorter timed digests. Taken together these observations suggest that digestion time could be a major tool for tailoring ECM hydrogel platforms towards specific applications.

6.5 Conclusions

We have determined that the solubilization approach used for preparing hydrogels from tissue derived matrix has a fundamental effect on the organization of the component proteins in a hydrogel. This results in a range of different gelation kinetics and mechanical properties that can be achieved by modifying solubilization approach. We also thoroughly characterized the protein profile of the samples and how they change with increased digestion time. It is also clear that digestion time plays a major role in rheometrical properties. It is likely that this increase in stiffness and branching was responsible for increased SAEC proliferation on the shorter timed digests. Investigation of this concept can lead to more tailored materials for specific biomaterial and modelling applications.

Chapter 7: Conclusion and Future Research

The decellularization approach we used was validated with respect to gross reduction iwn potential immunogenic sources, and characterized the depletion of essential lung ECM proteins. In the future we are interested in investigating additional decellularization approaches, or swapping out detergents as the field advances and better approaches are found. I also have an idea: if we can significantly and consistently reduce the cross-sectional area of the tissue, then that would allow us to use a triton-X100 only decellularization. Lung tissue is well suited to a perfusion decellularization approach, but because we are only interested in isolating matrix proteins and not as interested in preserving the architecture of lung structures (airways, vasculature, and alveoli) a suspension technique could be better suited. Cross sectional area could be controlled and reduced by sectioning into uniform chunks, freezer milling the intact lung and then decellularizing the resulting powder, or using a slicing technique to isolate thin slices from the tissue. Ultimately, the approach we used was robust in generating uniformly decellularized lung matrix for processing.

During our investigation we have thoroughly characterized a lung derived ECM hydrogel that can be used to suspend cells or drugs in a liquid and then self assembles to encapsulate the payload at a target location. The mechanical properties and gelation mechanics of the hydrogel were determined to be similar to those derived from heterogeneous soft tissues such as heart, brain, and adipose sources. We have also confirmed that the proteins in the hydrogel are able to

bind and sequester growth factors like KGF. This added functionality is specifically of interest for additional study. For example, instead of using the hydrogels to deliver cells that secrete pro-regenerative factors, like MSCs, it might be possible to harvest and collect these cytokines in vitro and load them into the gel for delivery. Another use could be to load the hydrogels with a desired factor and coat the proteins for in vitro assays or onto an implantable device in vivo.

The feasibility experiments we completed determined that lung ECM hydrogels are able to maintain encapsulated viability, and are not likely to cause unintended differentiation of encapsulated stem cells. We were also able to relieve a key concern, that the protein binding reservoir does not significantly inhibit entry or exit of bioactive factors from encapsulated cells or from the environment. We also found that the 3D culture of hMSCs in the hydrogel does not inhibit immunomodulation signaling pathways that are essential to their value. Our first attempt to investigate the immunogenicity of the material was relatively successful; while ECM hydrogels do not immediately indoctrinate naive macrophages into a shocking anti-inflammatory, pro-regenerative fury, they also do not polarize them toward being pro-inflammatory. While we already have some significant in vivo findings that show increased retention of cells delivered in a gel, I think future studies will have us doing a full scale delivery of stem cells into an animal model for lung disease. I think that many of the findings outlined in this dissertation will lead to a new dosing protocol that can resolve an induced injury for some significant, quantifiable, positive outcomes.

Our final aim was to start looking into changes in our solubilization protocol and to make novel observations regarding new ways to tailor and control ECM hydrogel properties.

Specifically, altering the ECM digestion duration has allowed us to characterize controllable properties including hydrogel branching/density, gelation kinetics and mechanics, and the profile and volume of solubilized proteins in the pre and post gelled samples. We have started to investigate the effect of these changes on cell culture and have found that cells respond differently depending on the digestion duration used for the gel. This is a huge area for future research because tailorable ECM hydrogels could make them more competitive in more applications, including cell and drug delivery, biomaterial coating, and as an in vitro platform for cell-ECM interaction. In the future these new gels need to be evaluated for differences in immunogenic potential, ability to sequester bioactive molecules or charged drugs, and ability to support and maintain encapsulated MSCs.

The process to translate a project from the bench to clinical use is a long and complex process that will have increased or relaxed hurdles to address depending on the classification of the material or treatment. In 1997 the FDA overhauled the classification system that determines if a product derived from human cells, tissue, and cellular and tissue-based products (referred to as HCT/Ps). With the new guidelines there was a line drawn between the regulation of newly defined 361 HCT/Ps and the more highly regulated 351 HCT/Ps which are regulated like drugs, devices, and/or biological products[96]. The statement that pushes most decellularized products is that the tissue has been more than minimally manipulated, and through several examples the FDA has determined that decellularization of most tissues is more than minimally manipulative and therefore subject to more stringent guidelines[97]. This classification is subject to interpretation and can depend heavily on the claims made by the producer and how it is advertised, for example: acellular dermis is a 361 HCT/P if advertised for use as a skin covering; however, if it

is advertised for promoting for revascularization or remodeling host tissue it is no longer regulated as a 361[97].

Our ECM hydrogel will almost definitely fall under the more stringent guidelines and with the addition of drugs, biologics, or cells would be subject to the guidelines defined by the Center for Biologics Evaluation and Research, which includes combination materials including: autologous cells and delivery device to treat diseases[97]. Some major requirements that will need to be met stem from both the Donor eligibility and the Current Good Tissue Practice guidelines (CGTP), which have been initiated to prevent the initiation, transmission, or spread of communicable diseases. These include baseline requirements for donor screening, testing, tissue storage, labelling, packing, and distribution[96]. The whole production space will need to be controlled to limit sources of contamination and the steps for producing the material will need to be thoroughly evaluated for potential breakdowns. Additionally, we will need to investigate a means for terminal sterilization of the material which can be at the end of the milling step as long as the digestion steps are completed in sterile environments with sterilized digestion components. One approach for terminal sterilization would be exposing the decellularized tissue or ECM powder to 0.1% periacetic acid and then rinsing with sterilized DI or PBS and lyophilizing under sterile conditions. Another approach recently used for a fully formed cartilage derived hydrogel is sterilization under ultraviolet light for up to 1.5 hours[98].

No matter what changes and approaches are used for bring the production up to FDA standards, the final product will need to be extensively evaluated for changes in baseline properties due to method changes, and evaluated for batch to batch variation. The FDA approval process for new drug or biologic can be seen in figure 7.1. We are still in the prototype and

development phase, however, we can plan and conduct research with an eye towards the standards necessary for the FDA approval process, for a smoother translational process.

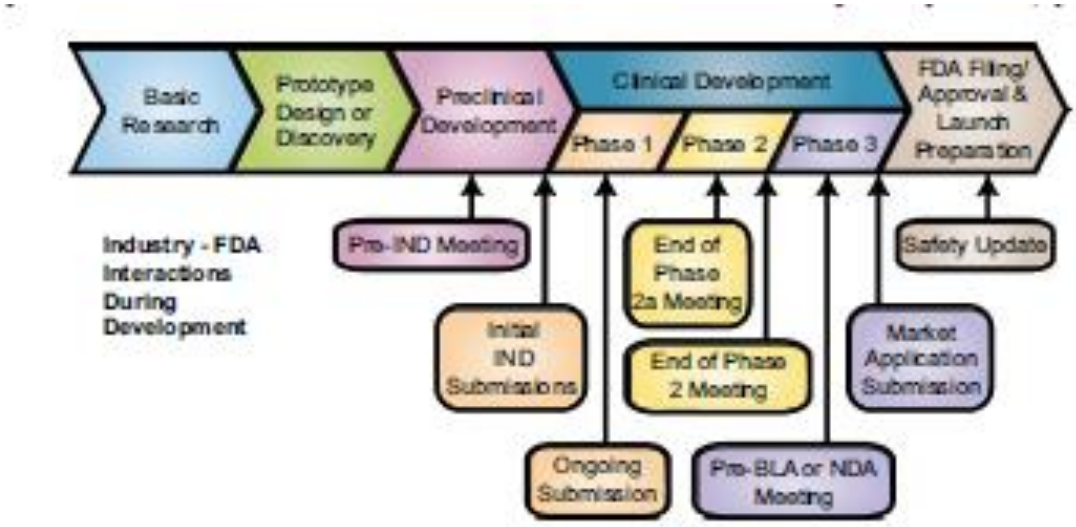

Figure 7.1 Generalized FDA Approval Process for Drugs and Biologics While we are still in the prototype design and discovery phase for Lung Derived ECM Hydrogels we can plan for future Preclinical development, which includes feasibility, iterative testing, and safety data collection; prior to testing in humans[99].

The results of our investigation indicate that an ECM hydrogel is a promising platform for cell and drug delivery. The isolated porcine extracellular matrix has already seen expanded use in several projects as a base material for electrospun scaffolds as well as the production of ECM nanoparticles. Additionally, we have identified many new impactful targets for future research.

References

1. Kochanek, K. D., Xu, J., Murphy, S. L., Miniño, A. M. & Kung, H.-C. National vital statistics reports. *Natl. Vital Stat. Rep.* **59,** 1 (2011).
2. Labiris, N. R. & Dolovich, M. B. Pulmonary drug delivery. Part I: Physiological factors affecting therapeutic effectiveness of aerosolized medications: Physiological factors affecting the effectiveness of inhaled drugs. *Br. J. Clin. Pharmacol.* **56,** 588–599 (2003).
3. Shah, N. D., Shah, V. V. & Chivate, N. D. Pulmonary drug delivery: A promising approach. (2012).
4. D'Agostino, B., Sullo, N., Siniscalco, D., De Angelis, A. & Rossi, F. Mesenchymal stem cell therapy for the treatment of chronic obstructive pulmonary disease. *Expert Opin. Biol. Ther.* **10,** 681–687 (2010).
5. Weiss, D. J., Casaburi, R., Flannery, R., LeRoux-Williams, M. & Tashkin, D. P. A Placebo-Controlled, Randomized Trial of Mesenchymal Stem Cells in COPDMesenchymal Stem Cells for COPD. *CHEST J.* **143,** 1590–1598 (2013).
6. Wang, D., Morales, J. E., Calame, D. G., Alcorn, J. L. & Wetsel, R. A. Transplantation of Human Embryonic Stem Cell–Derived Alveolar Epithelial Type II Cells Abrogates Acute Lung Injury in Mice. *Mol. Ther.* **18,** 625–634 (2010).
7. Olsson, B. *et al.* in *Controlled Pulmonary Drug Delivery* (eds. Smyth, H. D. C. & Hickey, A. J.) 21–50 (Springer New York, 2011).
8. Hogg, J. C. & Timens, W. The Pathology of Chronic Obstructive Pulmonary Disease. *Annu. Rev. Pathol. Mech. Dis.* **4,** 435–459 (2009).
9. Barnes, P. J. *et al.* Chronic obstructive pulmonary disease. *Nat. Rev. Dis. Primer* **3,** (2015).
10. Annoni, R. *et al.* Extracellular matrix composition in COPD. *Eur. Respir. J.* **40,** 1362–1373 (2012).

11. Celli, B., ZuWallack, R., Wang, S. & Kesten, S. Improvement in resting inspiratory capacity and hyperinflation with tiotropium in COPD patients with increased static lung volumes. *CHEST J.* **124,** 1743–1748 (2003).
12. Barnes, P. J. How corticosteroids control inflammation: quintiles prize lecture 2005. *Br. J. Pharmacol.* **148,** 245–254 (2006).
13. Criner, G. J. *et al.* Biologic Lung Volume Reduction in Advanced Upper Lobe Emphysema: Phase 2 Results. *Am. J. Respir. Crit. Care Med.* **179,** 791–798 (2009).
14. Taraseviciene-Stewart, L. & Voelkel, N. F. Molecular pathogenesis of emphysema. *J. Clin. Invest.* **118,** 394–402 (2008).
15. Carvalho, T. C., Peters, J. I. & Williams III, R. O. Influence of particle size on regional lung deposition – What evidence is there? *Int. J. Pharm.* **406,** 1–10 (2011).
16. Martin, T. R. Innate Immunity in the Lungs. *Proc. Am. Thorac. Soc.* **2,** 403–411 (2005).
17. Banchereau, J. & Steinman, R. M. Dendritic cells and the control of immunity. *Nature* **392,** 245–252 (1998).
18. Liu, Y.-J. Dendritic cell subsets and lineages, and their functions in innate and adaptive immunity. *Cell* **106,** 259–262 (2001).
19. Guilliams, M., Lambrecht, B. N. & Hammad, H. Division of labor between lung dendritic cells and macrophages in the defense against pulmonary infections. *Mucosal Immunol.* **6,** 464–473 (2013).
20. Lambrecht, B. N. Alveolar Macrophage in the Driver's Seat. *Immunity* **24,** 366–368 (2006).
21. Woodruff, P. G. *et al.* A Distinctive Alveolar Macrophage Activation State Induced by Cigarette Smoking. *Am. J. Respir. Crit. Care Med.* **172,** 1383–1392 (2005).
22. Nurwidya, F., Damayanti, T. & Yunus, F. The Role of Innate and Adaptive Immune Cells in the Immunopathogenesis of Chronic Obstructive Pulmonary Disease. *Tuberc. Respir. Dis.* **79,** 5 (2016).
23. Ding, D.-C., Shyu, W.-C. & Lin, S.-Z. Mesenchymal Stem Cells. *Cell Transplant.* **20,** 5–14 (2011).

24. Kode, J. A., Mukherjee, S., Joglekar, M. V. & Hardikar, A. A. Mesenchymal stem cells: immunobiology and role in immunomodulation and tissue regeneration. *Cytotherapy* **11,** 377–391 (2009).
25. Park, J. S. *et al.* The effect of matrix stiffness on the differentiation of mesenchymal stem cells in response to TGF-β. *Biomaterials* **32,** 3921–3930 (2011).
26. Kilian, K. A., Bugarija, B., Lahn, B. T. & Mrksich, M. Geometric cues for directing the differentiation of mesenchymal stem cells. *Proc. Natl. Acad. Sci.* **107,** 4872–4877 (2010).
27. Lee, J., Abdeen, A. A., Zhang, D. & Kilian, K. A. Directing stem cell fate on hydrogel substrates by controlling cell geometry, matrix mechanics and adhesion ligand composition. *Biomaterials* **34,** 8140–8 (2013).
28. Lau, A. N., Goodwin, M., Kim, C. F. & Weiss, D. J. Stem Cells and Regenerative Medicine in Lung Biology and Diseases. *Mol. Ther.* **20,** 1116–1130 (2012).
29. Mendez, J. J., Ghaedi, M., Steinbacher, D. & Niklason, L. E. Epithelial Cell Differentiation of Human Mesenchymal Stromal Cells in Decellularized Lung Scaffolds. *Tissue Eng. Part A* 140428074904005 (2014). doi:10.1089/ten.tea.2013.0647
30. Prockop, D. J. & Youn Oh, J. Mesenchymal Stem/Stromal Cells (MSCs): Role as Guardians of Inflammation. *Mol. Ther.* **20,** 14–20 (2012).
31. Oh, J. Y. *et al.* Anti-inflammatory protein TSG-6 reduces inflammatory damage to the cornea following chemical and mechanical injury. *Proc. Natl. Acad. Sci.* **107,** 16875–16880 (2010).
32. Choi, H., Lee, R. H., Bazhanov, N., Oh, J. Y. & Prockop, D. J. Anti-inflammatory protein TSG-6 secreted by activated MSCs attenuates zymosan-induced mouse peritonitis by decreasing TLR2/NF- B signaling in resident macrophages. *Blood* **118,** 330–338 (2011).
33. Milner, C. M. TSG-6: a multifunctional protein associated with inflammation. *J. Cell Sci.* **116,** 1863–1873 (2003).

34. Wisniewski, H.-G. & Vilcek, J. TSG-6: An IL-1/TNF-Inducible Protein with Anti-Inflammatory Activity. *Cytokine Growth Factor Reveiws* **8,** 143–163 (1997).

35. Lesley, J. *et al.* TSG-6 Modulates the Interaction between Hyaluronan and Cell Surface CD44. *J. Biol. Chem.* **279,** 25745–25754 (2004).

36. Matthay, M. A., Goolaerts, A., Howard, J. P. & Woo Lee, J. Mesenchymal stem cells for acute lung injury: Preclinical evidence: *Crit. Care Med.* **38,** S569–S573 (2010).

37. Lee, J. W., Gupta, N., Serikov, V. & Matthay, M. A. Potential application of mesenchymal stem cells in acute lung injury. *Expert Opin. Biol. Ther.* **9,** 1259–1270 (2009).

38. Mei, S. H. *et al.* Prevention of LPS-induced acute lung injury in mice by mesenchymal stem cells overexpressing angiopoietin 1. *PLoS Med.* **4,** e269 (2007).

39. Lee, J. W., Fang, X., Gupta, N., Serikov, V. & Matthay, M. A. Allogeneic human mesenchymal stem cells for treatment of E. coli endotoxin-induced acute lung injury in the ex vivo perfused human lung. *Proc. Natl. Acad. Sci.* **106,** 16357–16362 (2009).

40. Zhang, W.-G. *et al.* Regulation of transplanted mesenchymal stem cells by the lung progenitor niche in rats with chronic obstructive pulmonary disease. *Respir. Res.* **15,** 33 (2014).

41. Stucky, E. C., Schloss, R. S., Yarmush, M. L. & Shreiber, D. I. Alginate micro-encapsulation of mesenchymal stromal cells enhances modulation of the neuro-inflammatory response. *Cytotherapy* **17,** 1353–1364 (2015).

42. Garate, A. *et al.* Assessment of the Behavior of Mesenchymal Stem Cells Immobilized in Biomimetic Alginate Microcapsules. *Mol. Pharm.* **12,** 3953–3962 (2015).

43. Lu, S., Lee, E. J., Lam, J., Tabata, Y. & Mikos, A. G. Evaluation of Gelatin Microparticles as Adherent-Substrates for Mesenchymal Stem Cells in a Hydrogel Composite. *Ann. Biomed. Eng.* (2016). doi:10.1007/s10439-016-1582-x

44. Ingenito, E. P. *et al.* Autologous Lung-Derived Mesenchymal Stem Cell Transplantation in Experimental Emphysema. *Cell Transplant.* **21,** 175–189 (2012).
45. Badylak, S., Freytes, D. & Gilbert, T. Extracellular matrix as a biological scaffold material: Structure and function. *Acta Biomater.* **5,** 1–13 (2009).
46. Daly, A. B. *et al.* Initial Binding and Recellularization of Decellularized Mouse Lung Scaffolds with Bone Marrow-Derived Mesenchymal Stromal Cells. *Tissue Eng. Part A* **18,** 1–16 (2012).
47. French, K. M. *et al.* A naturally derived cardiac extracellular matrix enhances cardiac progenitor cell behavior in vitro. *Acta Biomater.* **8,** 4357–4364 (2012).
48. Gilbert, T., Sellaro, T. & Badylak, S. Decellularization of tissues and organs. *Biomaterials* (2006). doi:10.1016/j.biomaterials.2006.02.014
49. Hoshiba, T., Lu, H., Kawazoe, N. & Chen, G. Decellularized matrices for tissue engineering. *Expert Opin. Biol. Ther.* **10,** 1717–1728 (2010).
50. Nichols, J. E., Niles, J. A. & Cortiella, J. Production and utilization of acellular lung scaffolds in tissue engineering. *J. Cell. Biochem.* **113,** 2185–2192 (2012).
51. Petersen, T. H., Calle, E. A., Colehour, M. B. & Niklason, L. E. Matrix Composition and Mechanics of Decellularized Lung Scaffolds. *Cells Tissues Organs* **195,** 222–231 (2012).
52. Badylak, S. F., Valentin, J. E., Ravindra, A. K., McCabe, G. P. & Stewart-Akers, A. M. Macrophage Phenotype as a Determinant of Biologic Scaffold Remodeling. *Tissue Eng. Part A* **14,** 1835–1842 (2008).
53. Badylak, S. F. The extracellular matrix as a biologic scaffold material☆. *Biomaterials* **28,** 3587–3593 (2007).
54. Valentin, J. E., Badylak, J. S., McCabe, G. P. & Badylak, S. F. Extracellular matrix bioscaffolds for orthopaedic applications. *J. Bone Jt. Surg.* **88,** 2673–2686 (2006).

55. Bonvillain, R. W. *et al.* A Nonhuman Primate Model of Lung Regeneration: Detergent-Mediated Decellularization and Initial *In Vitro* Recellularization with Mesenchymal Stem Cells. *Tissue Eng. Part A* **18,** 2437–2452 (2012).

56. Johnson, T. D., Lin, S. Y. & Christman, K. L. Tailoring material properties of a nanofibrous extracellular matrix derived hydrogel. *Nanotechnology* **22,** 494015 (2011).

57. Seif-Naraghi, S. B. *et al.* Safety and efficacy of an injectable extracellular matrix hydrogel for treating myocardial infarction. *Sci. Transl. Med.* **5,** 173ra25–173ra25 (2013).

58. Martinez, F., Sica, A., Mantovani, A. & Locati, M. Macrophage activation and polarization. *Front. Biosci.* **13,** 453–461 (2008).

59. Petersen, T. H. *et al.* Tissue-Engineered Lungs for in Vivo Implantation. *Science* **329,** 538–541 (2010).

60. Price, A. P., England, K. A., Matson, A. M., Blazar, B. R. & Panoskaltsis-Mortari, A. Development of a Decellularized Lung Bioreactor System for Bioengineering the Lung: The Matrix Reloaded. *Tissue Eng. Part A* **16,** 2581–2591 (2010).

61. Wagner, D. E. *et al.* Can stem cells be used to generate new lungs? *Ex vivo* lung bioengineering with decellularized whole lung scaffolds: Ex vivo lung bioengineering. *Respirology* **18,** 895–911 (2013).

62. Badylak, S. F. Xenogeneic extracellular matrix as a scaffold for tissue reconstruction. *Transpl. Immunol.* **12,** 367–377 (2004).

63. Macher, B. A. & Galili, U. The Galα1,3Galβ1,4GlcNAc-R (α-Gal) epitope: A carbohydrate of unique evolution and clinical relevance. *Biochim. Biophys. Acta BBA - Gen. Subj.* **1780,** 75–88 (2008).

64. Badylak, S. F. Decellularized Allogeneic and Xenogeneic Tissue as a Bioscaffold for Regenerative Medicine: Factors that Influence the Host Response. *Ann. Biomed. Eng.* **42,** 1517–1527 (2014).

65. Naso, F., Gandaglia, A., Iop, L., Spina, M. & Gerosa, G. First quantitative assay of alpha-Gal in soft tissues: Presence and distribution of the epitope before and after cell removal from xenogeneic heart valves. *Acta Biomater.* **7,** 1728–1734 (2011).

66. Sokocevic, D. *et al.* The effect of age and emphysematous and fibrotic injury on the re-cellularization of de-cellularized lungs. *Biomaterials* **34,** 3256–3269 (2013).

67. Wagner, D. E. *et al.* Comparative decellularization and recellularization of normal versus emphysematous human lungs. *Biomaterials* **35,** 3281–3297 (2014).

68. Cortiella, J. *et al.* Influence of Acellular Natural Lung Matrix on Murine Embryonic Stem Cell Differentiation and Tissue Formation. *Tissue Eng. Part A* **16,** 2565–2580 (2010).

69. Singelyn, J. M. *et al.* Catheter-Deliverable Hydrogel Derived From Decellularized Ventricular Extracellular Matrix Increases Endogenous Cardiomyocytes and Preserves Cardiac Function Post-Myocardial Infarction. *J. Am. Coll. Cardiol.* **59,** 751–763 (2012).

70. Kwon, J. S. *et al.* Injectable extracellular matrix hydrogel developed using porcine articular cartilage. *Int. J. Pharm.* **454,** 183–191 (2013).

71. Wolf, M. T. *et al.* A hydrogel derived from decellularized dermal extracellular matrix. *Biomaterials* **33,** 7028–7038 (2012).

72. Young, D. A., Ibrahim, D. O., Hu, D. & Christman, K. L. Injectable hydrogel scaffold from decellularized human lipoaspirate. *Acta Biomater.* **7,** 1040–1049 (2011).

73. Freytes, D. O., Martin, J., Velankar, S. S., Lee, A. S. & Badylak, S. F. Preparation and rheological characterization of a gel form of the porcine urinary bladder matrix. *Biomaterials* **29,** 1630–1637 (2008).

74. Medberry, C. J. *et al.* Hydrogels derived from central nervous system extracellular matrix. *Biomaterials* **34,** 1033–1040 (2013).

75. Seif-Naraghi, S. B., Horn, D., Schup-Magoffin, P. J. & Christman, K. L. Injectable extracellular matrix derived hydrogel provides a platform for enhanced retention and delivery of a heparin-binding growth factor. *Acta Biomater.* **8,** 3695–3703 (2012).

76. Long, J. L. & Tranquillo, R. T. Elastic fiber production in cardiovascular tissue-equivalents. *Matrix Biol.* **22,** 339–350 (2003).

77. Frazier, S. B., Roodhouse, K. A., Hourcade, D. E. & Zhang, L. The Quantification of Glycosaminoglycans: A Comparison of HPLC, Carbazole, and Alcian Blue Methods. *Open Glycosci.* **1,** 31–39 (2008).

78. Wallis, J. M. *et al.* Comparative Assessment of Detergent-Based Protocols for Mouse Lung De-Cellularization and Re-Cellularization. *Tissue Eng. Part C Methods* **18,** 420–432 (2012).

79. Gilbert, T. W. Strategies for tissue and organ decellularization. *J. Cell. Biochem.* **113,** 2217–2222 (2012).

80. Petersen, T. H., Calle, E. A., Colehour, M. B. & Niklason, L. E. Matrix Composition and Mechanics of Decellularized Lung Scaffolds. *Cells Tissues Organs* **195,** 222–231 (2012).

81. Li, J. W. & Wu, X. Mesenchymal stem cells ameliorate LPS-induced acute lung injury through KGF promoting alveolar fluid clearance of alveolar type II cells. *Eur. Rev. Med. Pharmacol. Sci.* **19,** 2368–2378 (2015).

82. Butcher, D. T., Alliston, T. & Weaver, V. M. A tense situation: forcing tumour progression. *Nat. Rev. Cancer* **9,** 108–122 (2009).

83. Singelyn, J. M. & Christman, K. L. Modulation of Material Properties of a Decellularized Myocardial Matrix Scaffold. *Macromol. Biosci.* **11,** 731–738 (2011).

84. Brennan, E. P. *et al.* Antibacterial Activity within Degradation Products of Biological Scaffolds Composed of Extracellular Matrix. *Tissue Eng.* **12,** 2949–2955 (2006).

85. Reing, J. E. *et al.* Degradation products of extracellular matrix affect cell migration and proliferation. *Tissue Eng. Part A* **15,** 605–614 (2008).

86. Geer, D. J., Swartz, D. D. & Andreadis, S. T. Biomimetic Delivery of Keratinocyte Growth Factor upon Cellular Demand for Accelerated Wound Healing in Vitro and in Vivo. *Am. Hournal Pathol.* **167,** (2005).

87. Saluja, B., Li, H., Desai, U. R., Voelkel, N. F. & Sakagami, M. Sulfated Caffeic Acid Dehydropolymer Attenuates Elastase and Cigarette Smoke Extract–induced Emphysema in Rats: Sustained Activity and a Need of Pulmonary Delivery. *Lung* **192,** 481–492 (2014).

88. Goldblum, S. E., Wu, K.-M. & Jay, M. Lung myeloperoxidase as a measure of pulmonary leukostasis in rabbits. *J. Appl. Physiol.* **59,** 1978–1985 (1985).

89. Badylak, S. F., Taylor, D. & Uygun, K. Whole-Organ Tissue Engineering: Decellularization and Recellularization of Three-Dimensional Matrix Scaffolds. *Annu. Rev. Biomed. Eng.* **13,** 27–53 (2011).

90. Singelyn, J. M. *et al.* Naturally derived myocardial matrix as an injectable scaffold for cardiac tissue engineering. *Biomaterials* **30,** 5409–5416 (2009).

91. Chou, H.-C., Lin, W. & Chen, C.-M. Human mesenchymal stem cells attenuate pulmonary hypertension induced by prenatal lipopolysaccharide treatment in rats. *Clin. Exp. Pharmacol. Physiol.* (2016). doi:10.1111/1440-1681.12604

92. Waterman, R. S., Tomchuck, S. L., Henkle, S. L. & Betancourt, A. M. A New Mesenchymal Stem Cell (MSC) Paradigm: Polarization into a Pro-Inflammatory MSC1 or an Immunosuppressive MSC2 Phenotype. *PLoS ONE* **5,** e10088 (2010).

93. Crisostomo, P. R. *et al.* Human mesenchymal stem cells stimulated by TNF- , LPS, or hypoxia produce growth factors by an NF B- but not JNK-dependent mechanism. *AJP Cell Physiol.* **294,** C675–C682 (2008).

94. Kwon, Y. W. *et al.* Tumor necrosis factor-α-activated mesenchymal stem cells promote endothelial progenitor cell homing and angiogenesis. *Biochim. Biophys. Acta BBA - Mol. Basis Dis.* **1832,** 2136–2144 (2013).

95. Jablonski, K. A. *et al.* Novel Markers to Delineate Murine M1 and M2 Macrophages. *PLOS ONE* **10,** e0145342 (2015).

96. Guidance for Industry: Regulation of Human Cells, Tissues, and Cellular and Tissue-Based Products (HCT/Ps). (2007).

97. Solomon, D. R. HCT/P Regulatory Pathways and Jurisdiction: 361 HCT/P, Biological Product or Medical Device. (September).

98. Burnsed, O. A. *et al.* Hydrogels Derived from Cartilage Matrices Promote Induction of Human Mesenchymal Stem Cell Chondrogenic Differentiation. *Acta Biomater.* (2016). doi:10.1016/j.actbio.2016.07.034

99. Schneider, L. S. *et al.* Clinical trials and late-stage drug development for Alzheimer's disease: an appraisal from 1984 to 2014. *J. Intern. Med.* **275,** 251–283 (2014).

100. Pouliot, R. A. *et al.* Development and characterization of a naturally derived lung extracellular matrix hydrogel. *J. Biomed. Mater. Res. A* n/a–n/a (2016). doi:10.1002/jbm.a.35726

101. Price, A. P., England, K. a, Matson, A. M., Blazar, B. R. & Panoskaltsis-Mortari, A. Development of a decellularized lung bioreactor system for bioengineering the lung: the matrix reloaded. *Tissue Eng. Part A* **16,** 2581–2591 (2010).

102. Freytes, D. O., Martin, J., Velankar, S. S., Lee, A. S. & Badylak, S. F. Preparation and rheological characterization of a gel form of the porcine urinary bladder matrix. *Biomaterials* **29,** 1630–1637 (2008).

Appendices

Appendix A. Detailed Decellularization Protocol

PROTOCOL: (From Accepted Jove Article)

1) Decellularization and Hydrogel Preparation Protocol

1.1) Lung Decellularization (adapted from [100,101]):

1.1.1) Begin with en bloc porcine lung tissue with heart and vasculature intact.

1.1.2) Remove the heart carefully to keep the pulmonary artery intact for perfusion.

1.1.3) Carefully remove the connective tissue surrounding the trachea, bronchi, and vasculature.

1.1.4) Carefully remove one lung. Note: Retain sections for histology if desired.

1.1.5) Close disconnected bronchi with clamps or suture to prevent excess backflow.

1.1.6) Prepare the decellularization solutions and refrigerate at 4°C until needed (Table 1).

1.1.7) Perfuse the lung tissue 3 times with DI water through both vasculature and trachea. Perfuse vasculature first each time.

1.1.8) Perfuse both vasculature and trachea with Triton solution.

1.1.9) Submerge in Triton Solution for 24 hours at 4°C.

1.1.10) Perfuse vasculature and trachea 3 times with DI water to rinse.

1.1.11) Perfuse both vasculature and trachea with deoxycholate solution.

1.1.12) Submerge the tissue sections in deoxycholate for 24 hours at 4°C.

1.1.13) Perfuse vasculature and trachea 3 times with DI water to rinse.

1.1.14) Perfuse both vasculature and trachea with NaCl solution.

1.1.15) Submerge tissue in filtered NaCl solution for 1 hour at 4°C.

1.1.16) Perfuse vasculature and trachea 3 times with DI water to rinse.

1.1.17) Perfuse both vasculature and trachea with DNase solution.

1.1.18) Submerge tissue in filtered DNase solution for 1 hour at 4°C.

1.1.19) Perfuse both vasculature and trachea 5 times with PBS.

1.1.20) Dissect away noticeable cartilaginous tissue from conducting airways, leaving only respiratory zones.

1.1.21) Dissect tissue into 1” sections or smaller.

1.1.22) Remove excess liquid and freeze the tissue at -80°C. Retain sections for histology to ensure removal of cells and cellular debris, if desired.

1.2) Lung Processing

1.2.1) Lyophilize the tissue until all excess liquid is gone.

1.2.2) After lyophilization, freezer mill all tissue into fine powder. Store at -80°C until ready for use.

1.3) Micro-porous gel formation (8 mg/ml) (adapted from [100,102]):

1.3.1) Add 1% (w/v) of the decellularized powder and 0.1% (w/v) of pepsin to 0.01 M HCl, under constant agitation (should be able to see flow at the top level of liquid), at room temperature, for 48 hours.

Note: The powder is statically charged, so adding the HCl after the powder affords the opportunity to wash the excess off the tube walls.

1.3.2) After digestion for 48 hours, place the solution and reagents on ice for 5 minutes.

1.3.3) Using refrigerated 10% (v/v) 0.1 M NaOH, and 11.11% 10x PBS, bring the digested protein solution to physiologic pH of 7.4.

Note: The solution will now self-assemble into a micro-porous network at 37°C.

Appendix B. Scratch Assay Image Processing Methods

Scratch Assay Image Processing

Open Image J > Plugin > MRI Wound Healing 2 for MRI measure wound healing tool & Help Tool

1) If the images all have the same brightness > Take all the images and stack them
    a. Select all the images for a time point and drag into image j > image > stacks > images to stack [creates stack to be names] > save as (tiff)
        i. multiple images in one file now, access by scrolling
    b. Set the dimensions > use straight selection tool> draw bar on scale bar (hold shift to make horizontal) > analyze > set scale > Distance in pixels (for 4x, is 124 pixels); known distance (um); pixel aspect ratio (1.0); global (checked); press ok
    c. Adjust the brightness > image > adjust > brightness & contrast > change the settings until all of the images in the stack look reasonable> apply to all stacks> resave as imagestack_corrected
        i. If you ever close the stack it will ask if you want to disable the global, disable global (unchecked), check the second box. This was you don't have to reset the scale again
    d. Using the tool (ignore the help tool): [m]
        i. (right click) opens settings
        ii. (left click) make it run
        iii. 2 methods: variance or find edges (find edges is easier- only 2 parameters)

1. Find edges (only adjust min size, less control): parameters: radius open (always 1), min size (adjust 100k – 50k), variance & threshold don't effect find edges
2. Variance: Variance filter radius (); threshold ();

iv. Run Find Edges

1. Good for some scratch images but does not work as well as variance for most

v. Run Variance

1. Use the color picker tool to get an idea for threshold (range 1-155) (example, color picker on the middle of scratch, get 121; dark images, higher threshold; variance filter radius (1-10)

vi. Cropping> use the box tool to select an area > image > crop> resave the tiff as imagestack_cropped

e. Using the manual fixing tool

i. Go to the oval tool > right click> select brush tool>double click brush tool> select size (~50)

1. If from inside selection pushing outside it will increase the size
2. If you are outside pushing in you decrease the border

ii. Once you adjust something with the tool you need to click update

f. Data collection

i. ROI Manager> measure – will give you all of the individual selections regardless of image

ii. To merge selections: select the ones to merge> more> OR (Combine)> Update> it will update the first selection to include both> delete the second > now when you measure it will only have 1 measurement per image

g. Saving the ROI> show all> make sure none of the selections- are highlighted or it will only save 1. Save as a zip file
    i. Opening an ROI again> analyze > tools> ROI Manager> more> open > zip file
    ii. When you bring the stack back open the selections are already synced to the images
    iii. To save an image with the yellow borders still drawn on you would:
        1. In ROI manager > Flatten> for all images (yes)> file> save as> imagestack_adjusted_withborders
        2. You can open the stack in image viewer to get the individual image from the stack, or unstack in image J> image> stacks> stack to images
        3. Another cool thing is you can fill the borders to get a cooler picture

h. Steps:
    i. Use one of the methods
    ii. Delete and merge selections
    iii. Adjust with tool
    iv. Measure the data

Notes:

1. Consider stacking the wells, not the time points, then when you scroll you should see the

2. Starting setting for variance: VFR: 5; Threshold: 120; Radius OPEN: 1; Min Size: 50000